DOWNSTREAM ETCHING OF INDIUM PHOSPHIDE AND INDIUM

WITH HYDROGEN ATOMS AND METHYL RADICALS

BY

MARK EDWARD ASTON

B.Sc. (Hons.), University of Liverpool, 1987


A THESIS SUBMITTED IN PARTIAL FULFILLMENT OF THE

REQUIREMENTS FOR THE DEGREE OF MASTER OF SCIENCE

in

THE FACULTY OF GRADUATE STUDIES

Department of Chemistry


We accept this thesis as conforming

to the required standard


THE UNIVERSITY OF BRITISH COLUMBIA

October 1990

© Mark Edward Aston, 1990.

5 1.

In presenting this thesis in partial fulfilment of the requirements for an advanced degree at the University of British Columbia, I agree that the Library shall make it freely available for reference and study. I further agree that permission for extensive copying of this thesis for scholarly purposes may be granted by the head of my department or by his or her representatives. It is understood that copying or publication of this thesis for financial gain shall not be allowed without my written permission.

Department of _____Chemistry_____

The University of British Columbia
Vancouver, Canada

Date _____11/10/96_____

# Abstract

The etching of indium phosphide and indium by H atoms and methyl radicals has been studied in a discharge flow system at temperatures between 25 and 300°C. The results indicate that the hydrogen atoms react with InP to produce In metal globules and $PH_{3(g)}$ at temperatures greater than 160°C. Methyl radicals were not found to react with InP. However these radicals were found to react with indium metal and the globules that are produced in the reaction of hydrogen atoms with InP. Reactions were conducted by alternately etching with H atoms and then with $CH_3$ radicals. Rate constants for these reactions were determined at 300°C and these values were found to be consistent with the continuous etch rates observed for a mixture of H atoms and $CH_3$ radicals.

The etched surfaces were studied by SEM, XPS and surface profilometry and their properties found to be consistent with the proposed mechanism for the reaction.

# Table of contents

# List of tables

# List of figures

# List of plates

# Acknowledgements

# 1  Introduction

The binary compounds formed from the elements of groups III and V are particularly interesting optoelectronic materials, both for their fundamental properties and for their device applications. The most well known of these materials is GaAs which has been employed in a multitude of devices, such as lasers and other photovoltaic type applications. InP is a relatively new material whose properties also make it suited for optoelectronic devices. One of the attractions for III - V compounds is that they crystallise with a high degree of stoichiometry. Excellent quality crystals can be grown which improves the device efficiency. However probably their major advantage lies in the fact that these materials have direct band gaps which result in high optical transition probabilities, giving high absorption coefficients.

## 1.2  Direct And Indirect Band Gap Semiconductors.

An important use for compound semiconductors is in optoelectronic devices which interconvert electrical and light energy. Most devices generally employ GaAs and similar materials which possess direct band gaps where  the conversion of hole - electron pairs to photons, and vica versa, occurs without a change in momentum[1]. Consequently, there is no need for a third body to carry off momentum, greatly increasing the probability of the interconversion. This can be explained further as follows.

In a regular structure like a crystal, the direction of electron momentum is an important factor, and the state density is in reality

a function of both energy and the momentum vector $k^2$. Typical band diagrams are illustrated in figure 1.1[3]. The horizontal axis represents the magnitude of the momentum vector along the [111] and [100] crystal axes.

The significance of the band diagrams lies in the fact that the minimum in the conduction band energy and the maximum in the valence band may occur at different values of momentum. Since the transition probability drops off exponentially with the energy difference, electron transitions virtually always occur between the valence band maximum and the conduction band minimum. When these extrema coincide in momentum, the material is a direct band gap semiconductor and transitions between bands thus require no change in momentum. Irradiation with light of the proper wavelength will create electron - hole pairs without any impediment, and excess charge carriers can easily recombine to produce light photons. Gallium Arsenide type materials are therefore effective convertors between light and electrical energy, and good materials for the fabrication of optoelectronic devices.

Silicon is not suitable for these applications as it is an indirect band gap semiconductor. Consequently creation or annihilation of electron - hole pairs requires an exchange of both energy and momentum. Light quanta carry no momentum, and thus an electron transition cannot involve a photon alone. An interaction with a lattice vibration or some other momentum source is also required and such three body interactions are unlikely.
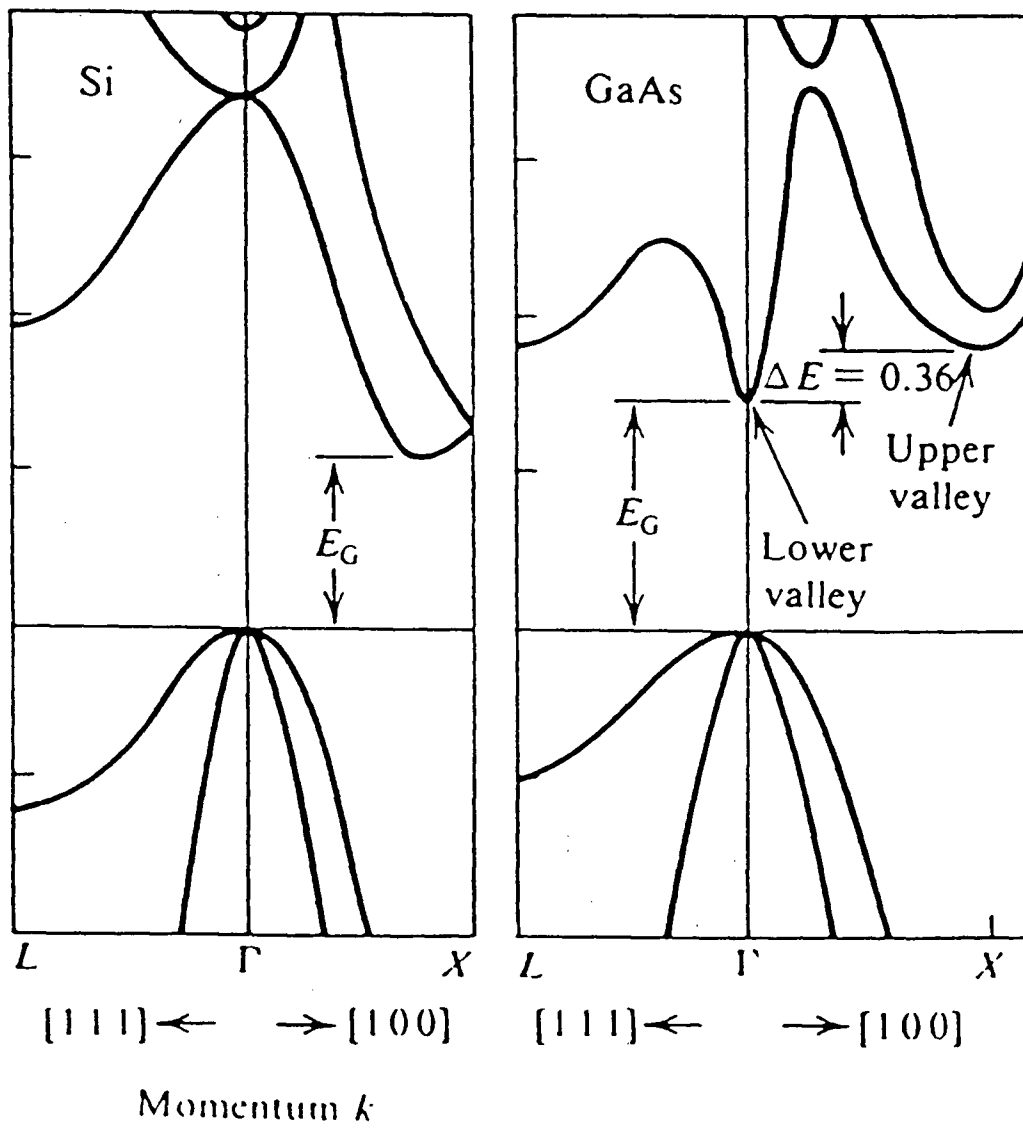
Figure 1.1.  Direct (GaAs) and indirect (Si) band diagrams.

3

## 1.3 Discussion of GaAs and InP

InP and GaAs are quite similar compound semiconductors (see table 1.1) GaAs being well established as a material for electronic devices. However, recently interest has shifted to InP as a replacement in some areas for a variety of reasons, some of which are indicated below.

The large electron mobility and greater saturated drift velocity give InP and GaAs an advantage in high speed applications[4] when compared to other semiconductors, such as silicon. Indeed researchers at AT&T laboratories have successfully fabricated 140 GHz bipolar transistors from InP/GaInAs, claimed to be the worlds fastest bipolar device. Traditional GaAs has a very high surface recombination velocity, so that a lot of current can leak through the surface of the device between the emitter and the base. Most GaAs bipolar work so far has therefore been done using 1 - 3 $\mu$m emitter stripes. InP on the other hand has a relatively low surface recombination velocity, so there is less leakage current at smaller dimensions (approx 0.3$\mu$m)[5].

A second key capability of InP is its radiation tolerance which offers substantial new horizons for InP when the devices are likely to be exposed to radiation such as, electrons, protons, neutrons, gamma and x-rays. InP solar cells all have at least twofold resistance to radiation than do comparable GaAs devices. Specifically, InP cells have tenfold greater resistance to electrons and protons than those of GaAs. Figure 1.2 compares Si, GaAs and InP solar cells in various natural radiation environments near Earth[6]. State of the art production efficiency in Si is 15 - 16 percent in GaAs

PROJECTED

STATE OF THE ART

Note : G.E.O => Geosynchronus Earth Orbit.
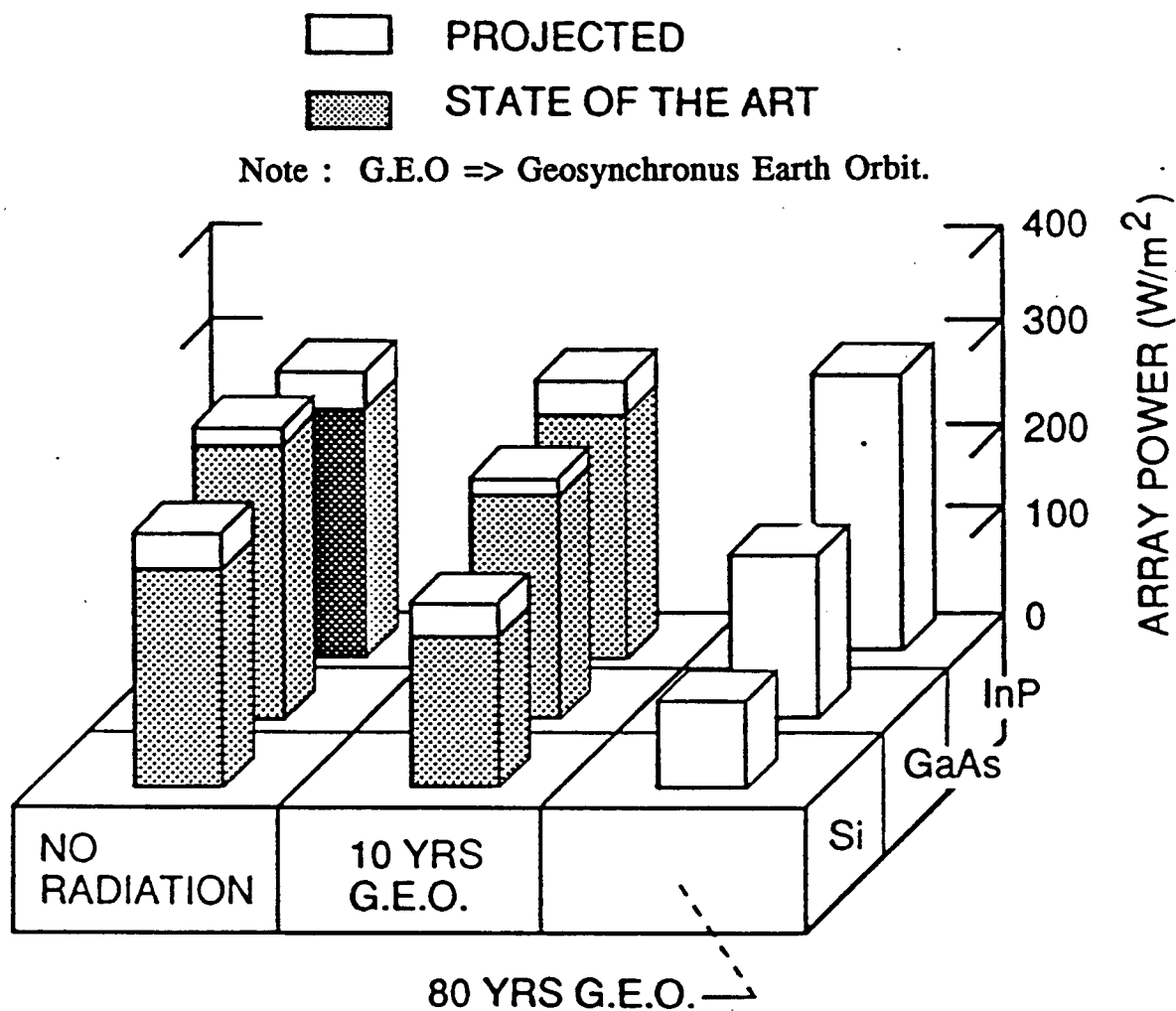


Figure 1.2. Comparison of solar cell power after radiation for Si, GaAs and InP.

Table 1.1.  Comparison between InP and GaAs.

| | InP | GaAs |
|---|---|---|
| Energy Gap 300K (eV) | 1.35 (direct) | 1.42 (direct) |
| Mobility, Electrons 300K ($cm^2$/V.s), Holes | 4500 100 | 5000-8000 300 |
| Crystal Structure | Zincblende | Zincblende |
| Lattice Constant (A) | 5.87 | 5.64 |
| Molecular weight | 145.79 | 144.64 |
| Density (g/$cm^3$) | 4.787 | 5.32 |
| Melting point (K) | 1330 | 1510 |
| $\Delta H_f$ (kcal/mole) | 134 | 128 |
| Absorption Coefficient at 0.5$\mu$m | $10^6$ cm$^{-1}$ | $5 \times 10^5$ cm$^{-1}$ |

17- 18 percent and in InP now up to 18.8 percent [7]. However, when these cells go into radiation environments there are large differences. For example after 10 years in geosynchronous Earth orbit, Si has lost 25% of its power; GaAs 10 - 15% and InP nothing.

Unfortunately an aspect where InP isn't at such an advantage is its cost, which may be prohibitively high when considering its use in devices requiring a large area of material, such as solar cells. The main expense incurred is due to the cost of the initial InP wafer which runs at around U.S$250 - $350 for a 2" sample. The corresponding Si being about $5.

Both InP and GaAs are well suited materials for solar cells having band gaps of 1.35 and 1.42 eV respectively, the optimal energy gap being estimated to be around 1.4eV[8]. It has been suggested that the improved radiation resistance of InP over GaAs is to be attributed to the better quality of the wafers used in processing the cells[9]. As well as this, InP has the added advantage that any radiation damage appears to be partially removed by exposure to light at room temperature[10].

### 1.4   The Solar Cell

A very basic solar cell can be envisaged as shown below in figure 1.3. With no external bias the photodiode will deliver power to a load resistance if irradiated by light with photons of sufficient energy. By making the collection area as large as possible, the solar cell will deliver a large photocurrent from direct illumination by sunlight. A solar cell with a collection area of 30 cm$^2$ and a power conversion efficiency of 10% will deliver 300 mW to a load in bright

7
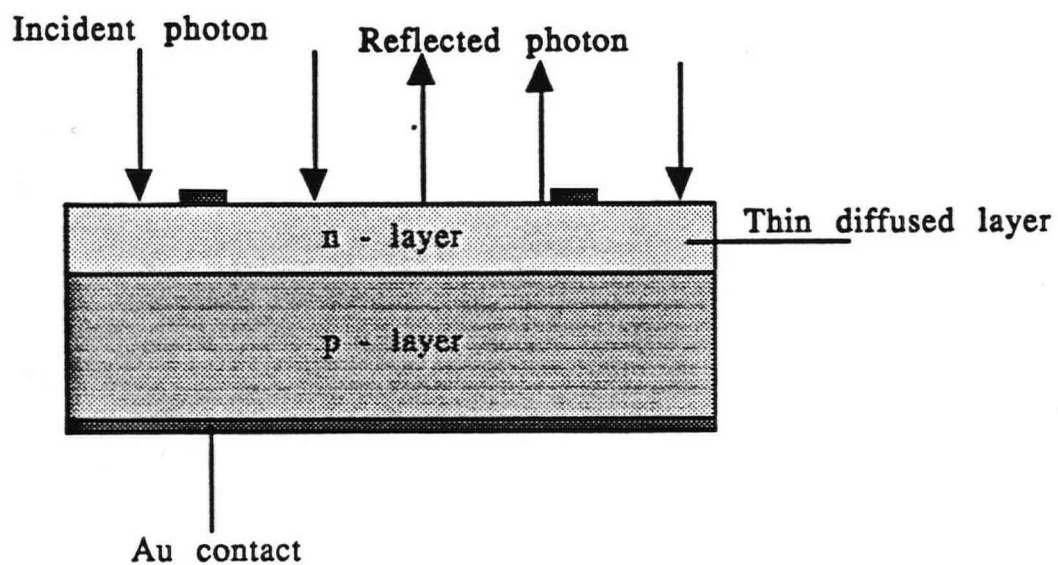
Figure 1.3. Simple InP solar cell.

sunlight[11]. Incident photons pass into the depletion region where they are absorbed, producing electron - hole pairs. The electrons drift towards the n - layer and the holes towards the p - layer, producing a reverse photocurrent.

Compound semiconductors are interesting as the relationships between band gap and composition gives the device designer the ability to control the spectral response by changing the composition. Also, the materials can be prepared in multi-layer structures by liquid or vapour phase epitaxial growth. Thus, there exists a wide range of possible compositions, absorption coefficients, ionization properties and device structures. The relationship between band gap, composition and lattice constant are represented in figure 1.4[12].

Since these compounds have direct transitions, the absorption coefficient rises steeply at the band edge to values of $10^4$ cm$^{-1}$ or more. These photodiodes can absorb efficiently in a layer only a few microns thick, leading to a small device structure and a fast carrier transit time. Indeed the InP solar cell technology has progressed so far that later in 1990 it is intended to launch satellites into space, powered by InP cells.

### 1.5 Indium Phosphide Wafer Growth

The most basic and commonly used technique for growing crystals is known as the Czochralski method. A schematic of the required apparatus is shown in figure 1.5.

The seed crystal is dipped into the melt and the melt temperature is adjusted until a meniscus can be supported by the seed. This is then slowly rotated and lifted. The major problem with
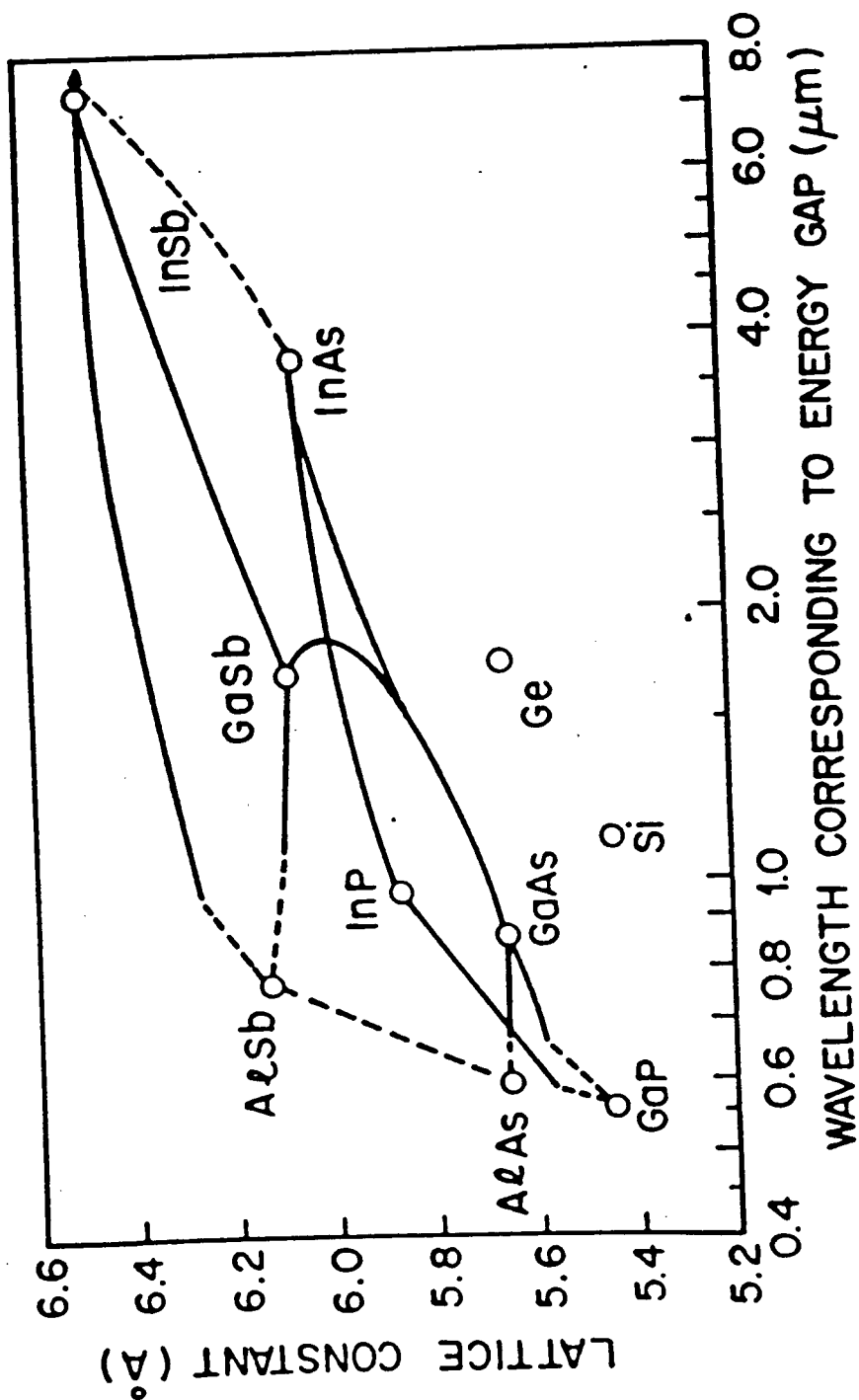
Figure 1.4. Plot of lattice constant against energy gap for selected semiconductors.
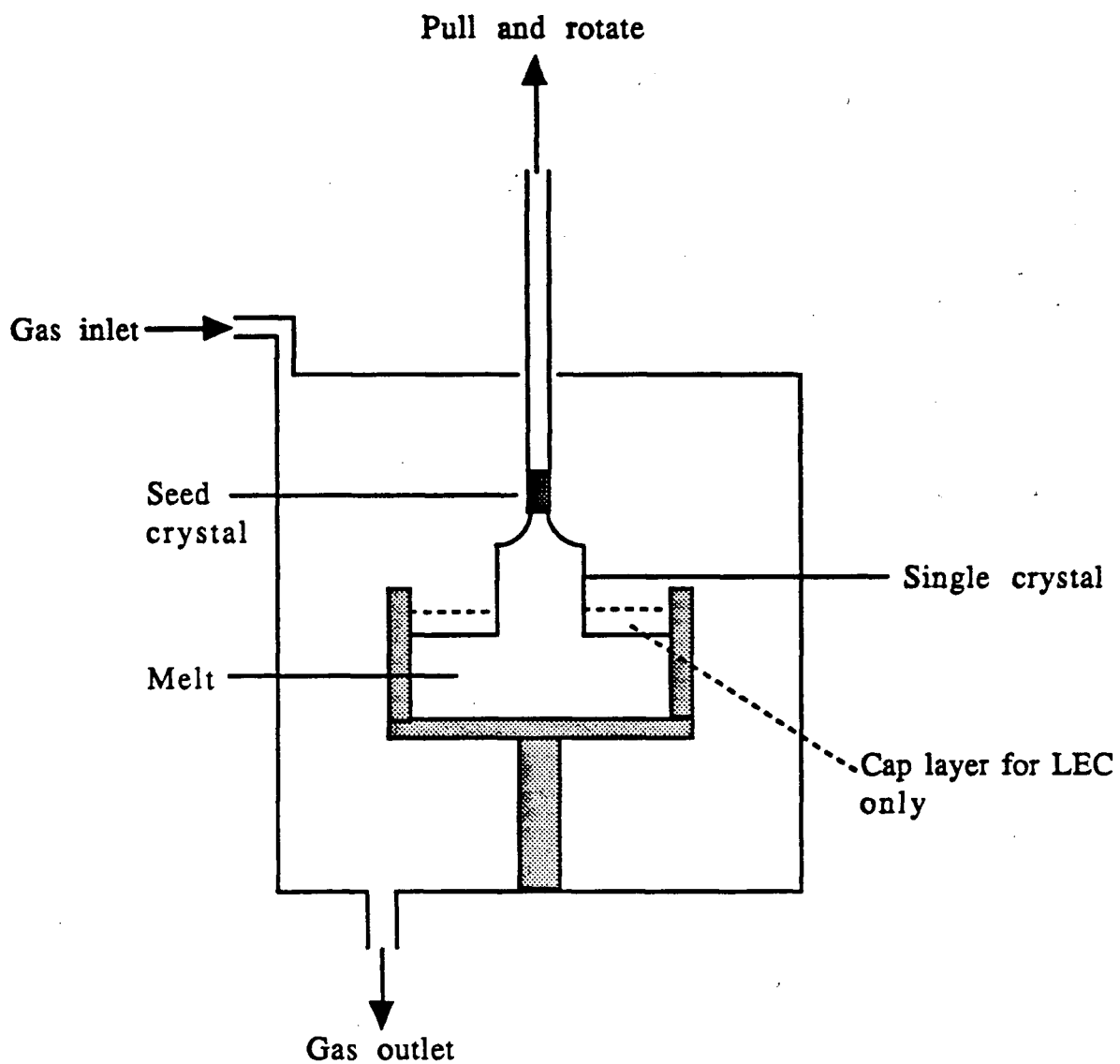
Figure 1.5.  Czochralski crystal growing apparatus.

this method for InP is that phosphorus is highly volatile, consequently the process has been adapted by encapsulating the melt with an inert compound. One such compound being $B_2O_3$. The cap of $B_2O_3$ prevents decomposition of the InP and this is known as Liquid Encapsulated Czochralski (LEC).

LEC is now the most common process for the large scale production of InP single wafers. One of the disadvantages with this type of wafer growth is that there is a high level of dislocations associated with wafers of large diameter. High quality substrates of InP are important for the advancement of high speed electronic, lightwave photonic and high performance solar conversion technologies. Single crystal substrates affect the quality of epitaxial layers and diffused or implanted regions in the substrate. Chemical purity determines the electrical properties of the substrates and structural perfection influences device yields, carrier recombination and device reliability. In view of these facts research is still being conducted into new and improved growth techniques. One such method, the Vertical Gradient Freeze method (VGF) was the first process which reported[13] (in 1986) the growth of large diameter ultra low defect density InP. The essential growth vessel is illustrated in figure 1.6.

A phosphorus over-pressure is maintained by having phosphorus heated by a lower zone heater. The stoichiometry is controlled by regulating the partial pressure of P over the melt. The upper zone heater heats the InP and this controls solidification and
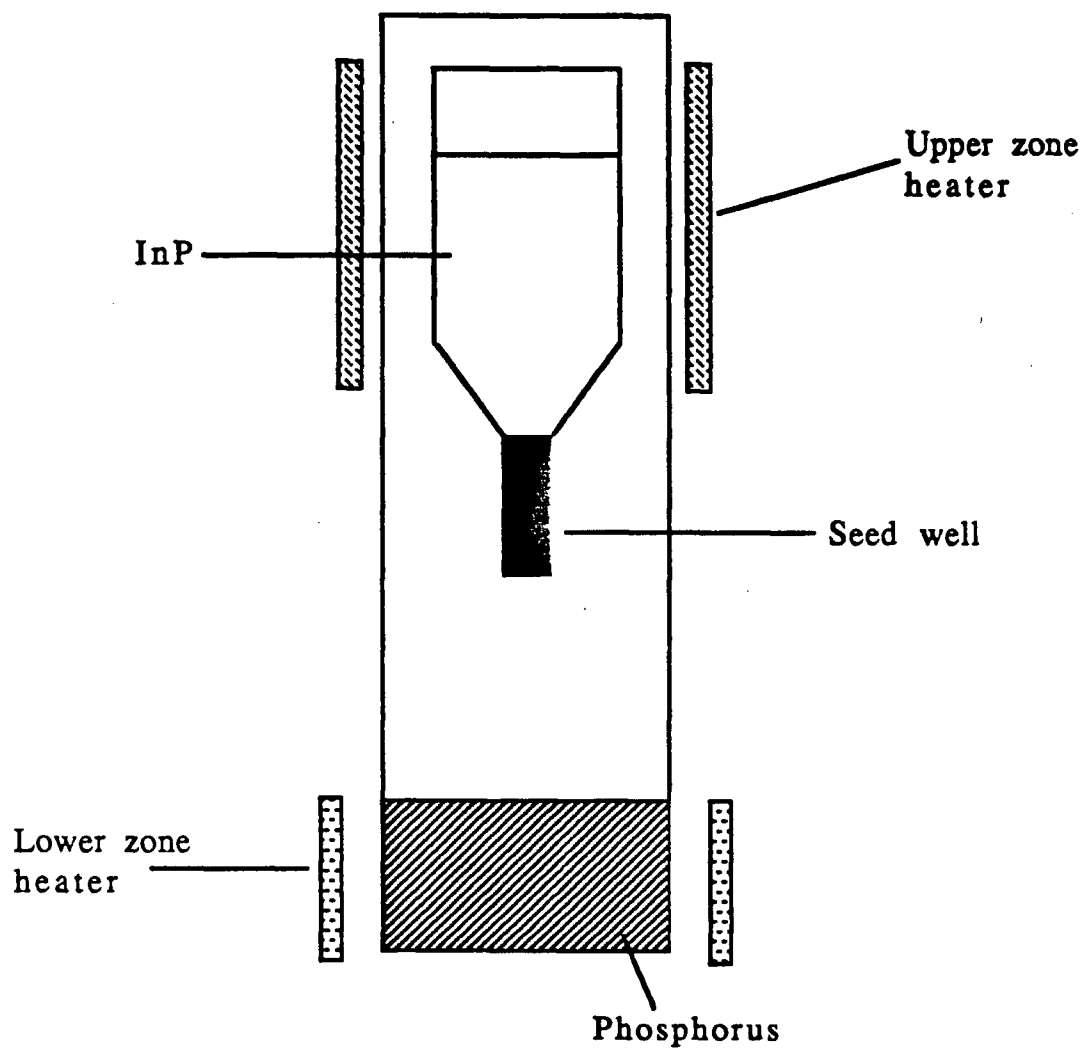
Figure 1.6.  Schematic of the growth vessel for VGF.

heat transfer during crystal growth. It is selected to melt the entire polycrystalline charge and the top portion of the seed. After a steady state has been achieved the upper zone is programmed to produce a cooling rate resulting in a growth rate of approximately 3mm/h. High quality wafers, with diameters over 2 inches, have been produced using this method.

### 1.6 Basic Wafer Fabrication

Once the ingot has been produced from the melt, it is sliced into wafers and the surface quality then improved by polishing. Next the imaging process is begun. Figure 1.7 gives a brief outline of how semiconductors are patterned.

Pretreatment of the wafer is the first step which involves mechanical and chemical cleaning as well as a short baking period. The wafer is now ready to be coated with photoresist. This is usually applied by spin coating which consists of a puddle of resist being dropped on to the substrate which is then spun around. Solvent is removed by softbaking whereby infrared, conduction and microwave heating is used to drive away the solvent and render the resist sensitive to radiation. The goal of exposure is to create a latent image of a desired pattern in the resist film with the mask being a passive tool that gives the resist its latent image. The substrate is either blanket exposed, step and repeat exposed, or scanned by a beam of radiation, see figure 1.8. In all cases, the result is an image closely matching the pattern of the photomask that has been laid down. One way of doing this is by repeatedly generating the reticle
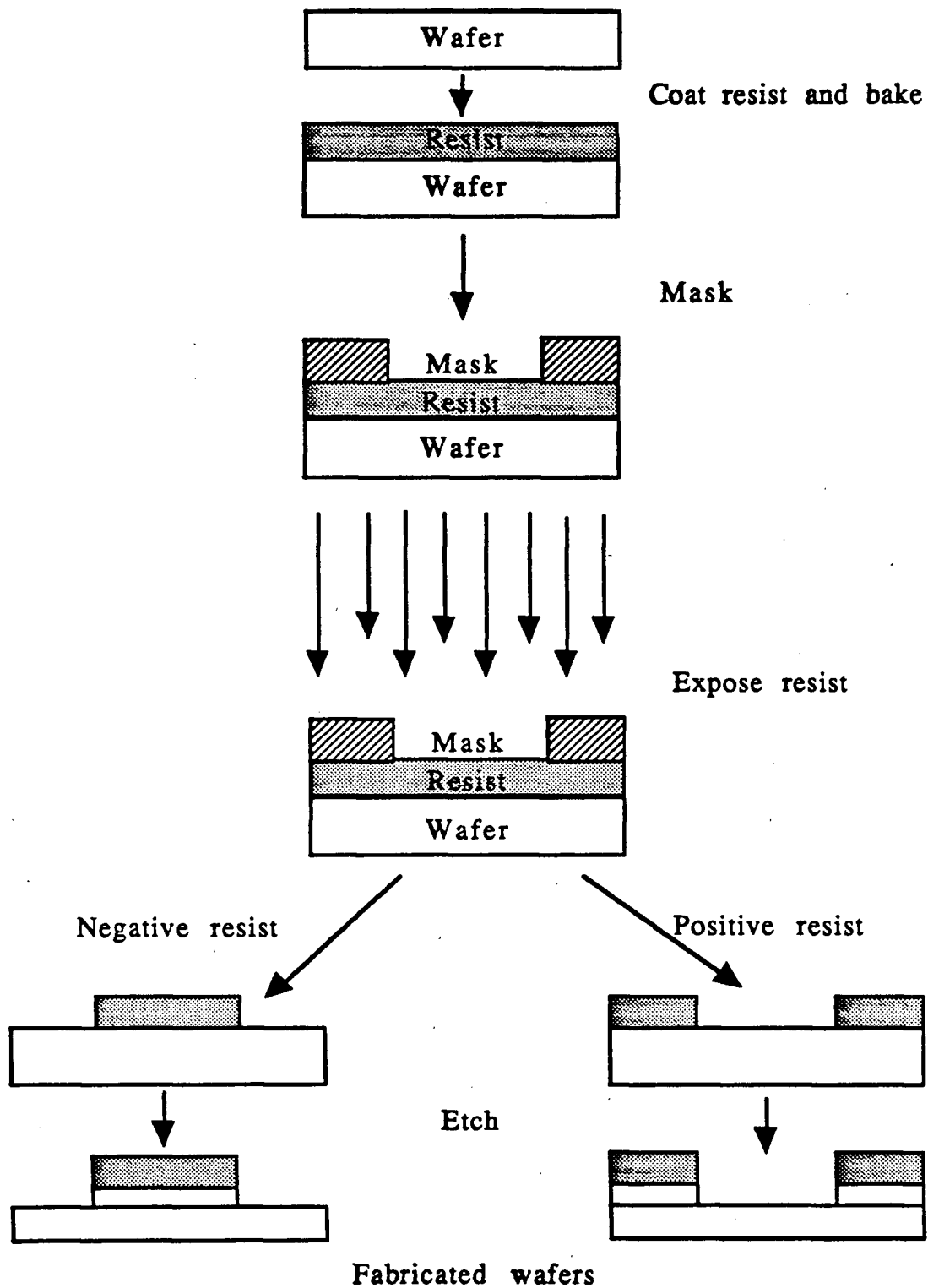
Figure 1.7. Resist imaging.

Reticle

Step - and repeat
generation of mask plate

Step - and repeat printing of
substrate from reticle
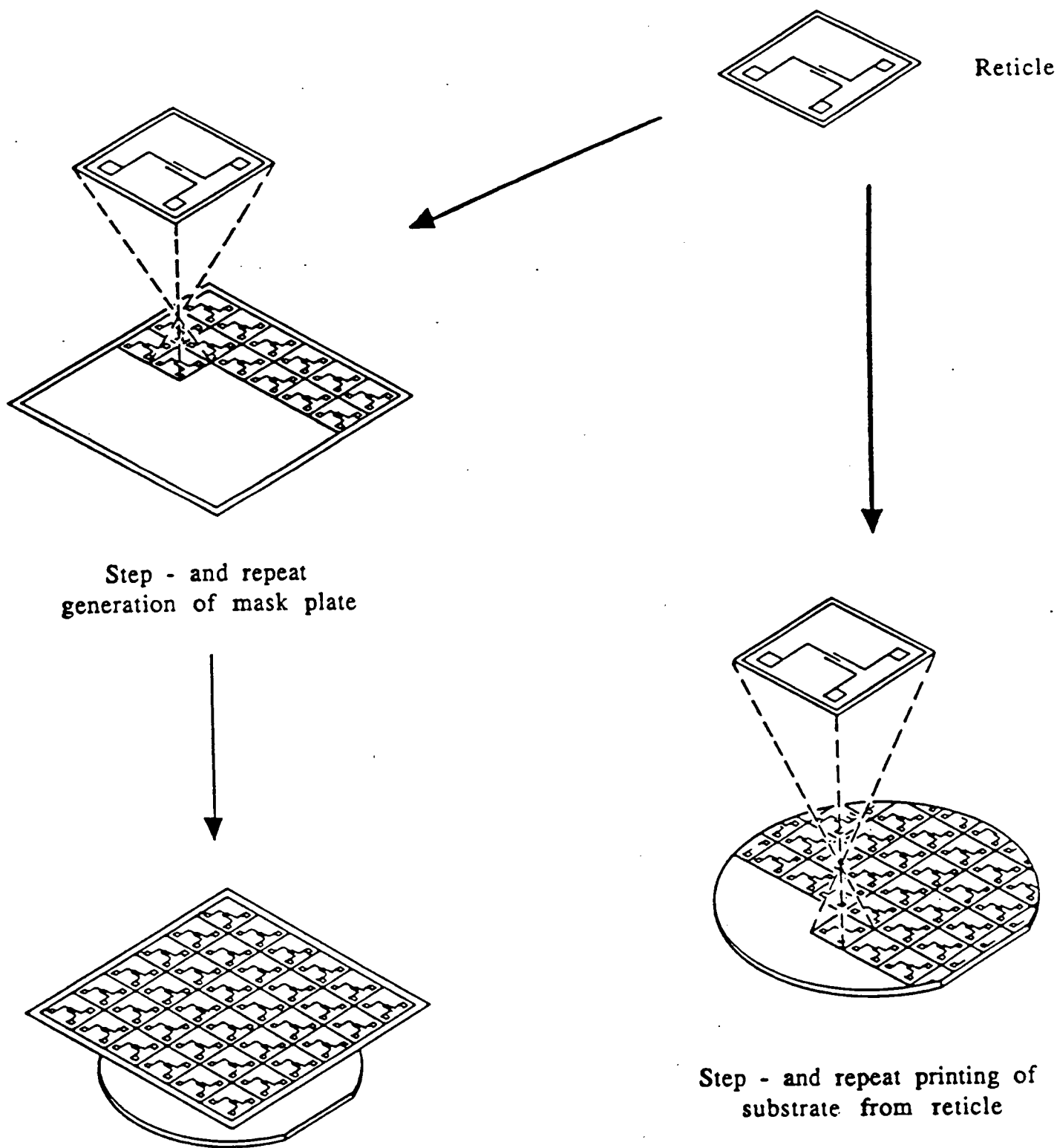
Figure 1.8.    Pattern generation.

pattern on the substrate, either directly or through an intermediate mask plate.

Developer is then sprayed over the exposed resist coating. The development process is one in which the developer selectively attacks and removes either exposed regions (positive resist) or unexposed regions (negative resist), and leaves behind the image to serve as the mask for etching purposes. Postbaking may be incorporated prior to etching in order to harden the resist further and make it chemically inert to the etchants.

The wafer is then ready to be etched with the unmasked semiconductor layer being removed. Following the etching process the resist is washed off usually by placing it in a heated resist stripping solution.

## 1.7 Etching processes

Etching has traditionally been performed using wet chemical methods, however, due to the use of thinner films and greater required control, dry methods are becoming increasingly sought after. Below follows a short discussion of wet etching and some dry etching techniques.

### 1.7.1 Wet etching

The substrate is immersed directly into a bath of etchant that attacks the semiconductor but leaves the resist or mask untouched. The reaction should, ideally, occur smoothly and be reproducible having products that are carried away from the surface quickly. The etch should also be anisotropic as shown in figure 1.9a. An
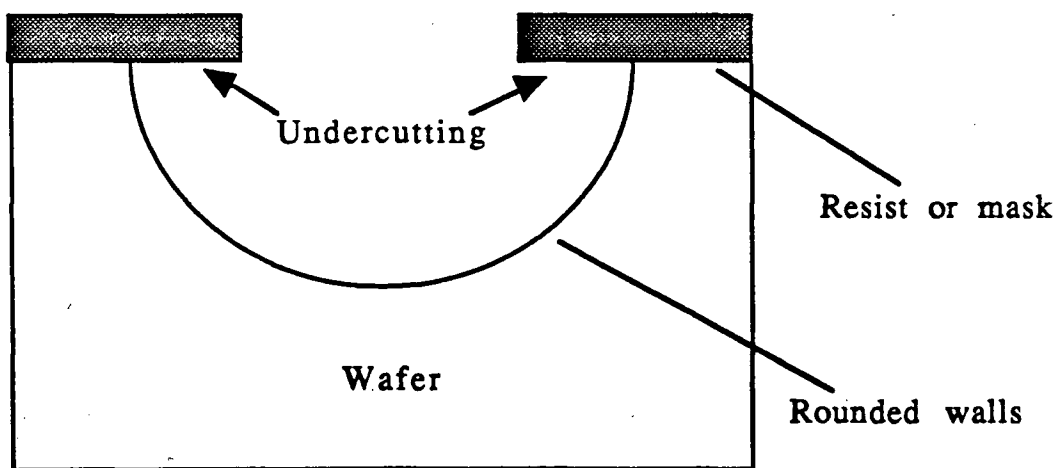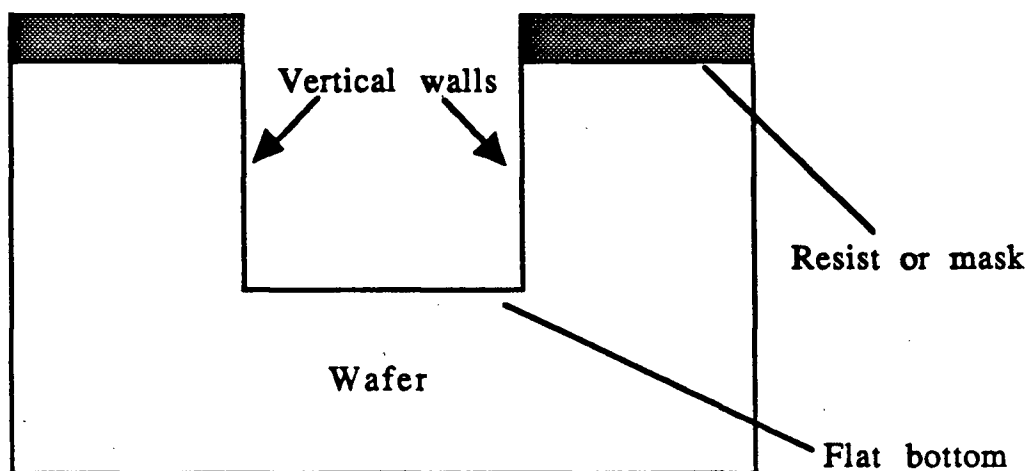
Figure 1.9 .a) Anistropic etch, note the vertical walls and flat bottom.
b) Isotropic etch, note the undercutting and rounded walls.

anisotropic etch profile is characterised by having vertical walls, a flat bottom with little or no resist erosion and an etched area not extending beyond the openings of the resist or mask. Consequently an accurate pattern transfer results.

If the etching does not occur very much faster in the vertical direction, as opposed to laterally, isotropic etching results as in figure 1.9b. Isotropic etching is associated with round walls, a curved bottom, undercutting and resist erosion.

The basic control parameters for wet etching are; concentration of reactants, reaction time, temperature and the amount of agitation. Unfortunately, most wet etching produces isotropic etches with some undercutting, pattern distortion and subsequently ill-defined surfaces with poor etch depth control. This has resulted in dry etching techniques being pursued in order to obtain better control.

### 1.7.2 Dry Etching

As well as obtaining accurate and reproducible pattern transfer there are numerous other requirements for dry etching processes. Production specifications mean that wafer to wafer reproducibility should be less than 3.5%[14] as well as maintaining good uniformity across the wafer, while keeping the selectivity high. Processes should be available to vary slope angles to permit controlled slope etching when required for certain devices. These requirements along with more obvious ones such as cost and safety must all be reached in order to make the technique feasible. Some of the more common dry etching techniques presently used are described below.

### 1.7.3 Sputter and ion beam etching

The sputtering process is typically run in a vacuum chamber in which a plasma is created by breaking down a heavy noble gas, such as argon, at $10^{-3}$ Torr. Two electrodes are set up and electrons are passed between them causing ionisation of the gas molecules. The electrons and positive ions are accelerated towards opposite electrodes and create ion bombardment on the electrode surface. An avalanche effect is created as more collisions occur. The wafer which is mounted on the cathode is sputtered and the surface removal by momentum transfer occurs, with the by products scattered towards the anode.

Sputter etch rates are fairly consistent for most materials, being in the 0.1 - 0.5 $\mu$m/min range. Very thick resist layers have to be used since removal rates for the resist and film are very similar, thus equal thickness' of resist and film are etched, subsequently its applications are limited by its poor selectivity. However, a high degree of anisotropy is possible since the ions arrive perpendicular to the surface.

Ion beam etching is a similar technique whereby high energy ions are directed towards a solid. Again anisotropy is very good. Unfortunately, high temperatures result causing the resists to flow and also making their removal difficult, thus limiting the use of this method.

### 1.7.4 Reactive ion etching (RIE)

Reactive ion etching involves both chemical reaction and physical sputtering. The ions formed are usually highly reactive and

20

are formed in an electric field at low pressure. They are subsequently accelerated to the substrate where they displace atoms through two processes; physical displacement and chemical reactions forming volatile by-products. RIE is highly anisotropic and good sidewall etch angle control is achieved. The process may be carried out at less than 0.1 Torr .

### 1.7.5 Reactive ion beam etching (RIBE)

RIBE works on the principle of an ionised beam created by the introduction of gas that will generate a reactive beam. A typical system might be as shown in figure 1.10. The reactive ions are produced in the plasma that is generated and are removed from the plasma by grids at a potential of between 500 - 1000 V. The highly energetic and reactive ions are directed, as a uniform beam, perpendicular to the wafer to provide anisotropic etching. RIBE is based on a combination of chemical and physical reactions; the gas composition is responsible for volatilizing the semiconductor, while leaving the resist or mask unaffected. The amount of gas used needs to be controlled in order to produce uniform results, and the power of the beam requires optimizing so that a sufficient etch rate is produced while maintaining adequate etch selectivity.

### 1.7.6 Plasma Etching

Plasma etching usually occurs at low pressure in the 0.01 - 1 Torr range. An electrical discharge generates reactive radicals and ions from the gas although the extent of ionisation is small. The first
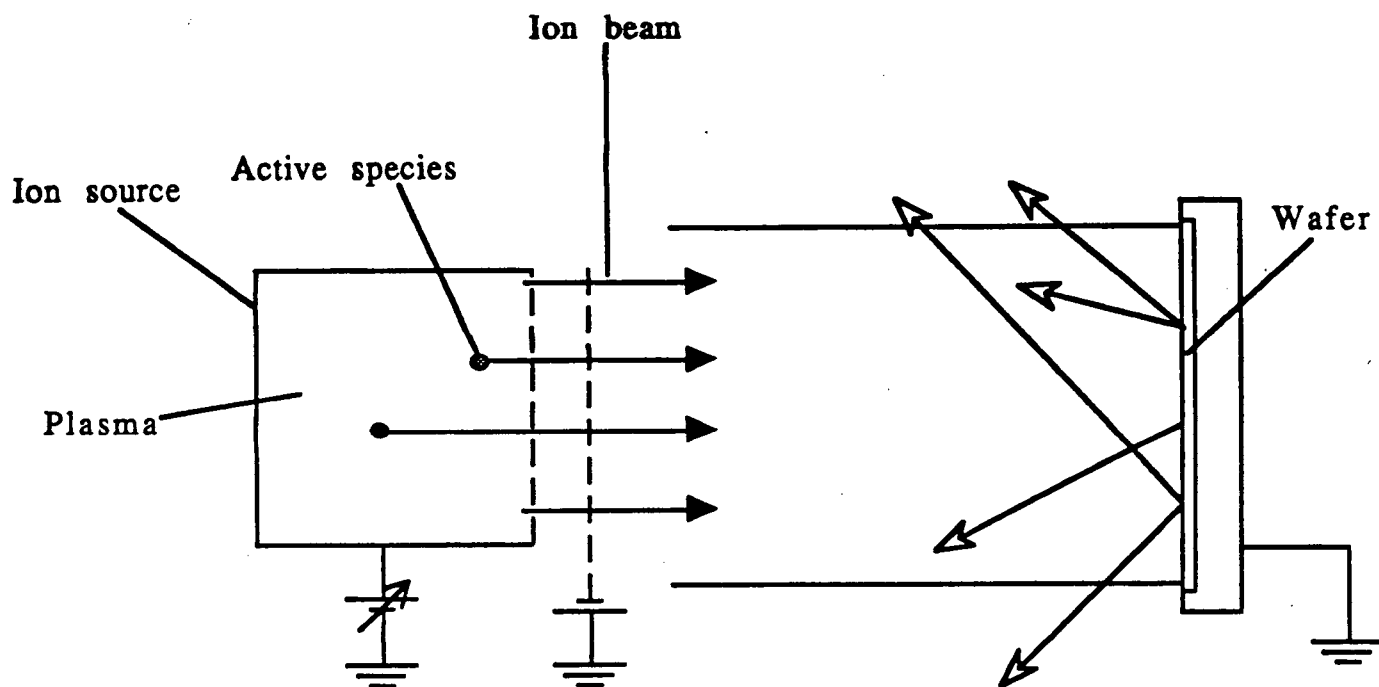
Figure 1.10.  Simple apparatus for reactive ion beam etching.

type of plasma etching equipment commonly used was based upon a barrel reactor, see figure 1.11. There is little control with this system as the rate of reaction alters with the changing temperature which results from heating by the plasma. Uniformity of etch is difficult to achieve. Subsequently a planar reactor was developed as illustrated in figure 1.12. A certain degree of temperature control is obtained by heating or cooling the lower electrode and uniformity of etch is improved by using a radial gas flow.

In both of the above techniques the semiconductor substrates are immersed in the plasma where energetic charged species impinge. While ion bombardment may be part of the reaction chemistry it also can sputter-deposit material from the reactor and cause device degradation by inducing chemical or structural changes. This is avoided if the wafers are placed downstream of the discharge and the gas is pumped over the wafers. Unfortunately, due to the short lifetimes of these species they usually cannot travel very far before recombination occurs.

## 1.8 Previous Work

Much work has been undertaken on etching InP by various methods, mostly involving halogens or halogenated mixtures which have been demonstrated to be efficient etchants[15,16,17,18]. Unfortunately, such processes involving halogen containing plasmas entail safety risks, corrosion of the vacuum system and highly variable results for the III - V compounds[19].
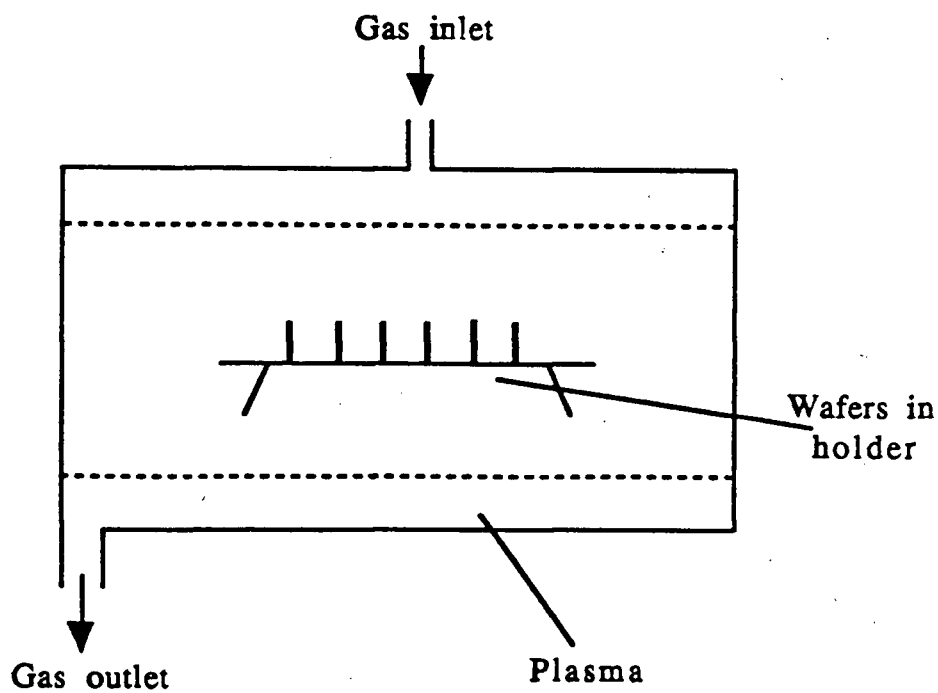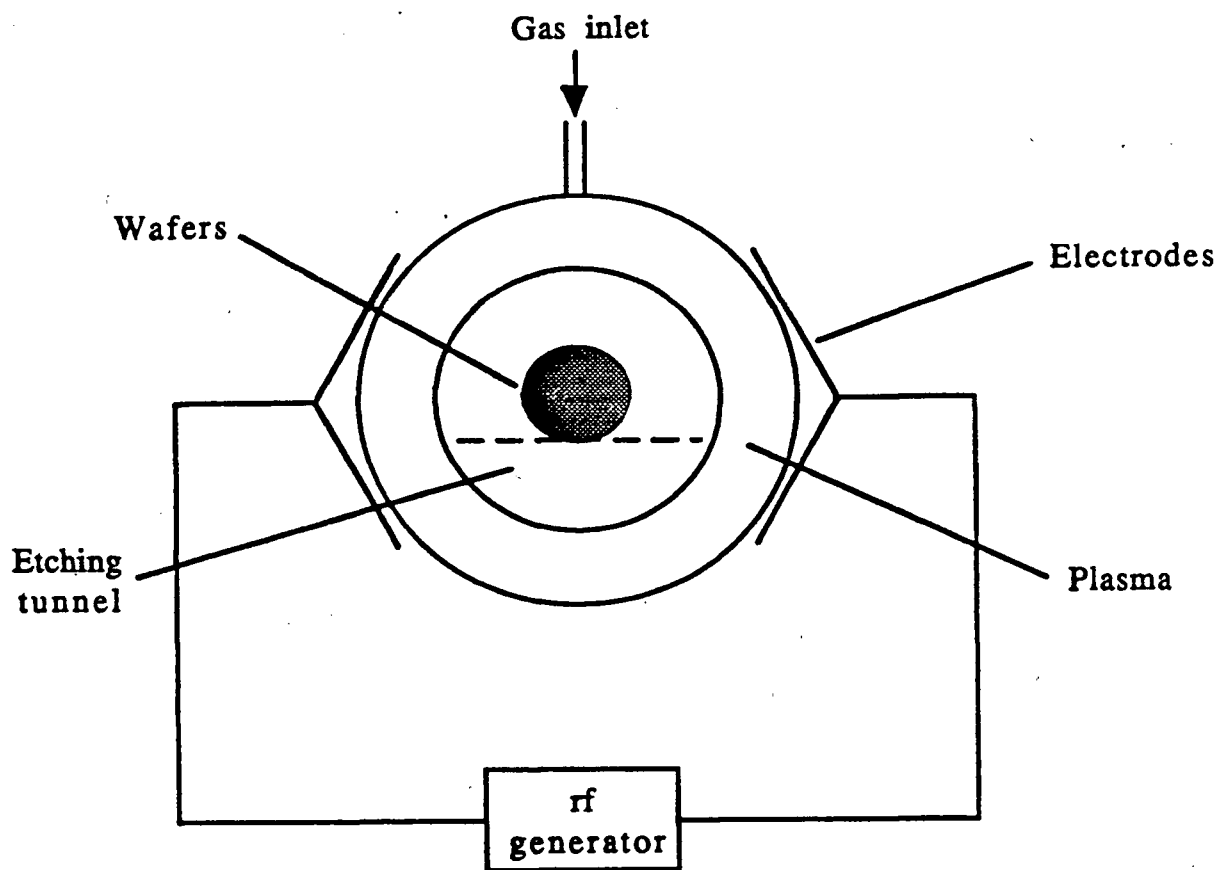
Figure 1.11. a) End view of a barrel reactor. b) side view.
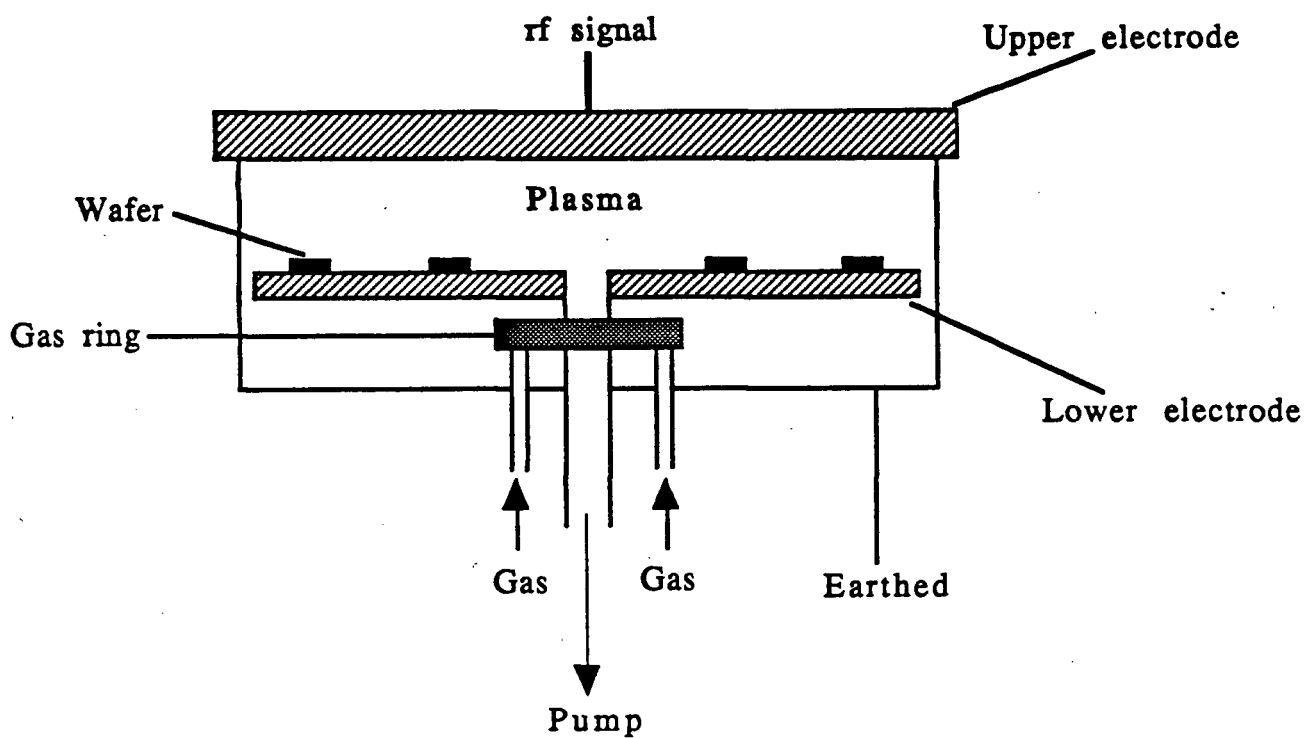
Figure 1.12.    Planar plasma reactor.

Consequently, by 1982 research had already started on hydrogen plasma etching under Chang et al[20]. A barrel plasma reactor was used, providing a high hydrogen atom concentration, but poor temperature control. Etching of both InP and its oxide were found to occur although an etch rate was not given. After prolonged etching the surface appeared very rough due to some form of segregation which left the surface indium rich. Both uniformity and repeatability were said to be poor. In a later paper Chang et al[21] used mass spectroscopy to detect the products of the reaction and found phosphorus hydrides formed.

A subsequent paper by Tu[22] observed that at low microwave power phosphorus was removed up to a depth of 0.8 nm at room temperature before reaction stopped. At much higher power levels the etch continued and left an indium rich surface, unfortunately the temperature control at higher power levels was not as good. The excess indium on the surface was found to rapidly oxidise even at $10^{-6}$ Torr due to residual water vapour.

Ethylene dibromide (EDB) was reacted with InP[23] using a two zone heated furnace. The InP was located at the lower temperature end (120 - 540 °C) while the hot zone was maintained between 600 - 900 °C to decompose the EDB which yielded a more reactive species. Etching was achieved with an etch rate between 0.002 - 1.0 $\mu$m/min. In the range 240 - 300 °C the surface morphology was said to improve.

RIE using a $CH_4/H_2$ mixture in argon was performed by Niggebrugge et al in 1985[24]. This produced a smooth etch which was attributed mainly to chemical etching by $CH_4$ from the fact that when

CH$_4$ was replaced by Ar (which is known to sputter) the etch rate decreased and the surface morphology degraded. When H$_2$ was used alone no reaction was observed to occur, although little information as to the conditions used were given. A steady increase in the etch rate was achieved as the ratio of CH$_4$/H$_2$ was increased up to 1 : 5 whereupon polymer formation inhibited the reaction. Doughty et al[25] obtained an etch rate of 70 nm/min via RIE with CH$_3$I and polymer formation was suggested as the cause of the surface roughness. It was also reported that ion beam assisted etching of InP with an I$_2$/Ar mixture provided anisotropic etching although the etch rate was very small when I$_2$ predominated in the mixture. This would tend to indicate a sputtering process. The temperature was below 40 °C and the pressure was 0.001 Torr. It was proposed that I$_2$ was the etchant.

Henry[26] performed a similar experiment to Niggebrugge who observed an etch rate of 70 nm/min with a CH$_4$/H$_2$ mixture, however, the temperature of the reaction was not stated. Matsui[27] reported similar etch rates of 20 - 60 nm/min for RIE of a C$_2$H$_6$/H$_2$ mixture.

InP was etched by RIE in a 10% CH$_4$/H$_2$ gas mixture by Roberts et al[28] where it was thought that ion bombardment played an important role in the etching. XPS confirmed a surface deficiency in P.

### 1.9 Purpose of study

The study was conducted to investigate the dry etching of InP with H atoms and CH$_3$ radicals by etching downstream of the discharge. This eliminates any mechanism due to physical sputtering

and purely chemical etching can then be studied. It was proposed to establish the nature of the etchant species and to examine the process in order to provide a suitable alternative to etch InP other than with a Cl based etchant.

## 2 Experimental

### 2.1 Materials

The hydrogen used was obtained from Linde. It was extra dry having a minimum purity of 99.95%. The major contaminants were oxygen (10ppm) and moisture (10ppm). The methane used was supplied by Matheson Gas Products and was Ultra Pure (>99.99%).

The gas cylinders were connected to the flow system with copper tubing of 1/4" diameter. Connections to and in this tubing were made with Cajon Ultra-torr fittings. A constant "over pressure" of approximately 10 p.s.i was maintained in the delivery system using Matheson two-stage high purity regulators with stainless steel diaphragms. All gas delivery lines were purged with their respective gases before each set of experiments.

The iodomethane used was obtained from BDH Chemicals as was the phosphoric acid which was used to coat the glass walls in the discharge region to prevent recombination of atoms.

The indium phosphide sample was in the form of a multilayer wafer. It was supplied by Bell Northern Research and was fabricated using a metal-organic chemical vapour deposition (MOCVD) process the crystal face being <100>. Its structure is illustrated in figure 2.1,
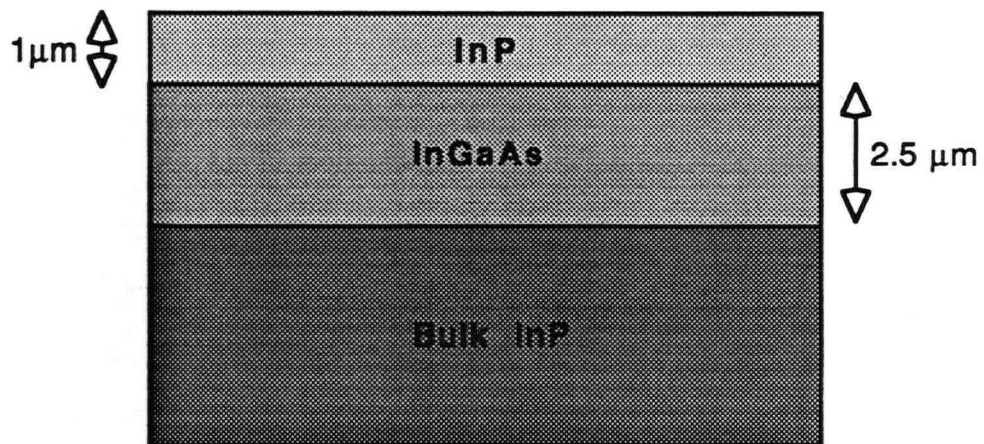
Figure 2.1. The composition of the sample wafer.

the top layer of InP was doped with $5 \times 10^{16}$ atoms/cm$^3$ Si and the composition of the second layer was In$_{0.53}$Ga$_{0.47}$As.

## 2.2 Apparatus

The apparatus was designed to obtain a fast flow of hydrogen atoms over the sample and through to the atom flow detector. Atoms were produced via a microwave discharge with the sample being located 15 cm downstream of the plasma. The extent of the reaction was monitored by two techniques, interferometry and profilometry, which will be discussed later. The major components of the apparatus are illustrated schematically in figures 2.2 and 2.3.

### 2.2.1 Flow System

The flow system starts with the hydrogen inlet line connected via a needle valve to 1/4" steel tubing. This leads to the major part of the flow system which is of pyrex and is connected by a Cajon O-ring fitting. The discharge area is followed by a light trap and then an inlet for the iodomethane which is connected by a needle valve to the iodomethane reservoir.

The sample holder is located inside 0.37" pyrex tubing which is surrounded by heating tape. Further down this tube is the atom probe and then a Cajon O ring fitting to 1/2" steel tubing. The flow system is completed by an Alcatel Molecular Drag Pump (5010) which is also backed by a Sargent -Welch two stage Duo-seal rotary vacuum pump. The vacuum pump was connected to the flow system with a small length of heavy walled rubber tubing, this helped prevent vibrations from the pump being transferred to the rest of
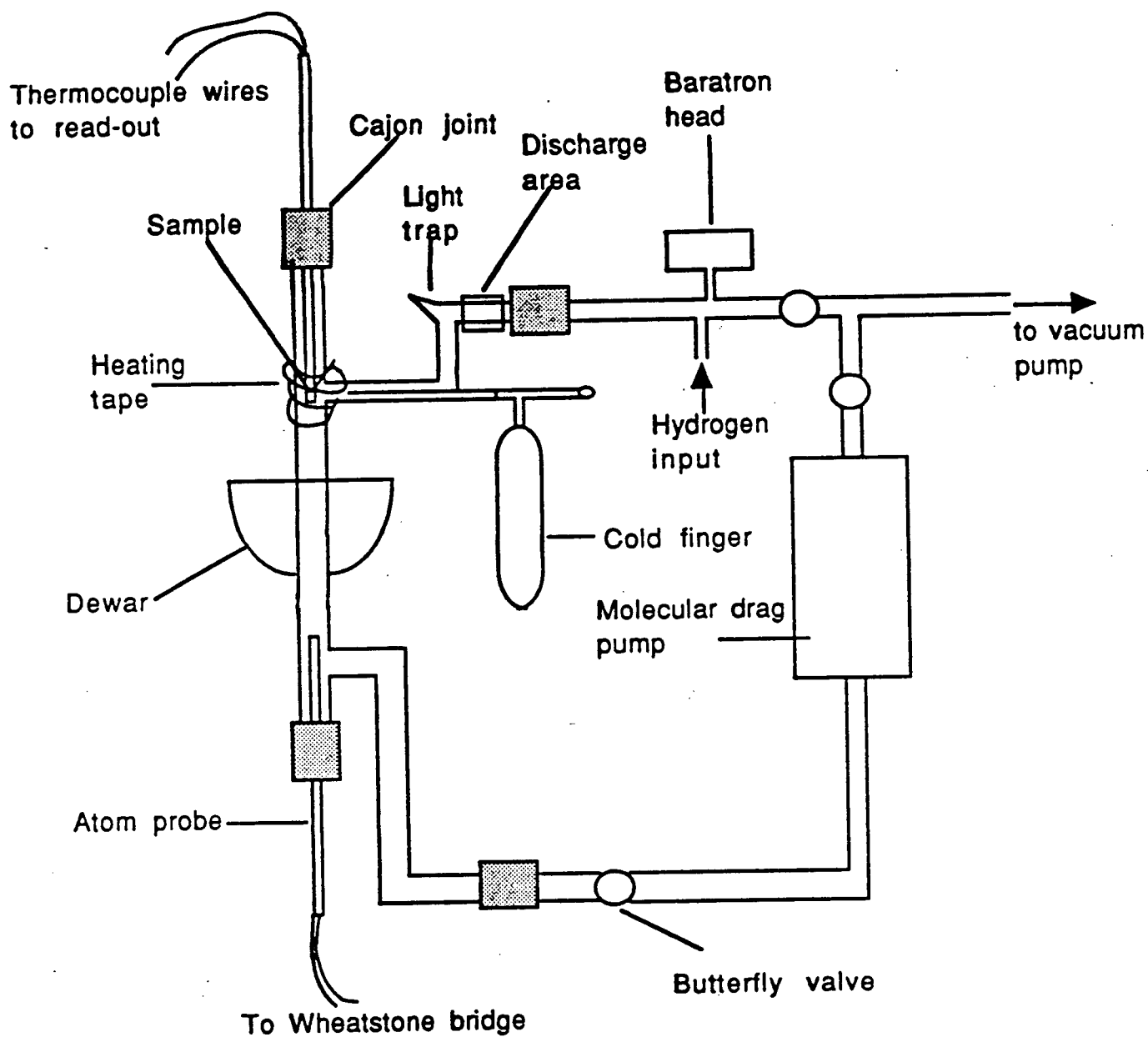
Figure 2.2. Flow system.

31
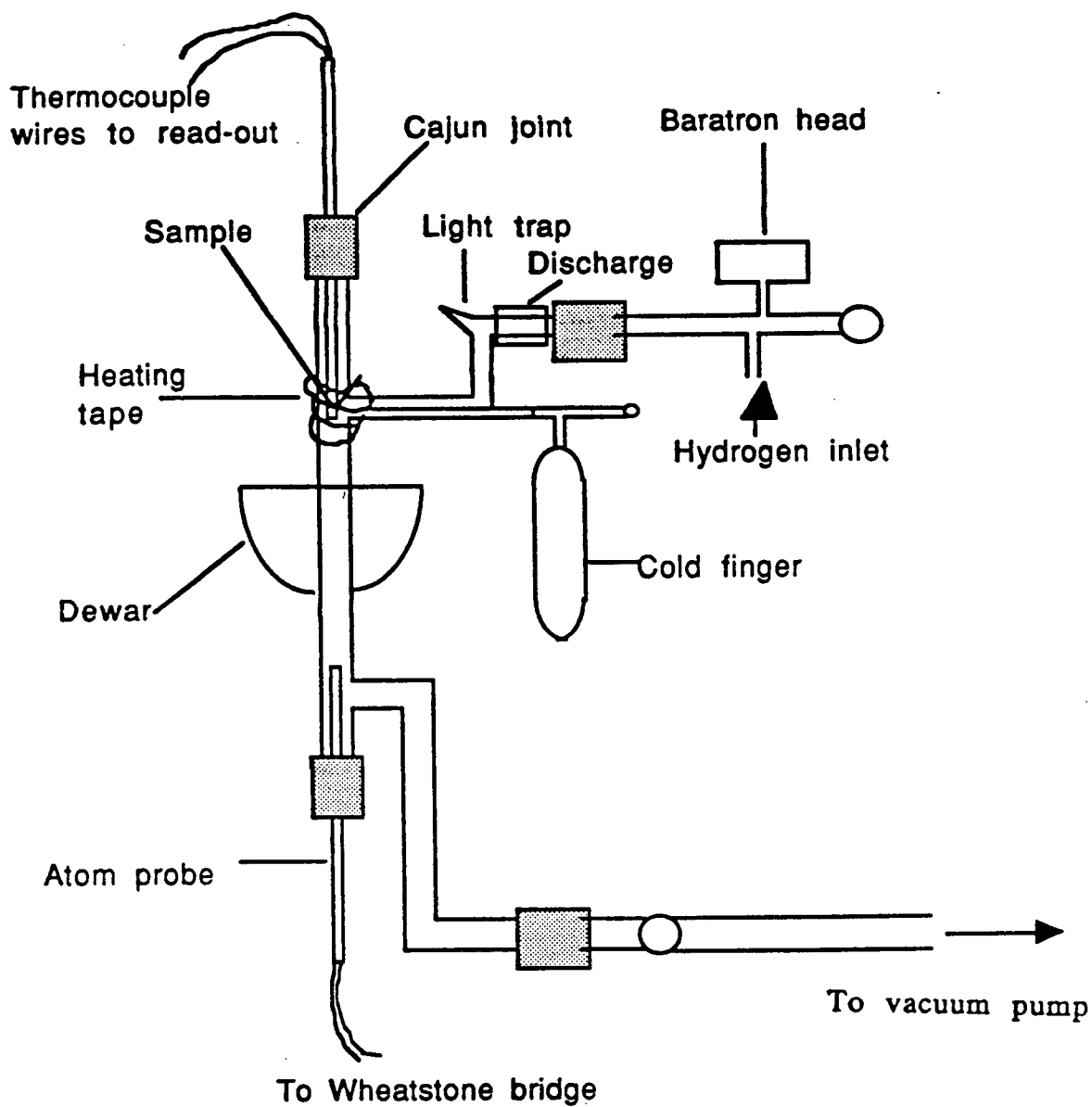
Figure 2.3. Slow flow system.

the apparatus. The pressure is measured by an MKS pressure transducer (type 122A) with a range of 10 Torr and is located opposite the hydrogen inlet. The transducer is connected to either a chart recorder or digital readout.

The discharge area consists of a standard 2.5 GHz coaxial cavity housed over the glass tubing. Microwaves are produced with an E.M.I. Microtron 200 (30-200W) unit, and coupled to the discharge tube with a quarter wave cavity that was tuned (with a reflected power meter) to reduce the reflected power to 5 - 10 %.

For some of the experiments the system shown in figure 2.3 was used. This did not include the molecular drag pump and consequently provided smaller flow rates.

### 2.2.2 Sample Holder

The sample probe consists of a 9mm (O.D) capillary tube with one end shaved away as shown in figure 2.4. A silicon wafer, which acts as a heat sink, was fixed to the glass using a high temperature epoxy cement while also incorporating a thermocouple to the underside of the Si. As the sample holder enters the system vertically two 'glass springs' were required to hold the InP sample in place. The sample was masked by sandwiching the InP wafer between the Si heat sink and a smaller Si wafer on top. The opposite end of the holder was sealed with epoxy.

Later it was found necessary to alter the sample holder as the temperature recorded did not appear to be that of the wafer surface. In order to obtain a more accurate measure of the substrate temperature the thermocouple was fixed with epoxy directly to the

Glass springs

Thermocouple
point

Silicon wafer
as mask

Silicon wafer

Indium Phosphide
sample

Capillary
tube

Torr
sealed
end

To thermocouple readout
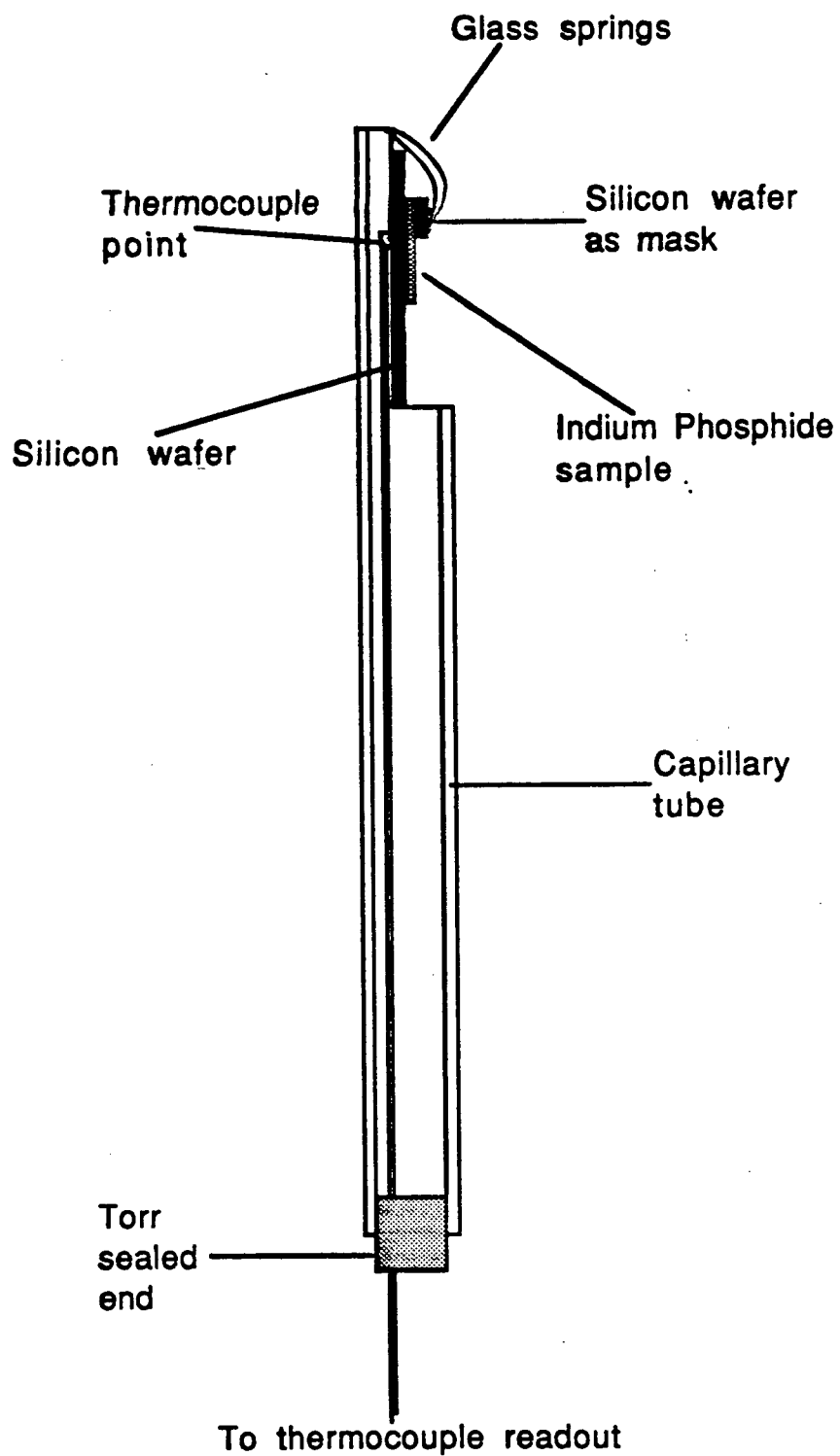
Figure 2.4. Sample probe.

back of the sample, ensuring that there was very little Torr - seal in between to impair thermal contact.

### 2.2.3 Laser Interferometry

The extent of the etch was monitored by laser interferometry. A 0.5 mW HeNe continuous wave laser (632.8 nm) was aligned perpendicular to the sample surface. The laser beam was reflected off the surface to a photodiode connected to a chart recorder via an adjustable amplifier. The photodiode was positioned directly on top of the HeNe laser trying to minimise the angles of incidence and reflection.

Interference between the radiation reflected from the InGaAs layer and that reflected from the etching surface produced a sinusoidal intensity as a function of time. The relationship between etch rate and peak period is as follows (see Appendix A);

$$\text{Etch Rate} = (\lambda/2\eta).1/t \qquad \text{nm/min}$$

where;

$\lambda$ = wavelength of radiation (632.8 nm),

t = time between peaks (mins),

$\eta$ = refractive index of InP (3.16).

## 2.2.4 <u>Isothermal calorimetric detection (ICD) of hydrogen atoms</u>

The technique used to determine the flow of hydrogen atoms present in the system was based upon initial work by Bonhoeffer[29] which has since then been developed further by Le Roy[30].

A coil of platinum wire attached to a glass probe (figure 2.5) is inserted into the system at the appropriate position (see diagram of system). Hydrogen is passed through the system with the discharge on and is partially dissociated. As the atoms pass over the spiral of platinum they recombine and heat the coil, thus raising its resistance. A current, $i_1$ is simultaeously passed through the wire and the resistance of the platinum is measured using a Wheatstone bridge. With the discharge off and the flow of hydrogen unchanged the current is increased to a value, $i_o$ so that the bridge is again balanced and the resistance (and therefore temperature) of the platinum wire are restored to its initial value. The electronic circuitry for the Wheatstone bridge set up is illustrated in Appendix C.

The atom flow can be calculated from the following;

$$\text{Atom flow} = \Delta(i^2)R/(4.18D/2) \quad \text{moles/second}$$

where,

$\Delta(i^2) = i_o^2 - i_1^2$

R = resistance of platinum ($\Omega$)

D = dissociation energy of bond formed (cal/mole)

4.18 = conversion factor of power to heat ($s^{-1}$)

Torr sealed end

Steel rods

Pt wire

Glass tube

Torr sealed end

To Wheatstone bridge
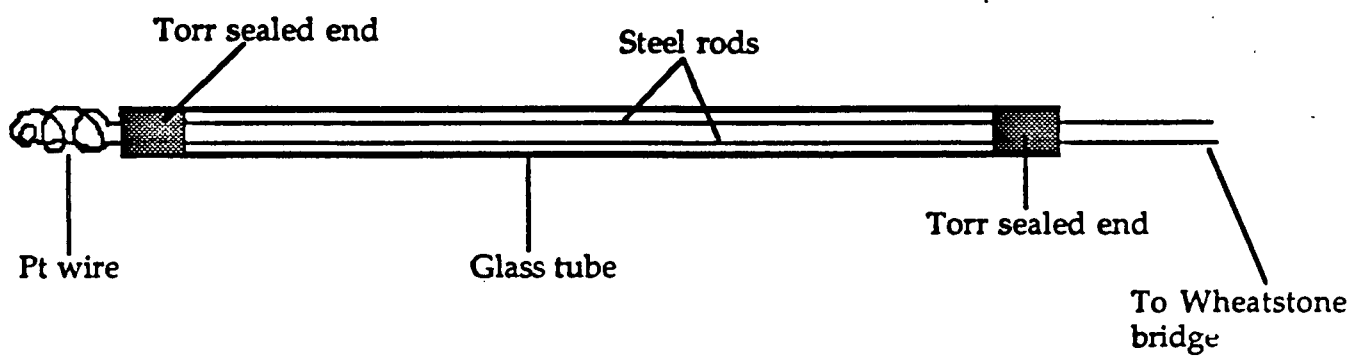
Figure 2.5.  ICD probe.

## 2.3  General Procedure

Hydrogen was flowed through the system past the baratron head and into the discharge area which had been coated with phosphoric acid. This had been baked to convert it to $P_2O_5$ by removing most of the water. The hydrogen and hydrogen atoms, produced by the discharge, flow over the wafer and sample holder. The sample was externally heated using heating tape around the glass walls and a thermocouple attached to the probe recorded the sample temperature.

The sample was heated to the required temperature under a small flow of hydrogen to prevent any oxidation. When the sample reached a steady temperature, the pressure of hydrogen was set by altering the flow and the discharge was started. Depending upon the initial temperature of the wafer, recombination of hydrogen atoms on the probe increased the temperature. At 300°C this heating effect was not detectable.

The hydrogen atoms were measured by balancing the bridge with the discharge on and then re-balancing later, at the same flow, with the discharge extinguished.

Iodomethane ( $CH_3I$ ) was pumped on before each run while solidified under liquid nitrogen. The tube was then sealed off and warmed to room temperature using a heat gun. The methyl radical flow could be calculated by assuming a 1:1 reaction with hydrogen atoms under excess $CH_3I$, having previously measured the atom flow. The major reaction expected was,

$$CH_3I_{(g)} + H_{(g)} = HI_{(g)} + CH_{3(g)} \quad k = 10^{10} \text{ l.mol}^{-1}.\text{s}^{-1}.$$

This seemed reasonable[31,32] since the $CH_3$ recombination reaction would be small due to the very small partial pressure of $CH_3$ present. The reaction is given below and is written as being bimolecular. At the

$$2CH_{3(g)} = C_2H_{6(g)} \quad k = 2 \times 10^9 \text{ l.mol}^{-1}.\text{s}^{-1}.$$
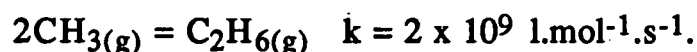
pressures used it is likely that this reaction is actually termolecular requiring the presence of a third body, this would also reduce the extent of the recombination compared with the formation of $CH_3$.

The abstraction of a H from $CH_3$, and the addition of one to form methane would both be limited at the temperatures and partial

$$CH_{3(g)} + H_{(g)} = H_{2(g)} + CH_{2(g)} \quad k = 10^8/10^9 \text{ l.mol}^{-1}.\text{s}^{-1}.$$

$$CH_{3(g)} + H_{(g)} = CH_{4(g)} \quad k = 10^{10} \text{ l.mol}^{-1}.\text{s}^{-1}.$$
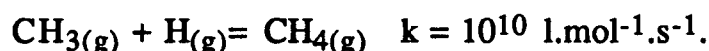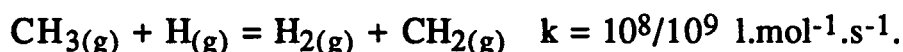
pressures used in the study. The later may also require the presence of a third body for the reaction to occur.

The $CH_3I$ flow was controlled using a fine needle valve and pressure changes noted. Excess $CH_3I$ was trapped out using a dry ice/acetone mixture in the dewar.

The glass system was cleaned periodically using hot concentrated potassium hydroxide, washed with distilled water and very dilute phosphoric acid. It was observed that surface recombination losses on the phosphoric acid coated surfaces were small and that hydrogen atoms could be pumped for considerable distances from the discharge region[33].


## 2.4 Methods Of Analysis

Several methods were used to examine the etched surfaces. Interferometry was performed concurrently with the etch

experiments and was the primary method used for following the reactions. However, profilometry was also used on a majority of the samples as this could be used to verify any etch rates obtained via interferometry. Profilometry also gave an insight into the surface roughness of the etched wafer.

The composition of the samples was determined using X-Ray Photoelectron Spectroscopy (XPS) and the surface morphology was examined by Scanning Electron Microscopy (SEM). These methods are described briefly below.

### 2.4.1 Profilometry

As part of the surface of each sample was masked by a small wafer of Si, thus providing a reference of height, it was possible to examine the etched surface by profilometry. Each surface was scanned twice by a Tencor alpha-step 200 profilometer whereby a small stylus is passed across the surface recording the depth. The etch depth, and consequently, etch rate could be calculated and the surface roughness of each sample examined. The length of sample scanned by the stylus was 400 $\mu$m, this being from across the masked to the etched areas.

### 2.4.2 S.E.M

The S.E.M uses a very fine, narrow beam of electrons ~40 Å in diameter, to scan the surface of a sample and generate secondary electrons. These are accelerated by a positive voltage over to the electron detector, see figure 2.6.
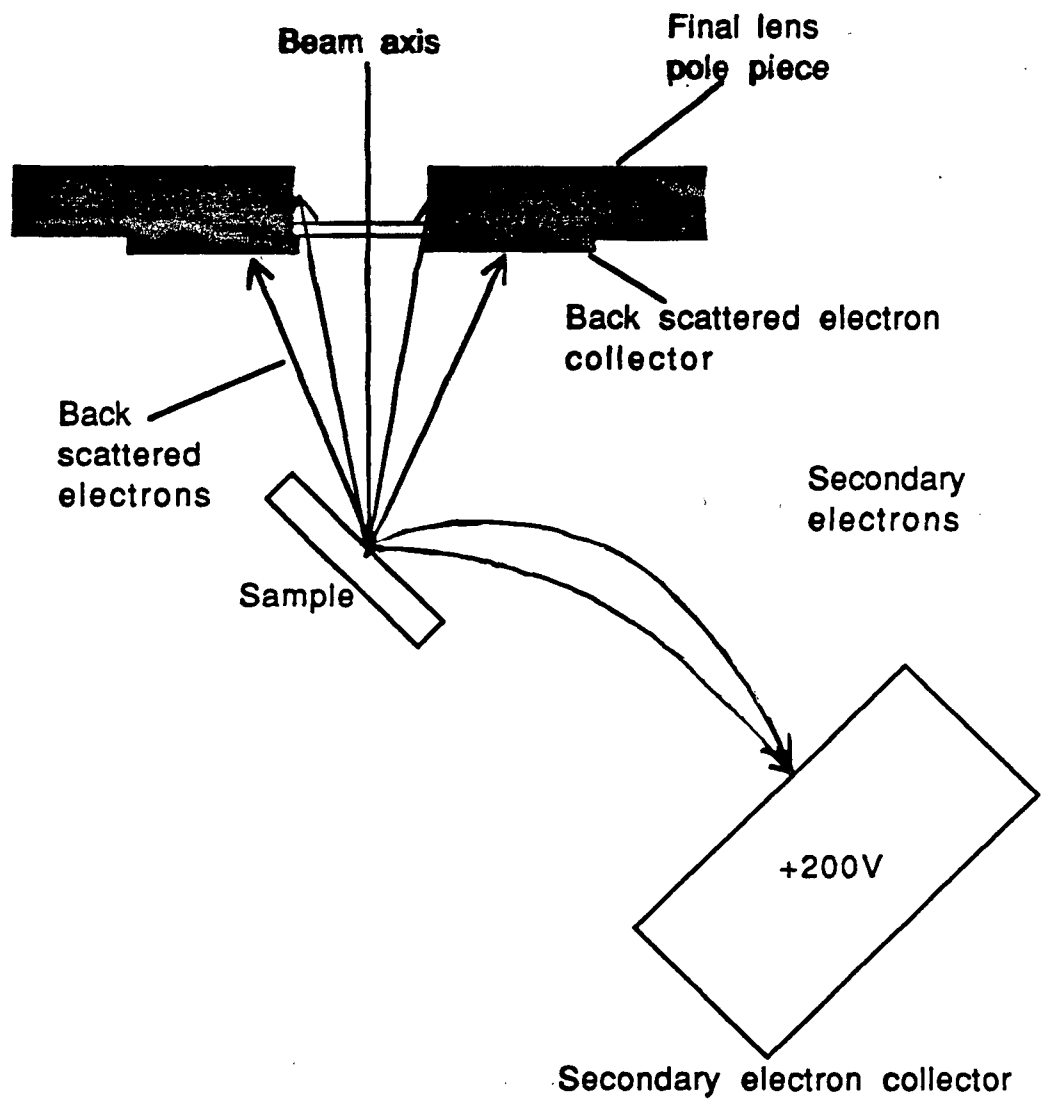
Figure 2.6. Detection system for S.E.M. The secondary electrons produced near the surface of the sample by the impact of the primary beam and by the back scattered electrons, have less energy and are readily attracted to a collector held about 200 volts positive with respect to ground.

The configuration of the detector prevents most of the high-energy back scattered electrons from entering the detector, since they have a much poorer resolution than the secondary electrons. The S.E.M used in these studies was a Hitachi S-570. The operating voltage was 20 kV with a back-scattered resolution of about 0.7 μm and an x-ray resolution of 1 μm. The secondary electron resolution is 25 Å to 100 Å depending upon beam diameter.

The signal from the photomultiplier is scanned onto the cathode ray tube synchronously with the scanning of the primary beam across the specimen surface, building up a surface image.

### 2.4.3 XPS

X-ray photoelectron spectroscopy was used to analyse the surface of the wafers using a Leybold Micro Area 200 XPS. This technique was chosen over EDX as it only examines a 5 nm depth of the surface compared to 100 nm by EDX. Both the masked and etched regions of the samples were examined with a spatial resolution of 200 μm.

The major peaks looked at were,

$$In \; 3p_{5/2} \quad 444 \; eV$$
$$P \; 2p \quad 130 \; eV$$
$$C \; 1s \quad 285 \; eV$$

These results were used to give surface compostions for In:P as well as identifying any possible hydrocarbon or oxide formation.

# 3 <u>Results and Discussion</u>

## 3.1 <u>Hydrogen atom flow</u>

Because the hydrogen atom flow was measured at either 4 or 11 cm downstream from the sample it was necessary to determine the loss of hydrogen atoms between the detector and the wafer. This was done for both fast and slow flow systems at the operating temperatures. It was observed that the ratio of atoms at the wafer to that at the detector was independent of the temperature although the atom concentration measured differed slightly upon altering the temperature. The presence of the sample probe was found to have a negligible effect on atom flow. Representative plots are shown in figures 3.1, 3.2 and 3.3. Consequently atom flows at the sample could be calculated from measuring the flow further downstream.

## 3.2 <u>Hydrogen molecule flow</u>

The hydrogen molecule flow rates were determined as follows. The volume of the glass system was calculated to be 203 $cm^3$. The pressure of the $H_2$ was recorded, after the glass section was isolated, with $H_2$ flowing for different initial pressures. The slope, dP/dt, was then calculated.

The flow of $H_2$ is found from;

$$dn/dt = dP/dt \cdot V/RT.$$

Tables 3.1 and 3.2 give the results for the initial starting pressures of $H_2$ at 25°C. Figure 3.4 and 3.5 show these results plotted. Figure 3.6 shows two typical chart recordings of the

43

Figure 3.1. Graph of atom flow against the position of the atom detector below the sample wafer for the fast flow system. 33W, 25°C, 0.30 Torr pressure $H_2$.

Figure 3.2. Graph of atom flow against position of the atom detector below the sample wafer for the fast flow system. 33W, 300°C, 0.30 Torr pressure $H_2$.
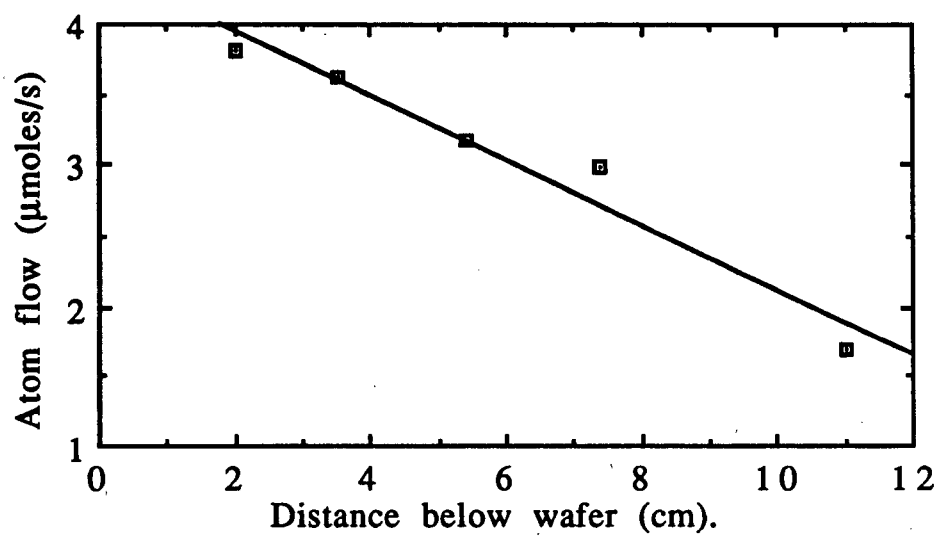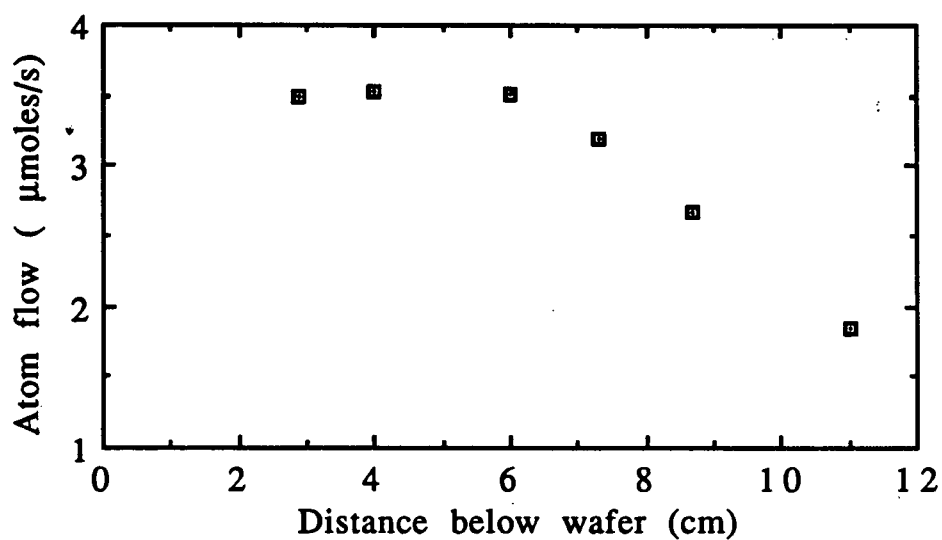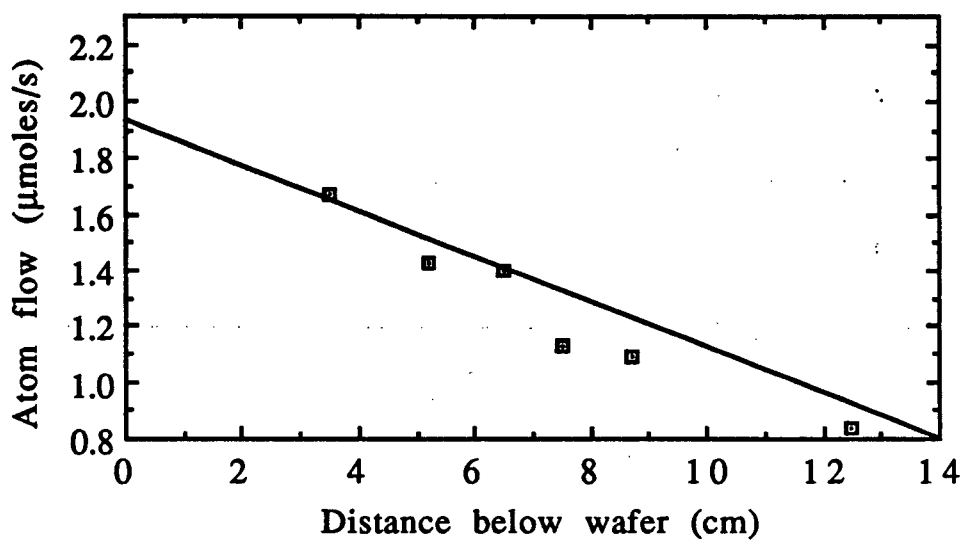
Figure 3.3. Graph of atom flow against the position of the atom detector below the sample wafer for the slow flow system. 33W, 25°C, 1.50 Torr pressure $H_2$.

Table 3.1. Flow rates of $H_2$ at various pressures for the fast flow system.

| Initial pressure (Torr) | Initial pressure (Pa) | dP/dt (Pa/min) | dn/dt x$10^{-3}$ (moles/min) |
|---|---|---|---|
| 0.10 | 13.3 | 2010 | 0.165 |
| 0.15 | 20.0 | 3449 | 0.283 |
| 0.20 | 26.7 | 5565 | 0.456 |
| 0.25 | 33.3 | 7450 | 0.610 |
| 0.30 | 40.0 | 8951 | 0.733 |
| 0.35 | 46.7 | 11272 | 0.924 |
| 0.40 | 53.3 | 12266 | 1.00 |
| 0.45 | 60.0 | 15165 | 1.24 |
| 0.50 | 66.7 | 17141 | 1.40 |
| 0.55 | 73.3 | 17999 | 1.47 |
| 0.60 | 80.0 | 20517 | 1.64 |
| 0.65 | 86.7 | 16905 | 1.39 |
| 0.70 | 93.3 | 24799 | 2.03 |
| 0.75 | 100.0 | 23491 | 1.92 |
| 0.80 | 106.7 | 27251 | 2.23 |
| 0.85 | 113.3 | 25025 | 2.05 |
| 0.90 | 120.0 | 25545 | 2.09 |

Table 3.2. Flow rates of $H_2$ at various pressures for the slow flow system.

| Initial pressure (Torr) | Initial pressure (Pa) | dP/dt (Pa/min) | dn/dt $\times 10^{-4}$ (moles/min) |
|---|---|---|---|
| 0.2 | 26.7 | 1137 | 0.90 |
| 0.3 | 40.0 | 1727 | 1.41 |
| 0.5 | 66.7 | 2619 | 2.13 |
| 0.7 | 93.3 | 4185 | 3.41 |
| 0.9 | 120.0 | 5285 | 4.30 |
| 1.1 | 146.6 | 9083 | 7.39 |
| 1.3 | 173.3 | 11888 | 9.68 |
| 1.5 | 200.0 | 11666 | 9.49 |
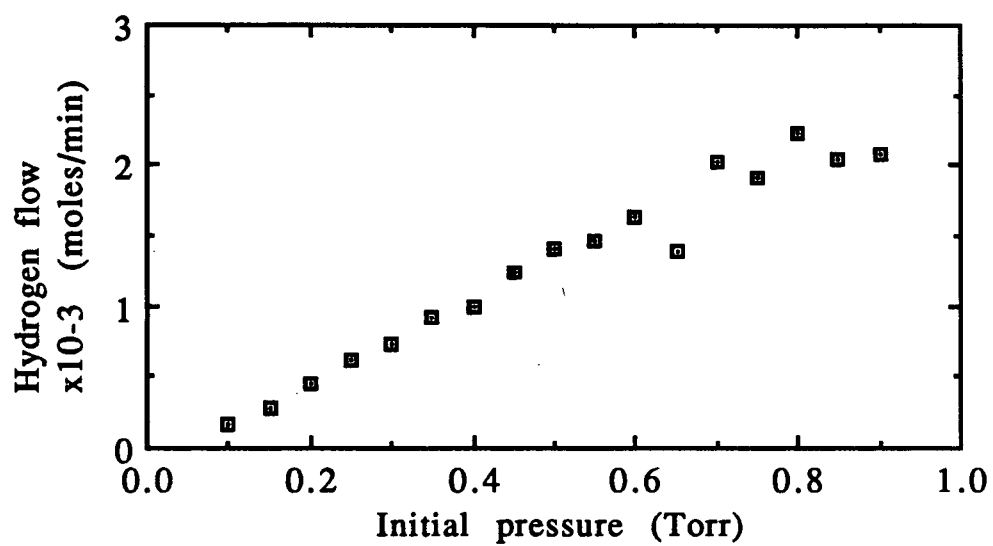
Figure 3.4. Graph of hydrogen flow against pressure for the fast flow system.
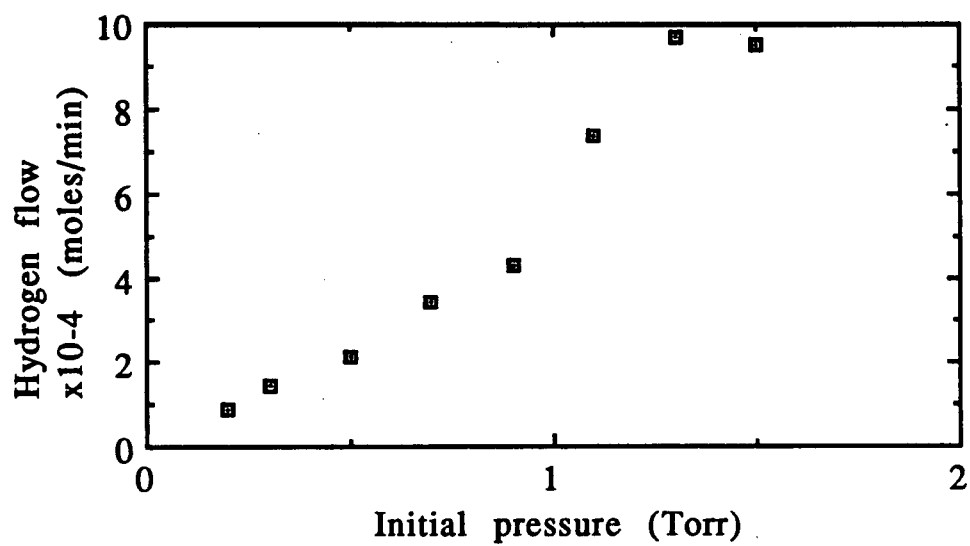
Figure 3.5. Graph of hydrogen flow against pressure for the slow flow system.
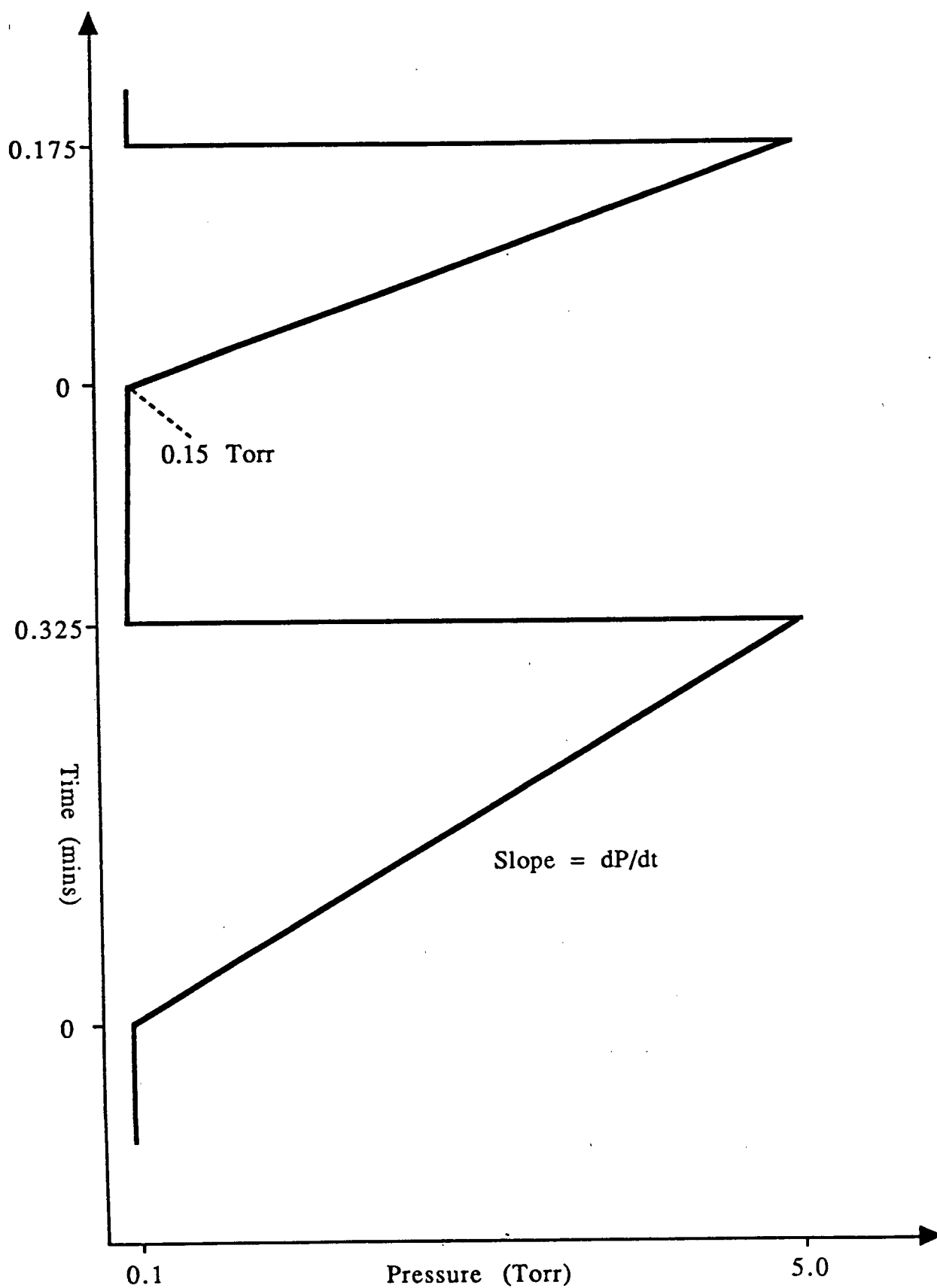
Figure 3.6. Pressure against time for 0.1 Torr and 0.15 Torr starting pressure.

The axis labels and values in the figure are:

- Vertical axis: Time (mins), with marked values 0.175, 0, 0.325, 0
- Horizontal axis: Pressure (Torr), with marked values 0.1 and 5.0
- 0.15 Torr (dashed line label)
- Slope = dP/dt

pressure rise on shutting off the glass section of the fast flow system.

## 3.4 Partial pressure of H and $H_2$

Knowing both the H and $H_2$ flow rates allows one to calculate their partial pressures as follows.

Assuming the ratio of the flows is equal to the ratio of the partial pressures,

$$P_H/P_{H2} = F_H/F_{H2} \qquad (3.1)$$

$$\text{where, } F_H = \text{H flow}$$
$$F_{H2} = H_2 \text{ flow}$$
$$\text{and } F_{H2} \gg F_H.$$

The total pressure is the sum of the partial pressures, thus;

$$P_{total} = P_H + P_{H2} \qquad (3.2)$$

substituting (3.1) in (3.2) yields

$$P_{total} = P_{H2} + P_{H2} \cdot F_H/F_{H2} \qquad (3.3)$$

therefore,

$$P_{H2} = P_{total}/(1 + F_H/F_{H2}) \qquad (3.4)$$

and,

$$P_H = P_{total}\{1 - 1/(1 + F_H/F_{H2})\} \qquad (3.5)$$

## 3.5 Temperature control

Our initial experiments using the fast flow system led us to believe that the InP etched at temperatures below 150°C. When the discharge was ignited the temperature reading rose rapidly and after

52

an initial induction period the sample was observed, by interferometry, to etch. A typical plot of the temperature rise as recorded by the thermocouple readout is shown in figure 3.7. It is seen that there is a rapid initial rise in the first 50 seconds, followed by a more gradual increase over the next few minutes. The final temperature recorded by the thermocouple was around 200°C. The sample in figure 3.7 etched after 44 seconds which corresponds to a temperature of 130°C. However because the sample platform was relatively thick, there could have been a time lag between the temperature of the sample surface and that recorded by the thermocouple. Consequently the temperature at which etching commenced could have been considerably higher than 130°C. This is discussed further in section 3.7.

When the initial starting temperature was increased the temperature rise was found to be far smaller, as shown in figure 3.8. The temperature rise starting at 51°C (figure 3.7) after 2 minutes was 110°C, however starting the discharge at an initial substrate temperature of 159°C (figure 3.8) produces only about a 20°C increase in the same period. This is somewhat surprising and suggests that the final sample temperature is nearly the same regardless of the temperature of the walls or the initial sample temperature. The answer could lie in a lower "recombination heating" at high temperature. However we did not investigate this problem further.

Using the slow flow system the temperature rise was found to be less pronounced, as shown in figure 3.9. The problem of keeping the temperature constant in order to obtain useful etch rates was

Figure 3.7. Graph of temperature against time of discharge for fast flow system. 75W microwave power, 51°C initial temperature, 0.20 Torr pressure $H_2$.
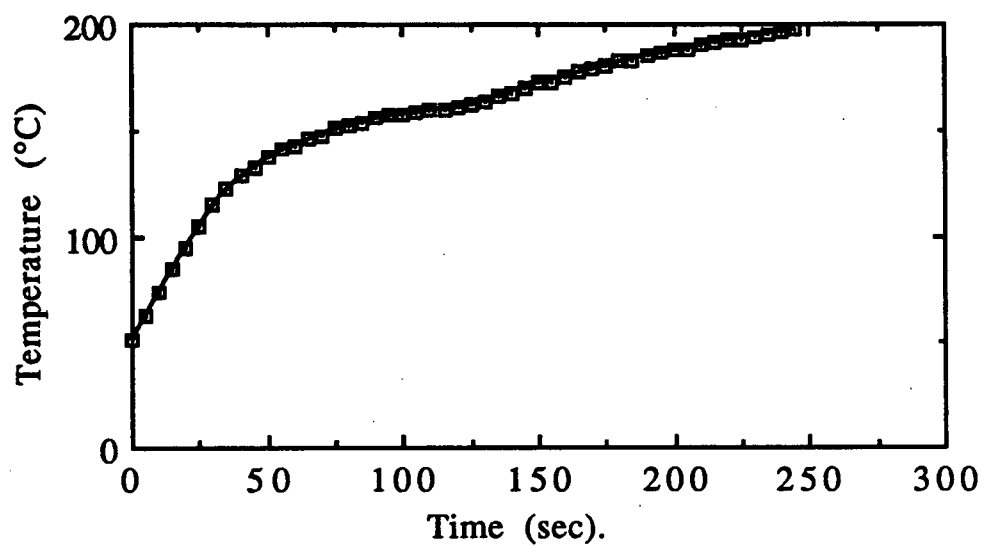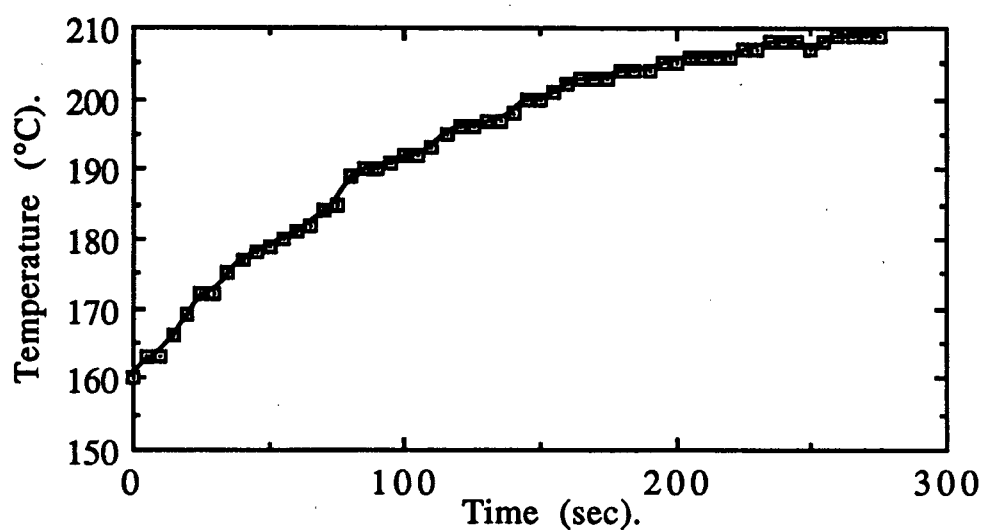
Figure 3.8. Graph of temperature against time of discharge for fast flow system. 75W microwave power, 159°C initial temperature, 0.20 Torr pressure $H_2$.
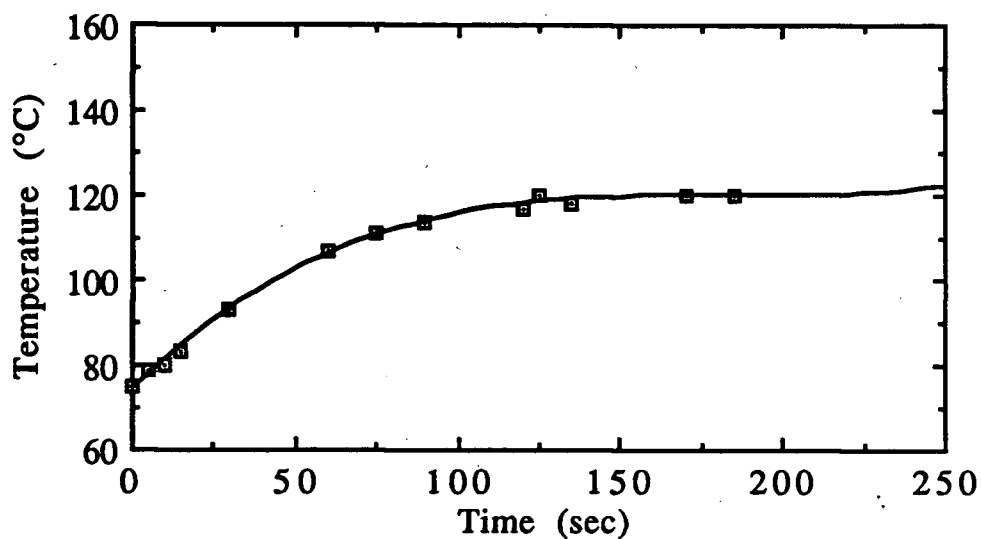
Figure 3.9. Graph of temperature against time for H recombination on InP using slow flow system. 35W microwave power, 1.50 Torr pressure, 0.14 μmoles/s atom flow.

overcome by using high initial substrate temperatures and experiments were conducted at 300°C, using both slow and fast flow systems. The temperature rise occurring between the start and finish of the etch being limited to 1 - 2 °C using small atom flows and 2 - 4 °C using higher atom flows.

The cause of this temperature rise would seem to be due to the recombination of H atoms on the surface of both the sample and probe. The reaction occurring is highly exothermic;

$$\text{surface} + 2H = H_2 + \text{surface} \qquad \Delta H = -420 \text{ kJ/mole}.$$

To ensure that this temperature rise was indeed due to recombination of H atoms and not to a hot gas stream the sample probe was wrapped in teflon tape. The rate of recombination of H atoms on teflon is known to be small. The temperature rise on starting the discharge is shown in figure 3.10. It can be seen that the temperature rise is reduced from about 45°C (figure 3.9) to about 22°C . Consequently this temperature rise is due mainly to this recombination, rather than from the presence of a hot gas stream.

### 3.6 Induction period prior to etching

When the initial substrate temperature was low there was a long induction period between initiation of the plasma and commencement of the etching. This varied with both temperature and atom flow but was found to occur to a far lesser extent at higher temperatures. It is unlikely that the longer induction periods are due to etching through the oxide layer as it is known that H atoms readily etch InP oxide[2]. The longer induction periods are probably due to heating up of the sample surface to a temperature where the
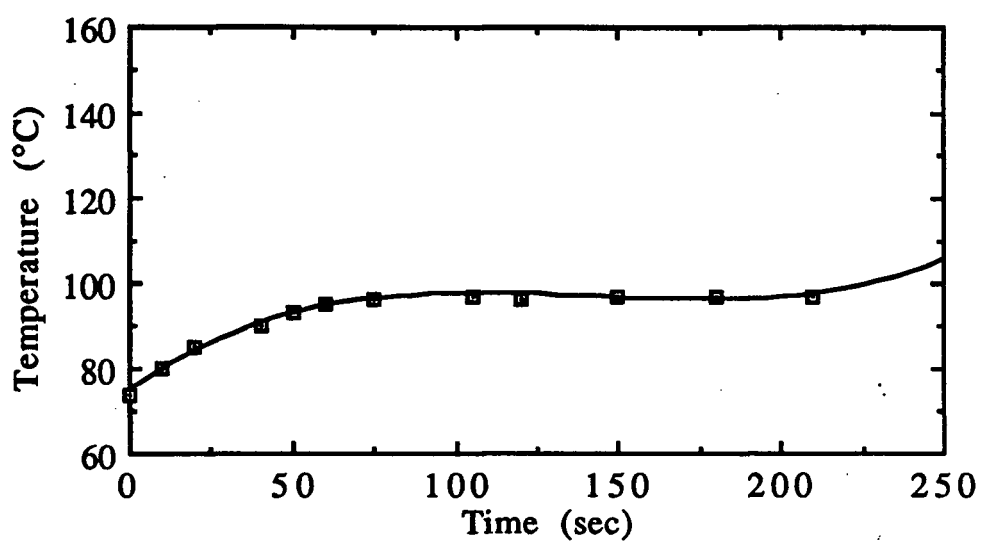
57

Figure 3.10. Graph of temperature against time for H recombination on teflon using slow flow system. 35W microwave power, 1.50 Torr pressure, 0.14 μmoles/s atom flow.

Table 3.3. Induction periods for etches at initial substrate temperatures of 100°C and 300°C.

| Sample # | Atom flow x10⁻⁶ (moles/s) | Initial temperature (°C) | Induction period (min:sec) |
|---|---|---|---|
| 111 | 1.03 | 102 | :54 |
| 112 | 0.90 | 104 | :57 |
| 113 | 0.88 | 98 | :53 |
| 114 | 1.22 | 96 | :29 |
| 115 | 0.97 | 99 | 1:22 |
| 116 | 2.18 | 88 | 2:34 |
| 117 | 0.78 | 102 | 1:19 |
| 118 | 1.77 | 104 | 1:39 |
| 119 | 1.72 | 100 | :42 |
| 124 | 1.91 | 316 | :2 |
| 125 | 1.49 | 300 | :10 |
| 126 | 1.50 | 300 | :4 |
| 128 | 2.35 | 300 | :14 |

InP readily etches. Table 3.3 gives induction times for a series of samples at initial substrate temperatures around 100°C. These may be compared to those given at 300°C where it is observed that there is a drastic reduction in the induction period. Also see figure 3.11. On average the time is reduced by at least an order of magnitude. It would seem that at the lower temperatures there is an additional factor involved, other than removing the oxide layer.

### 3.7 Starting temperature of the etch

For a given H atom concentration the etching of InP did not consistently start at any particular temperature registered by the thermocouple. Observing that the etching commenced at a lower read out temperature when the temperature was rising rapidly, we considered it possible that there was a temperature lag between the sample surface and the thermocouple. This could mean that the sample surface was already heated to say 200°C and was being etched although the thermocouple had not responded as rapidly and was recording a lower, incorrect, temperature. Consequently the sample was attached directly to the thermocouple and a faster responding temperature readout was employed, as described in the experimental section. With this arrangement the thermocouple readings reached a steady state much more quickly when the discharge was initiated.

In the first experiment with this new sample mount, the temperature of the substrate was initially heated to 75°C using the slow flow system and a low discharge power (33W). When the discharge was initiated the temperature rose slowly to a value that
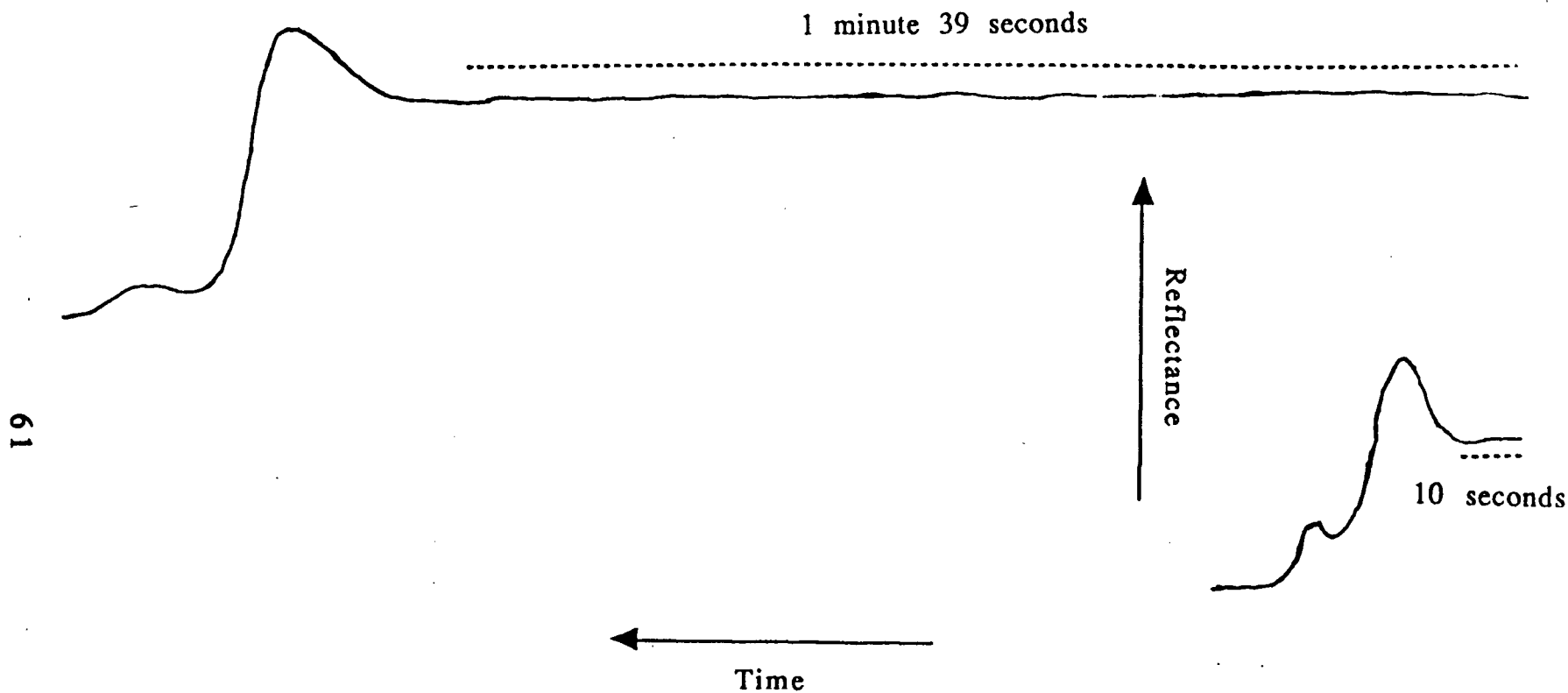
Figure 3.11. Top; interferogram for sample # 118 at an initial substrate temperature of 104°C, the induction period is 1 min 39 secs. Bottom; interferogram for sample # 125 at a substrate temperature of 300°C, the induction period is 10 secs.

could be set by changing the discharge power. The InP was observed, by interferometry, to etch only when the temperature reached 162°C. The experiment was repeated starting with a substrate temperature of 86°C and was found to commence etching at 160.5°C, (see table 3.4).

### 3.8 Comparison of etch rates from profilometry with those from interferometry

Table 3.5 compares the etch rates obtained by interferometry with those from profilometry for several samples. The etch depths are also given. While the etch rates obtained by both methods are comparable it can be seen that all etch rates from profilometric measurements are less than those calculated by laser interferometry. Those calculated from interferometry correspond to the etch rate for the first 0.1 μm of the sample, whereas those by profilometry are all for etch depths greater than 0.1 μm. This would indicate that the etch rate is decreasing as the etch depth increases.

### 3.9 Hydrogen atom etching

Laser interferometry was performed while the samples etched. Interferograms were produced showing the usual interference maxima and minima. As explained in the experimental section the etch rates can be found by measuring the time taken between interference peak maxima and substituting into equation (2.1). The etch rates of InP were measured at 300°C at various partial pressures of H at 0.30 Torr. These results are listed in table 3.6. Figure 3.12 shows a plot of the etch rate against low partial pressure

Table 3.4. Time and temperature readings for sample 183. Start of etch at 160.5°C.

| Power (W) | Time (mins) | Temp (°C) | Power (W) | Time (mins) | Temp (°C) | Power (W) | Time (mins) | Temp (°C) |
|---|---|---|---|---|---|---|---|---|
| 33 | :0 | 86 | | 5:45 | 126 | 60 | 15:30 | 153.5 |
| | :10 | 90 | | 6:00 | 127 | | 16:00 | 154 |
| | :20 | 93 | | 6:20 | 128 | | 16:30 | 155 |
| | :30 | 98 | | 6:40 | 129 | | 16:50 | 155 |
| | 1:10 | 105 | 50 | 7:00 | 130 | | 17:30 | 155 |
| | 1:30 | 107 | | 7:20 | 132 | | 18:00 | 155 |
| | 1:46 | 107 | | 7:40 | 134 | 62 | 18:20 | 156 |
| 40 | 2:15 | 110 | | 8:00 | 135 | | 18:30 | 156 |
| | 2:25 | 112 | | 8:40 | 138 | | 18:45 | 156.4 |
| | 2:40 | 112 | | 9:20 | 140 | 64 | 19:25 | 157 |
| | 3:00 | 114 | | 9:40 | 141 | | 19:45 | 157 |
| 45 | 3:15 | 115 | | 10:30 | 142 | 65 | 20:50 | 158 |
| | 3:30 | 115 | 55 | 11:20 | 146 | | 21:00 | 159 |
| | 4:00 | 159 | | 11:40 | 147 | | 21:20 | 159 |
| | 4:10 | 120 | 12:00 | 148 | | 23:50 | 160 |
| | 4:30 | 121 | | 12:40 | 149 | * | 24:10 | 160.5 |
| | 4:45 | 122 | 58 | 13:20 | 151 | | 24:20 | 160.6 |
| | 5:00 | 123 | | 13:40 | 151 | | 25:00 | 160.1 |
| | 5:20 | 124 | | 14:00 | 152 | | 25:30 | 160.1 |
| | 5:30 | 125 | | 14:30 | 153 | | 26:00 | 160.3 |

* Beginning of etch.

Table 3.5. Comparison of etch rates obtained by interferometry with those from profilometry on the same samples.

| Sample # | Etch depth ($\mu$m) | Etch rate ($\mu$m/min) by profilometry | Etch rate ($\mu$m/min) by interferometry |
|---|---|---|---|
| 57 | 0.46 | 0.46 | 0.49 |
| 61 | 0.19 | 0.34 | 0.40 |
| 62 | 0.17 | 0.12 | 0.27 |
| 100 | 1.52 | 1.41 | 1.52 |
| 106 | 0.19 | 0.47 | 0.63 |
| 108 | 1.52 | 3.26 | 3.64 |
| 114 | 0.28 | 1.41 | 1.54 |
| 122 | 0.18 | 0.13 | 0.14 |

Table 3.6. Results for etch rate of InP at 300°C, 44 Pa pressure and 33W microwave power.

| Sample # | Etch rate (μm/min) | $P_H$ (Pa) | Atom flow ($x10^{-6}$moles/s) |
| --- | --- | --- | --- |
| 131 | 0.04 | 1.108 | 0.36 |
| 125 | 0.47 | 7.575 | 2.98 |
| 133 | 0.029 | 0.655 | 0.22 |
| 135 | 0.018 | 0.361 | 0.12 |
| 136 | 0.056 | 1.672 | 0.56 |
| 139 | 0.045 | 1.185 | 0.40 |
| 145 | 0.714 | 7.724 | 3.08 |
| 148 | 0.134 | 5.230 | 1.91 |
| 149 | 0.454 | 4.258 | 1.57 |
| 150 | 0.454 | 8.314 | 3.28 |
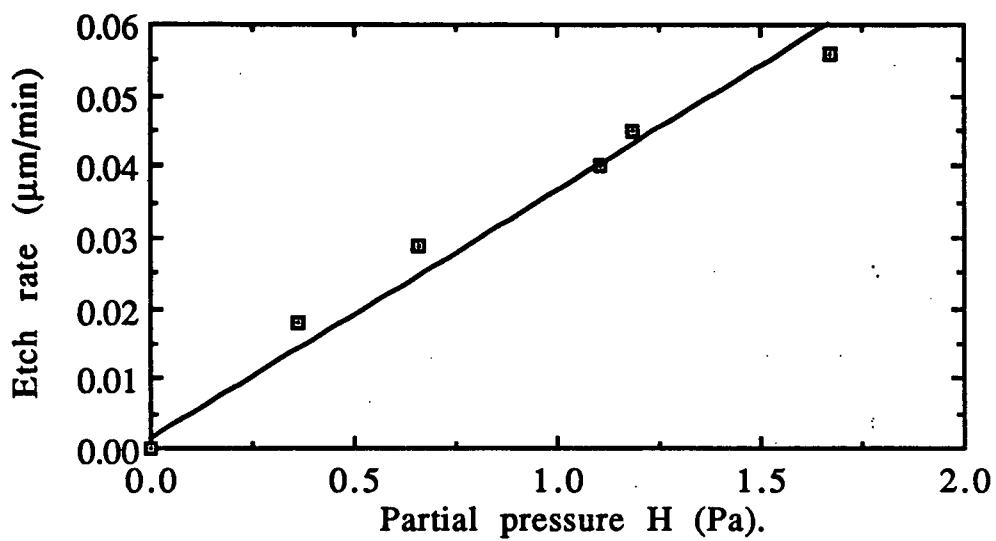
Slope ( $k_1$) = 0.0307 ± 0.0018 $\mu m.min^{-1}.Pa^{-1}$.

Figure 3.12. Graph of etch rate against partial hydrogen atom pressure at 44 Pa, 300°C, 33W microwave power for low atom flows.

of hydrogen. Even at 300°C there was quite a considerable heating effect at the higher atom flows resulting in a large amount of scatter in these readings. Figure 3.13 shows a plot of etch rates as a function of the partial pressures of H.

The surfaces of the wafers appeared to be roughened by the etching process which could be seen with a laboratory microscope. This roughness could be seen to be due to the presence of small silvery globules across the entire surface. Shown in plates 3.1, 3.2 and 3.2b are some typical SEM pictures taken of the etched samples. These show globules of various diameter up to 30 μm.

The results of an XPS analysis of a globule covered surface are given in table 3.7. The XPS spectrum of the etched surface is shown in figures 3.14, 3.15 and 3.16. The C 1s peak is referenced at 284.6 eV, requiring that all binding energies have to be corrected by 0.5 eV as the spectrum in figure 3.14 shows this peak at 285.1 eV. The pure In peak is found to be at 443.5 eV which is within 0.1 eV of where it is to be expected. However, there is a large shoulder on this peak at 444.8 eV which corresponds to an In suboxide[34]. It is seen from figure 3.15 and 3.16 and table 3.6 that the sample surface is completely depleted of P leaving it In rich. This would explain why the InP was found only to etch in bulk when the substrate temperature reached 160.5°C, since the melting point of In is 156.6°C. Consequently, it would seem that the surface P is etched away, leaving behind a layer of In. Subsequent reaction with H atoms cannot occur until the In is moved to uncover further P. As happens when the In melts and globulates. Tu et al[16] observed similar behaviour in that the reaction stopped after 0.8 nm of P had
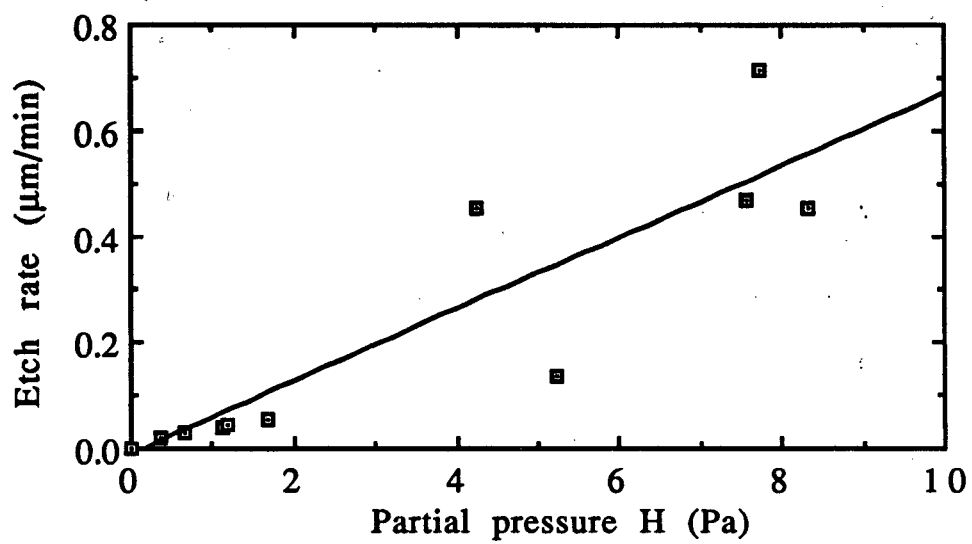
Figure 3.13. Graph of etch rate against partial hydrogen atom pressure at 44 Pa, 300°C, 33W microwave power for all atom flows.
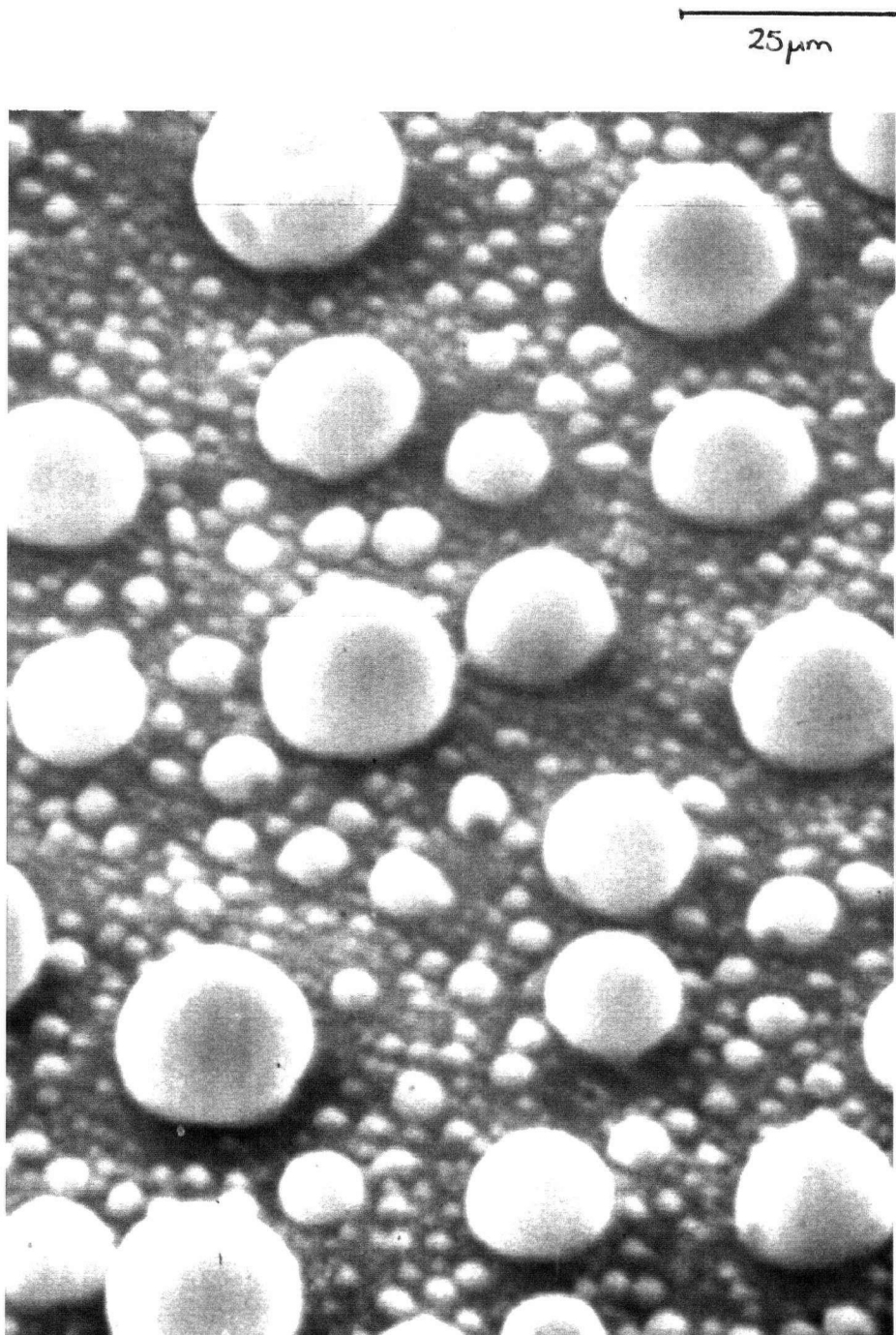
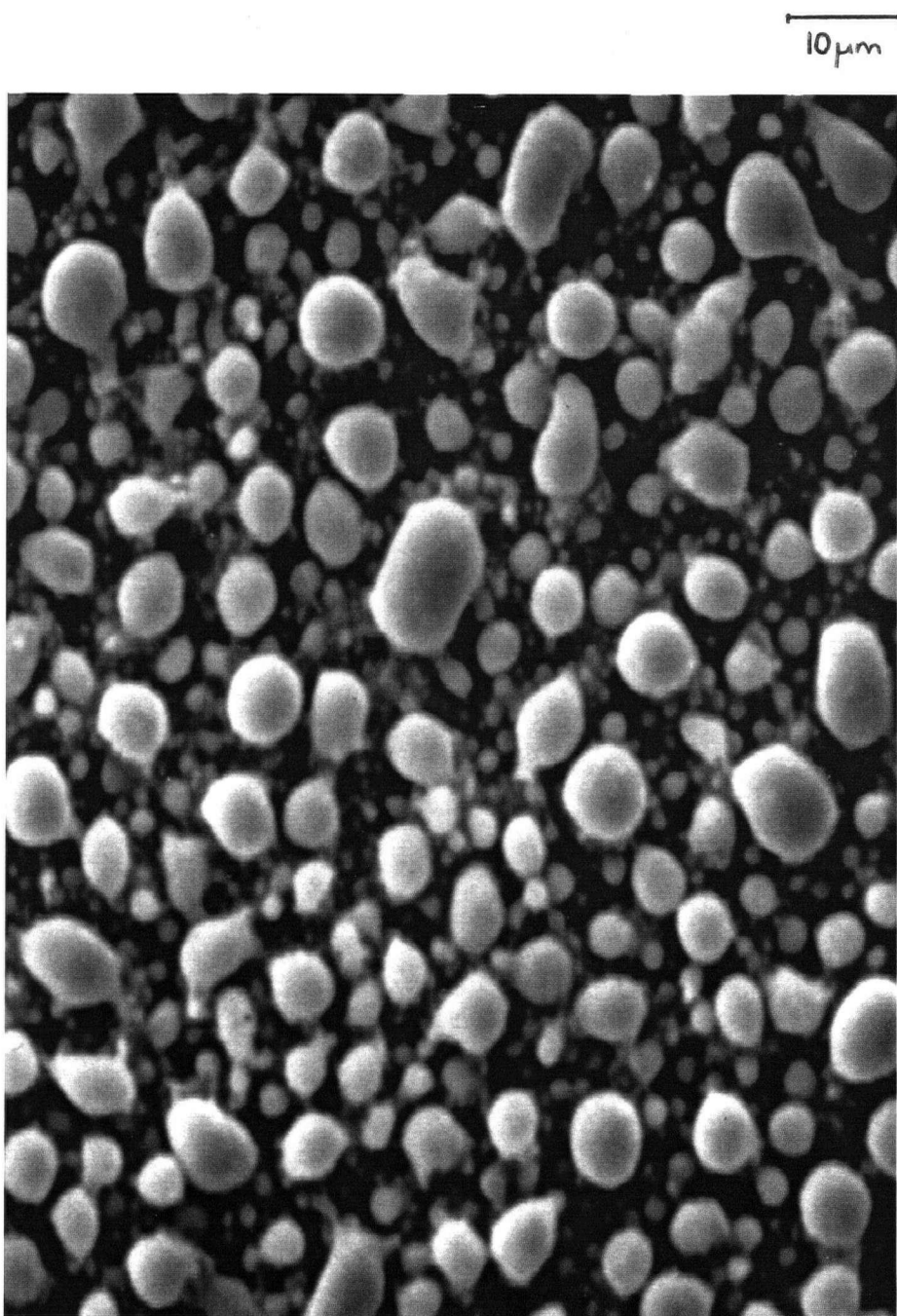Plate 3.1.  Sample # 149 H atom etched surface (300°C), x 6.0k largest globule 25μm.

Plate 3.2. Sample # 14 H atom etched surface (200°C) x 3.0k, largest globule
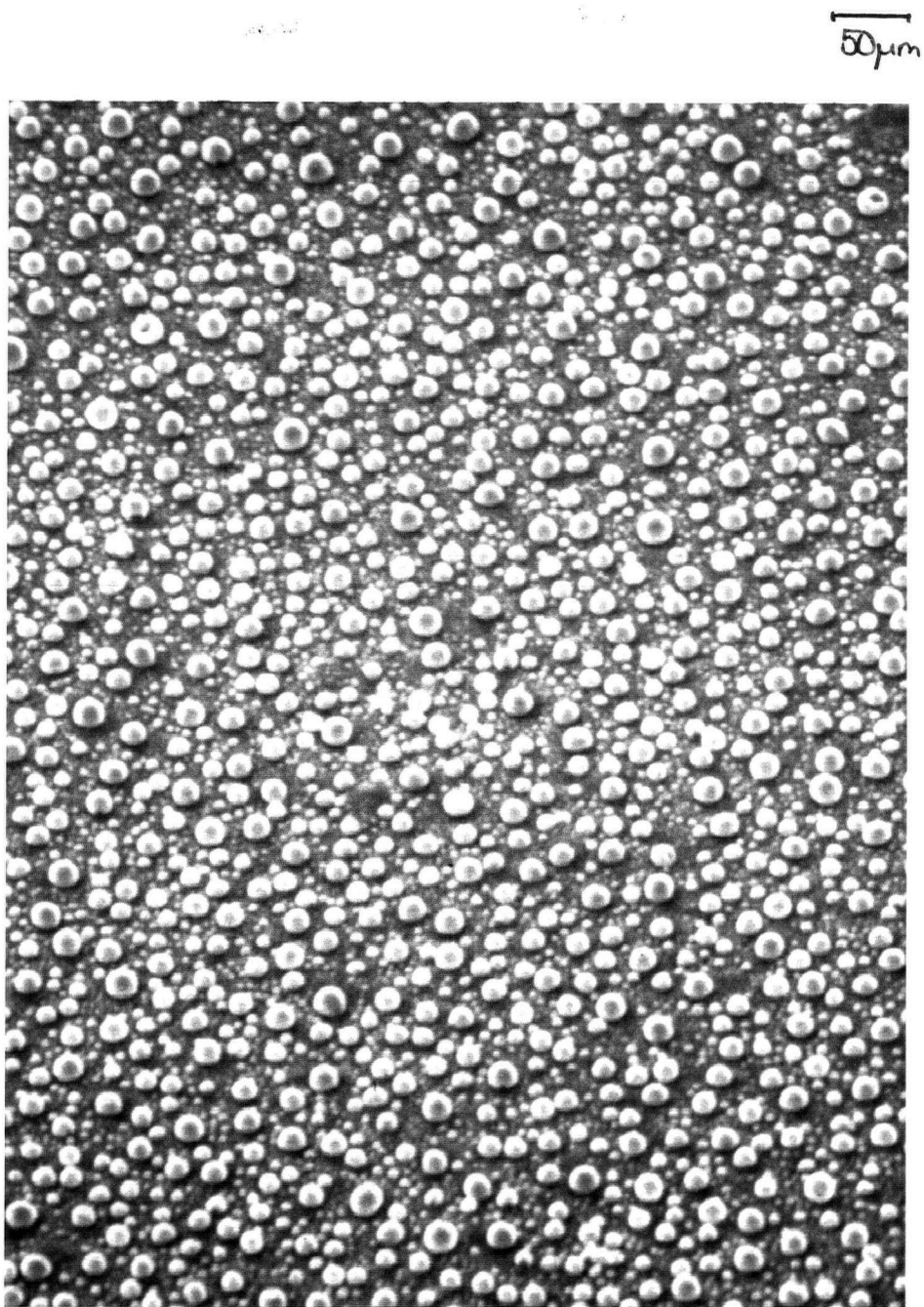10μm.

50μm

Plate 3.2b. Sample # 149 only magnified x 800.

Table 3.7.  Areas under peaks for an In covered surface.

| Peak | Etched region | Binding energy (eV) | Binding energy corrected (eV) |
|------|---------------|---------------------|-------------------------------|
| In $3d_{5/2}$ | $1.960 \times 10^3$ | 444.04 | 443.5,444.8(ox) |
| C 1s | $2.154 \times 10^2$ | 285.1 | 284.6 |
| P 2p | 0 | 132.8 | 132.3 |
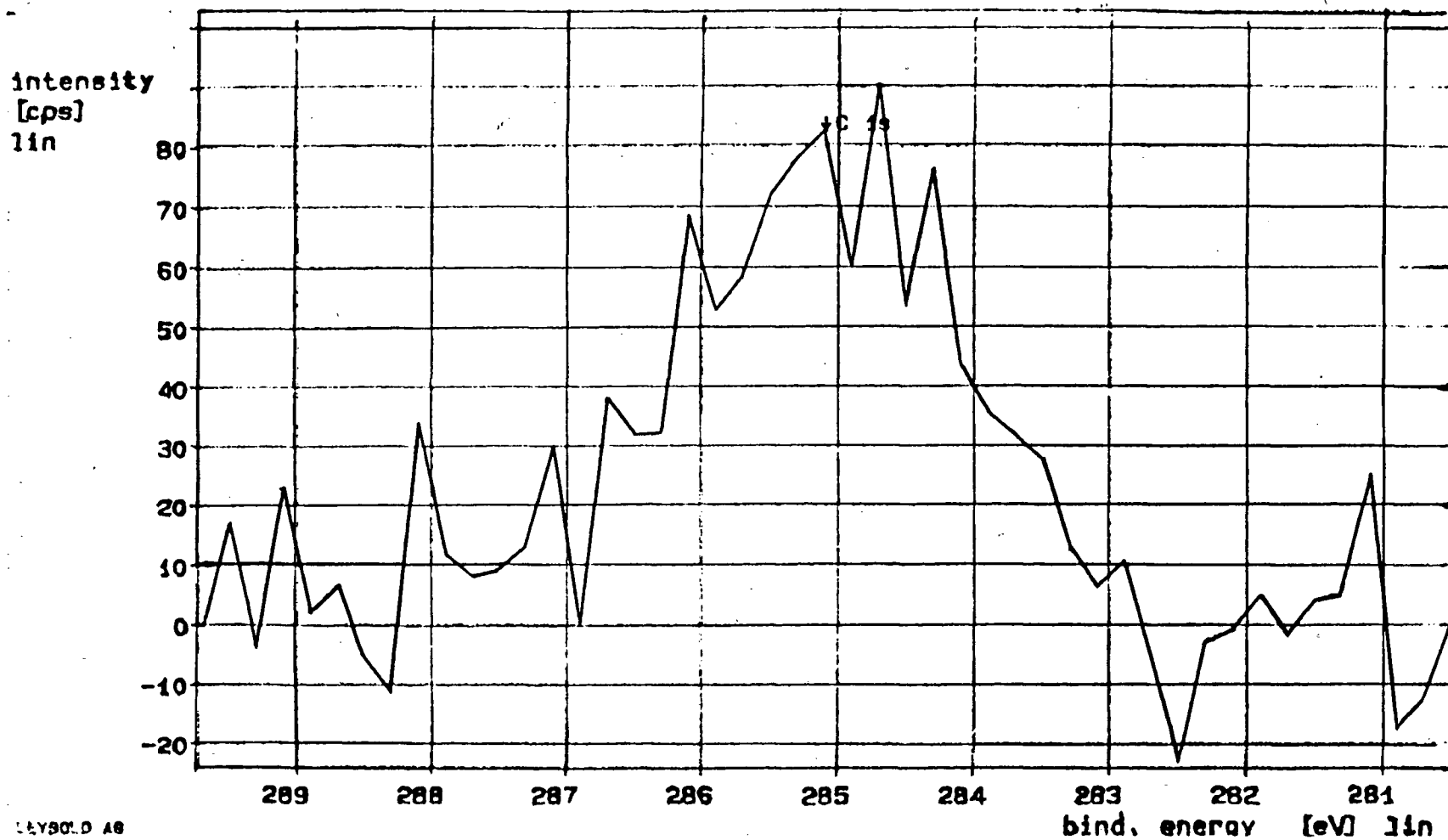
Figure 3.14 . XPS spectrum of C 1s region for sample # 6.

intensity
[cps]
lin

600

500

400

300

200

100

+ In 3d5/2

447    446    445    444    443    442    441

bind. energy   [eV]   lin

LEYBOLD AG

74
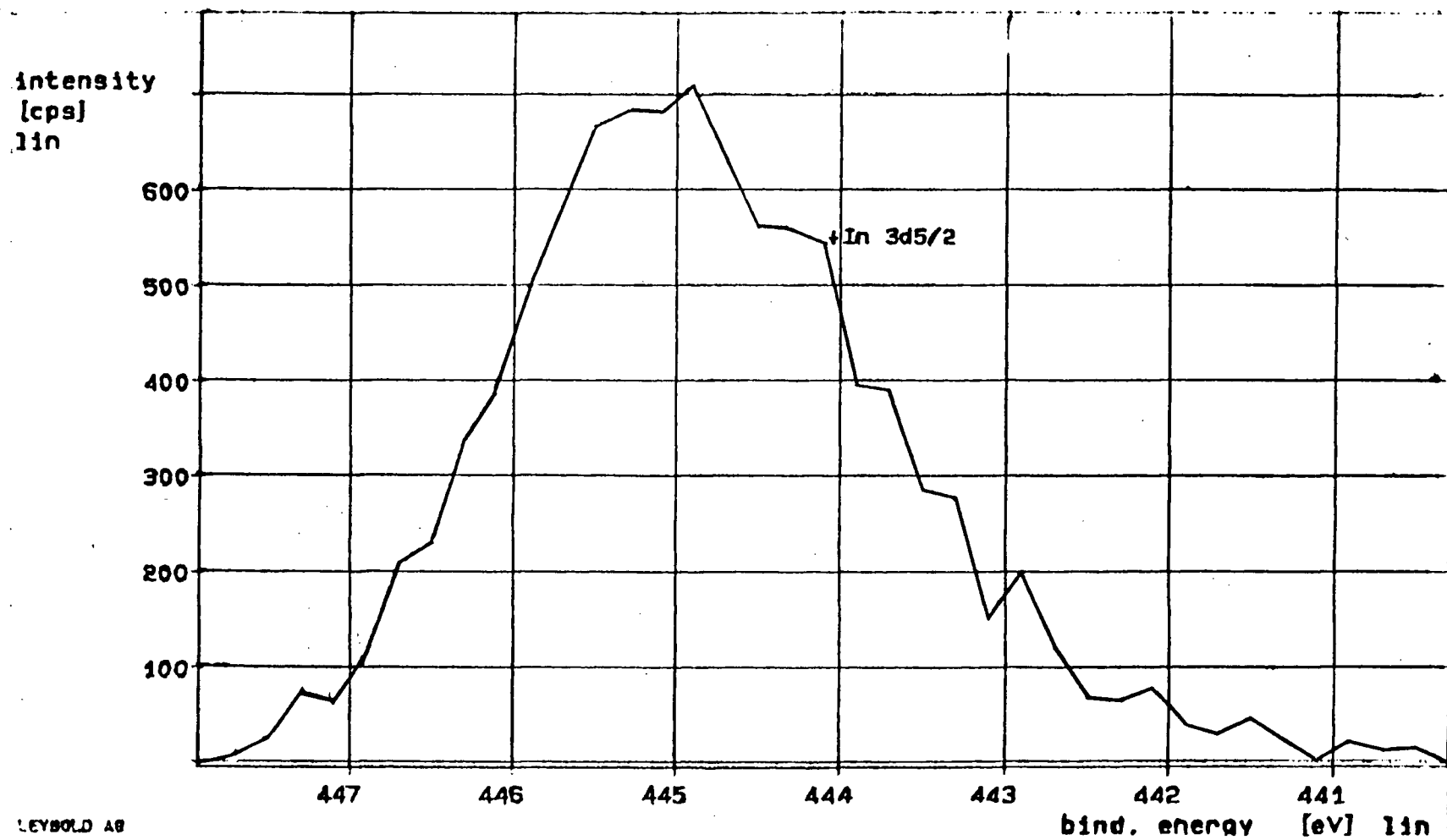
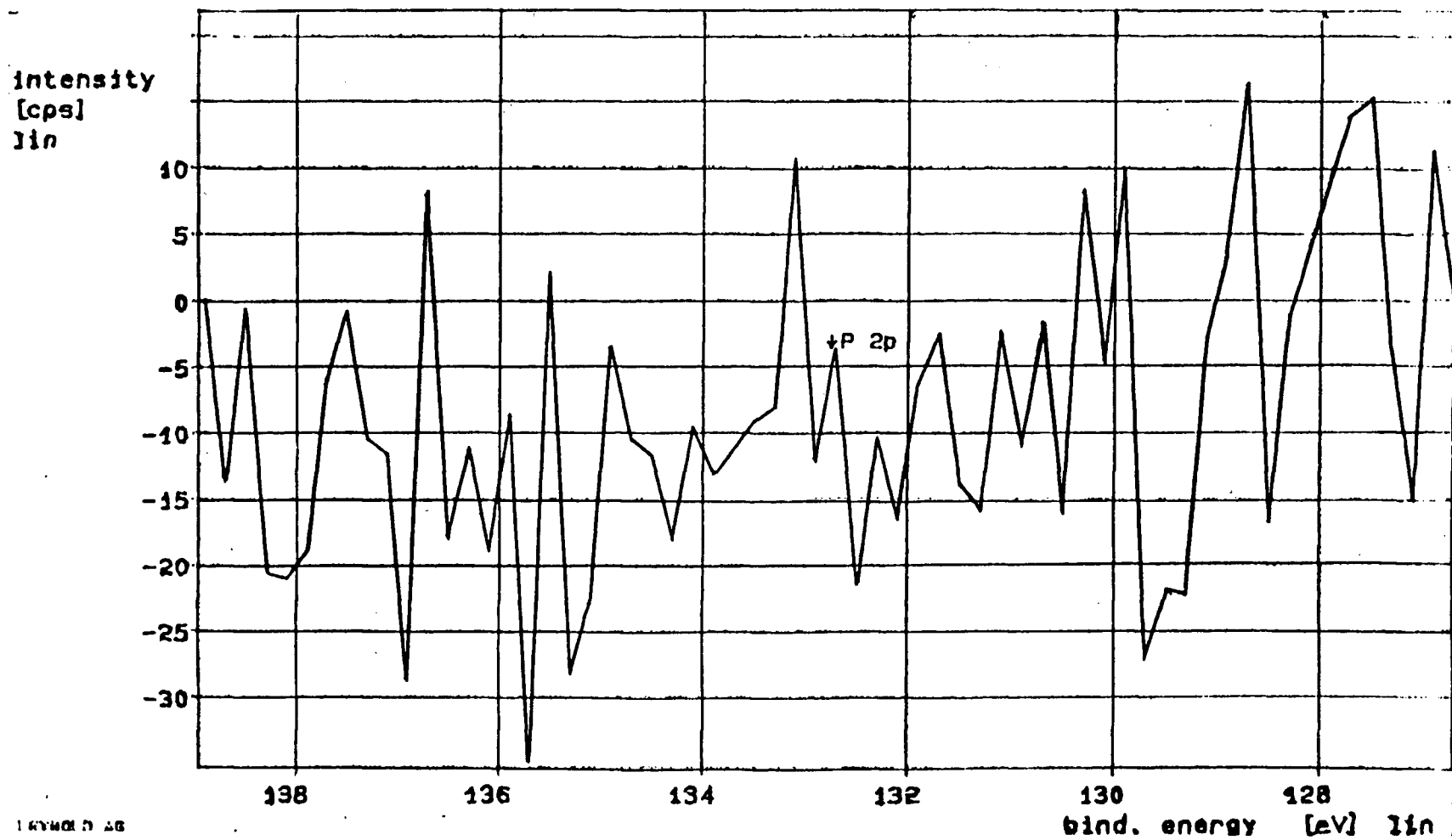Figure 3.15 .   XPS spectrum of In 3d5/2 for sample # 6.

Figure 3.16. XPS spectrum of P 2p for sample # 6.

been removed from the surface at room temperature. The large induction periods and poor repeatability of etches at lower temperature, which were discussed earlier, are both explained by the requirement that the sample surface be heated above the melting point of In, before the reaction can take place. Consequently, the long induction period found for samples etched at low temperatures (that is below the melting point of In) is due to one of two factors. The first is a short period (probably up to 20 seconds at most depending upon atom flow and temperature) while the oxide layer is removed. The second and more substantial period is due to the sample surface being heated, by surface recombination reactions, to temperatures higher than the melting point of In so that droplets can condense exposing the phosphorus to the H atoms. A typical interferogram of a H etched sample is shown in figure 3.17. It can be seen that there are only 2 'oscillations' before the reflected intensity drops to such an extent that further etching cannot be monitored in this manner. This is due to the formation of the In globules which scatter the incident beam of light. Although the large drop in reflected intensity is probably due to globulation, the positions of the maxima and minima do not appear to be greatly affected as the etch rates obtained by interferometry and profilometry are comparable at similar etch depths. Once the surface is covered in these globules the reflectance becomes so poor that the reaction can no longer be followed using interferometry. Since the average number of reflectance maxima obtained in any sample was 2, the maximun etch depth that can be measured by this technique is given by:

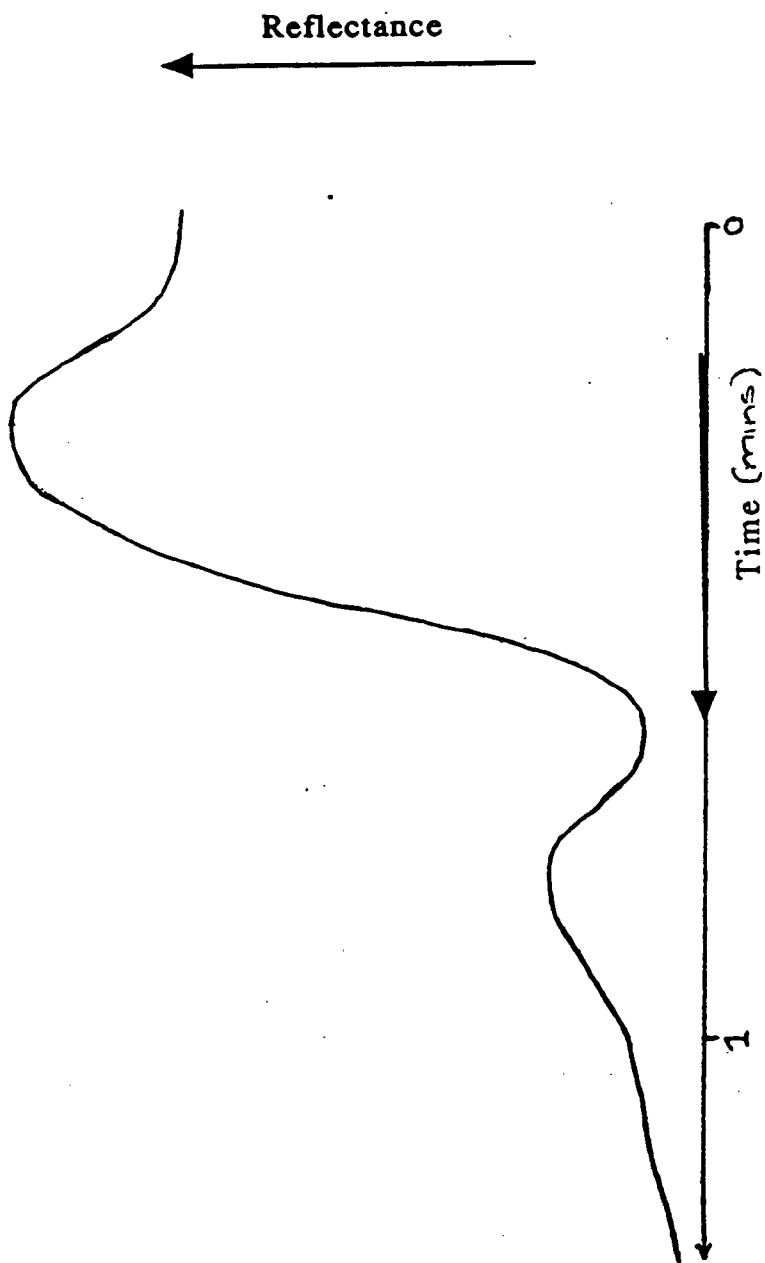$$\text{Depth (for 2 reflectance peaks)} = \lambda/2 \cdot \eta_{air}/\eta_{InP}$$

Reflectance

Time (mins)

0

1

Figure 3.17. A typical interferogram.

77

therefore,

$$\text{depth etched} = 0.1 \ \mu m$$

where,

$\lambda$ = wavelength of incident beam and

$\eta$ = refractive index


Consequently, the etch depths were also measured by profilometry. As stated in section 3.5 these etch rates are slower than those measured by laser interferometry. This is to be expected since at greater etch depths the formation of In on the surface masks more of the InP, restricting its exposure to the H atoms. Two typical profiles are shown in figure 3.18. As can be seen from these profiles the In globules accumulate together since parts of the etched surface are actually higher than the level of the areas that were masked with silicon. The location of these 'hillocks' are uniform throughout the wafer's surface. Comparison between wafers doesn't reveal any obvious trends in size or density of the droplets. It would be reasonable to postulate that the position, size and frequency of these hillocks was dependent upon, among other factors, temperature, etch time and atom flow. Surface defects and/or surface contamination could also affect their formation.
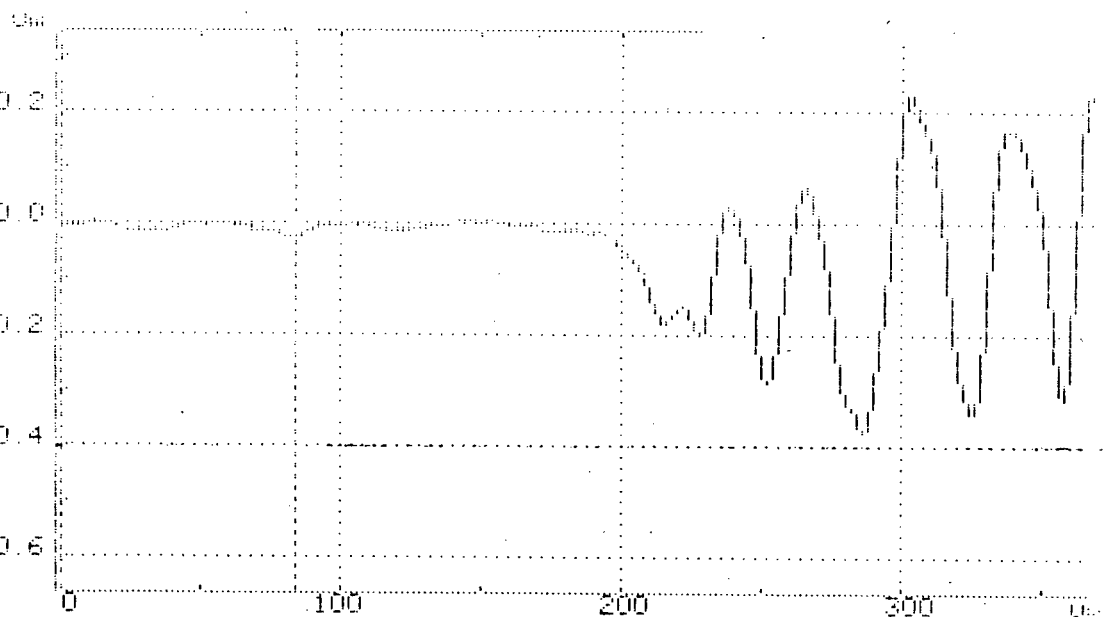

### 3.10 Rate constant ($k_1$) for H atom reaction

The data in figure 3.12 indicate a first order dependence upon the partial pressure of H ($P_H$) the rate constant, being $k_1$, for the reaction;
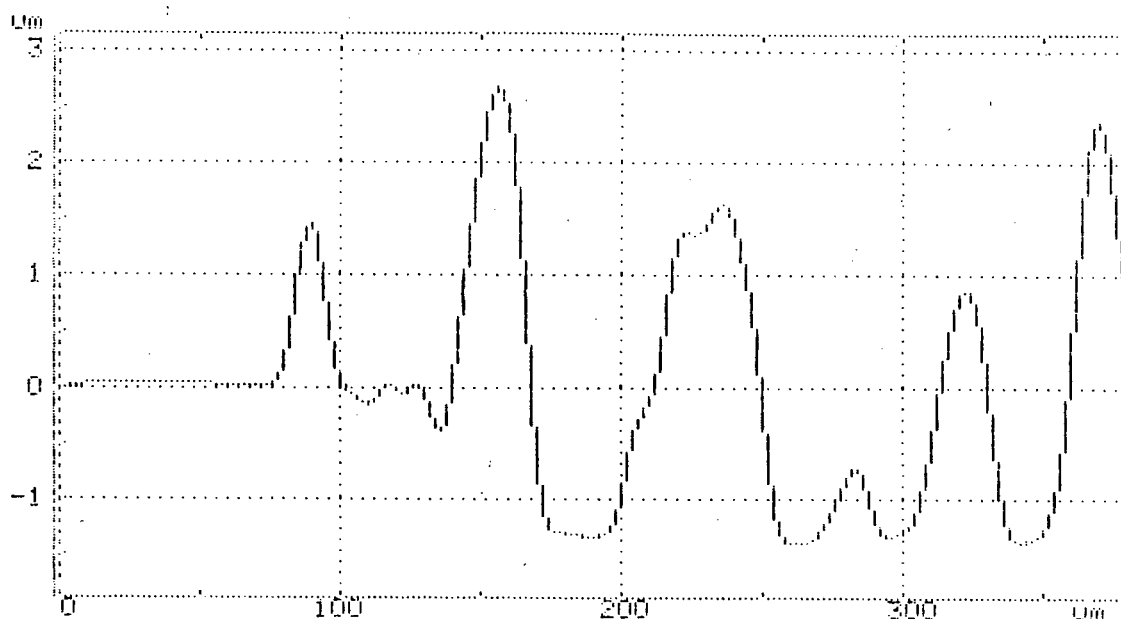
Figure 3.18. Profiles of sample # 100, top, and sample # 80,
bottom.

79

$$3H + InP = In + PH_3.$$
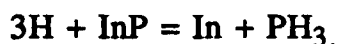
Because of the possibility of heating at high atom concentration the rate constant was calculated from the slope of the line in figure 3.12 . Using a least squares straight line fit with errors (see appendix B) in both coordinates gives,

$$k_1 = 0.0307 \pm 0.0018 \ \mu m.min^{-1}.Pa^{-1} \quad at \ 300°C.$$

### 3.11 Etching by methyl radicals

It is clear from the observations described earlier that H atoms remove only the P from InP. We therefore searched for an etchant for the indium that is compatible with the H atoms. In view of previous studies by others workers (see introduction) we chose to investigate the possibility that methyl radicals can form $(CH_3)_3In$. Since we have already prepared a known flow of hydrogen atoms a logical choice would be a reaction of hydrogen atoms which produces $CH_3$, in the gas stream before it encounters the substrate. The simplest reaction for this purpose is the reaction of hydrogen atoms with a methyl halide.

$$H_{(g)} + CH_3X_{(g)} = HX_{(g)} + CH_{3(g)}$$
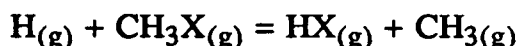
The choice of halide was governed by the need for a rapid reaction that produced a halogen atom that was least reactive so that secondary reactions were minimal. $CH_3I$ was therefore chosen because of the relative weakness of the $H_3C-I$ bond and the fact that F, Cl and Br atoms are more reactive.

Our preliminary experiments showed that the H atoms could be completely removed when an excess of $CH_3I$ was added about 3 - 4 cm upstream of the InP substrate.

When the discharge was ignited with a small $CH_3$ flow through the system no reaction with InP was seen to take place. This was repeated several times but the InP was not etched. Consequently the experiments were repeated starting with just a H atom flow whereupon the P was etched leaving behind the surface In. After a short period of H atom etching the $CH_3I$ was introduced into the gas stream. Figure 3.19 shows the resulting interferogram. Initially we observe the typical behaviour of the reflectance decreasing rapidly due to the globule formation, along with two peak maxima. At the top of the second interference peak, $CH_3$ was added and the reflectance rose steadily until it leveled off at a value approximately 25% less than that of the initial polished surface. The $CH_3I$ flow was then shut off and another interference pattern was produced by etching of the H atoms. The $CH_3$ was again added at a similar stage in the reaction and the etching process was found to be again repeatable.

It is seen that the $CH_3$ restores the reflectance of the sample back to a value that was similar, although slightly reduced from that before H atom etching. However on successive etches of the sample, the surface becomes increasingly roughened until a point is reached, (on the fifth cycle) where the reflectance does not rise significantly. The H atom etch rates as measured by interferometry after each indium clean up were found to be very similar. For the experiment shown in figure 3.19 these were; 0.27, 0.24 and 0.27 $\mu m/min$ respectively.

These reactions were generally run at around 250 - 300°C since the reaction of indium with $CH_3$ was not seen to occur at
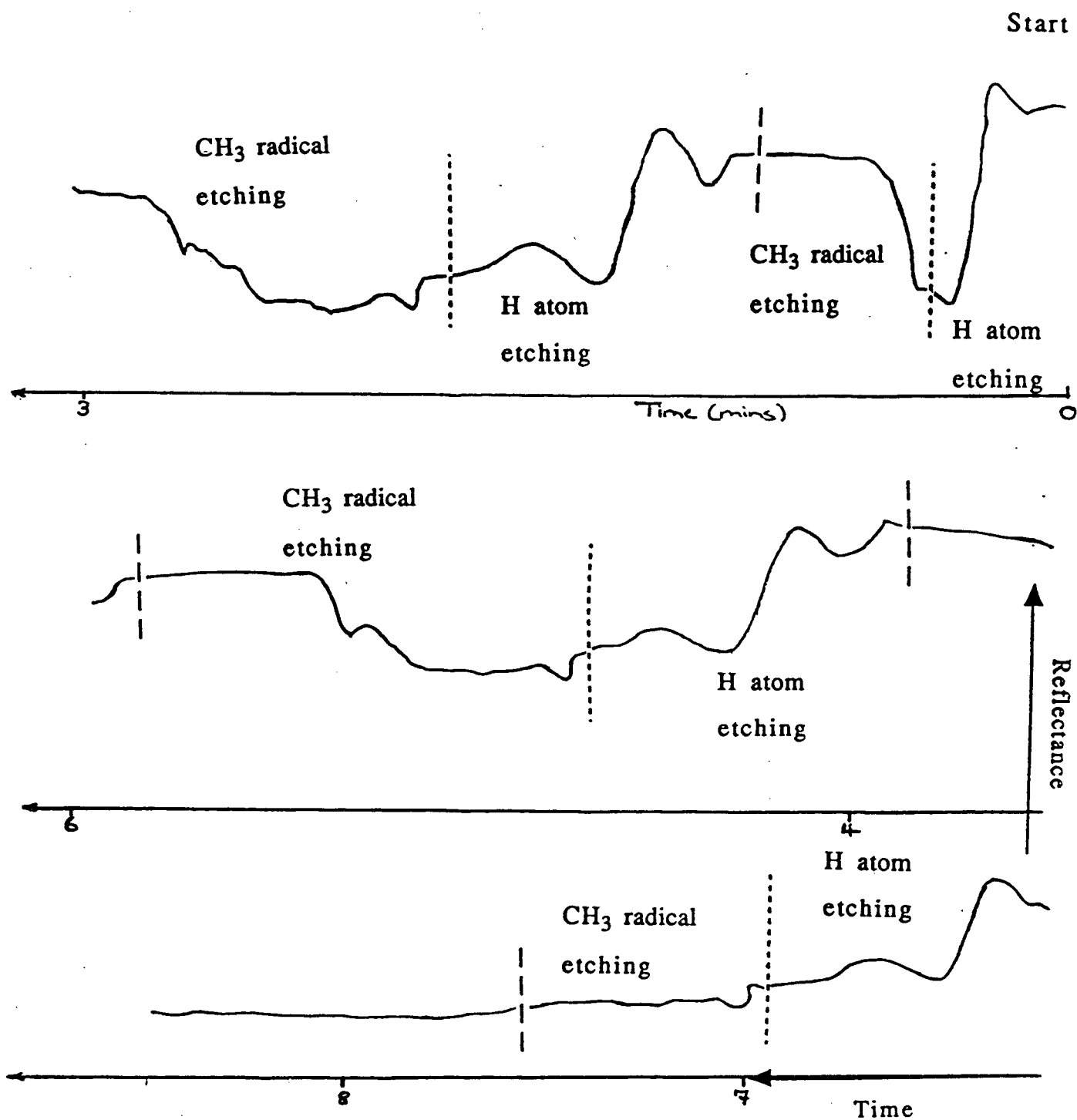
Figure 3.19. Interferogram for sample # 157. 33W microwave power, 215°C, 0.360 Torr pressure, fast flow system. ------- MeI flow started, _ _ _ MeI flow shut off.

temperatures much over 300°C where a brown residue was left behind. This was probably due to the decompostion of the $CH_3I$.

Experiments were run using $I_2$ instead of $CH_3I$ which should have produced iodine atoms through the reaction,

$$H_{(g)} + I_{2(g)} = HI_{(g)} + I_{(g)}$$
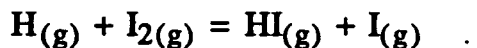
No etching by the I atoms was observed.


### 3.12  Examination of the surfaces

Several etching experiments were performed and stopped at various times during either the H or $CH_3$ etching. Each sample was subjected to XPS, SEM and profilometric analyses.


### 3.12.1  XPS analysis of the samples

Figure 3.20 shows the ratio of indium to phosphorus in the samples at various stages. It is clearly seen that the surface is quickly depleted of P on H atom etching. When the $CH_3I$ is added (dotted line) there is a rise in the reflectance which corresponds to the removal of excess In from the surface making the sample relatively smooth again. The composition at this stage has returned to $In_{0.5}:P_{0.5}$, as in the initial wafer.

The ratio of In:P was calculated by comparing the intensities of the In and P peaks on both masked and etched regions of each sample. The samples were also scanned for the presence of iodine, carbon and oxides. No iodine was found to be present and there was not a build up of carbon which indicates that polymer/hydrocarbon formation does not appear to be a problem, unlike what was found by other workers[35,18] when $CH_4/H_2$ discharges were used. However,
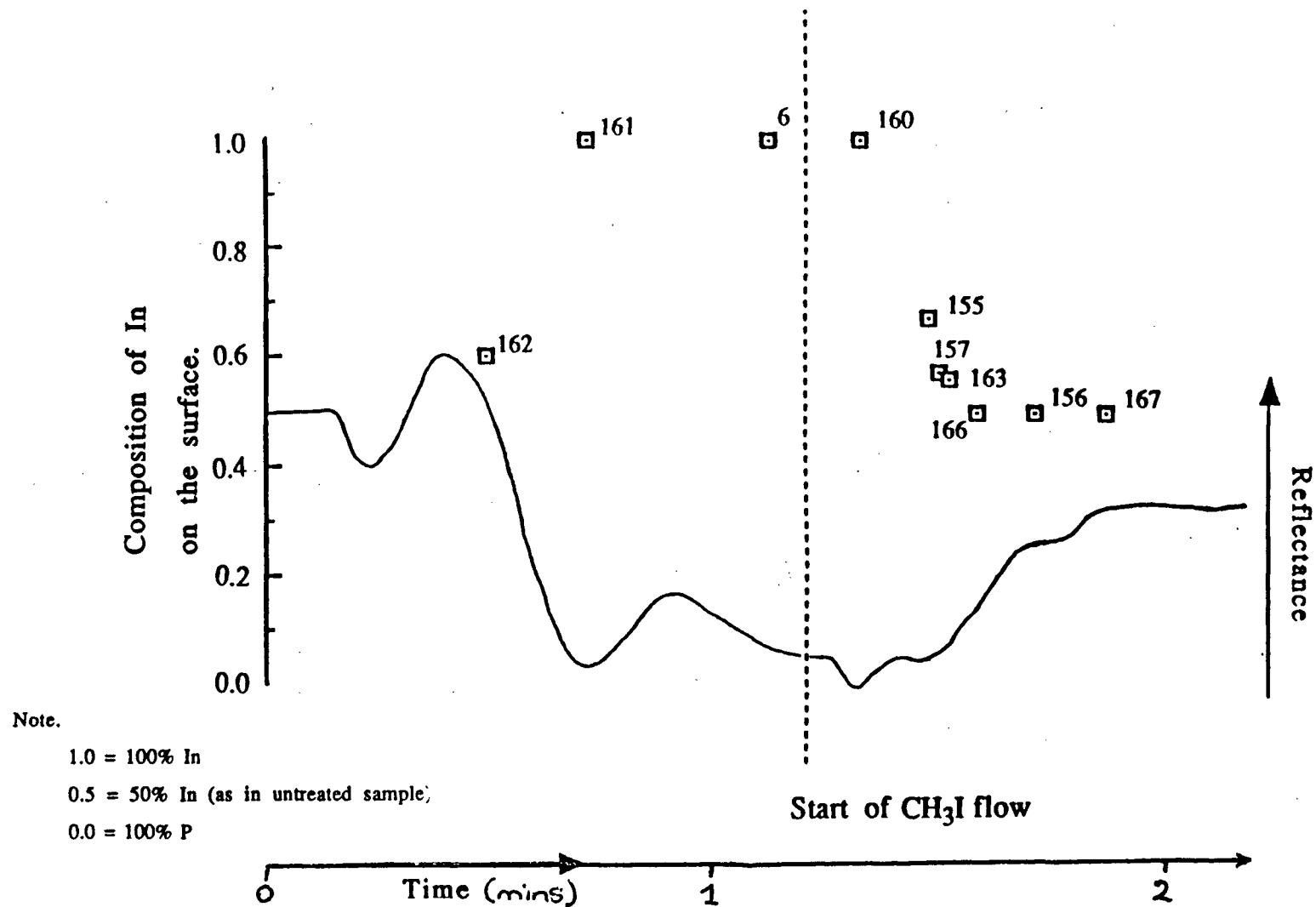
Figure 3.20.   Ratio of In in each sample at various stages shown during the process.

when the surfaces were scanned for oxygen, oxides were found to be present. Lau et al[25] studied oxide formation on InP using XPS and concluded that the oxide is not $InPO_4$ and that P and In oxides probably exist in separate phases. The In oxide was found not to be $In_2O_3$ and was assigned as a suboxide phase. Lau also stated that the surface oxidation peak on the P 2p spectrum overlaps with the bulk InP and was also due to the formation of a P suboxide. A weak broad peak with a chemical shift of around 4.5 eV was indicative of the formation of P oxide phases with a structure similar to a phosphate unit. In the samples examined by XPS the P oxide peak was also seen to be broad and located 4 - 5 eV from the P 2p signal, as shown in figure 3.21. The In oxide peak overlapped with the In 3d signal of the InP and a typical deconvolution is shown in figure 3.22. The In peak is found at 444.1 eV, compared with 443.9 eV by Lau et al. The In oxide peak is at 445.4 eV which is consistent with the literature, see figure 3.23. Table 3.8 gives the compositions for each sample including oxide compositions.

From the oxide measurements shown in table 3.8 H atom etching removes any oxide layer present. This confirms the observations by Chang et al[2]. The oxide that is found on the samples could mostly be due to small amounts of water present in the phosphoric acid coated walls and only partially due to subsequent oxidation on removal from the system, since all the samples were left in air for a similar period of time. Table 3.8 indicates that the longer the sample is exposed to the $CH_3$ flow, the greater the amount of oxide present. The formation of oxides in the presence of $CH_3 + I$ could be due to the presence of trace impurities in the system (eg, HO
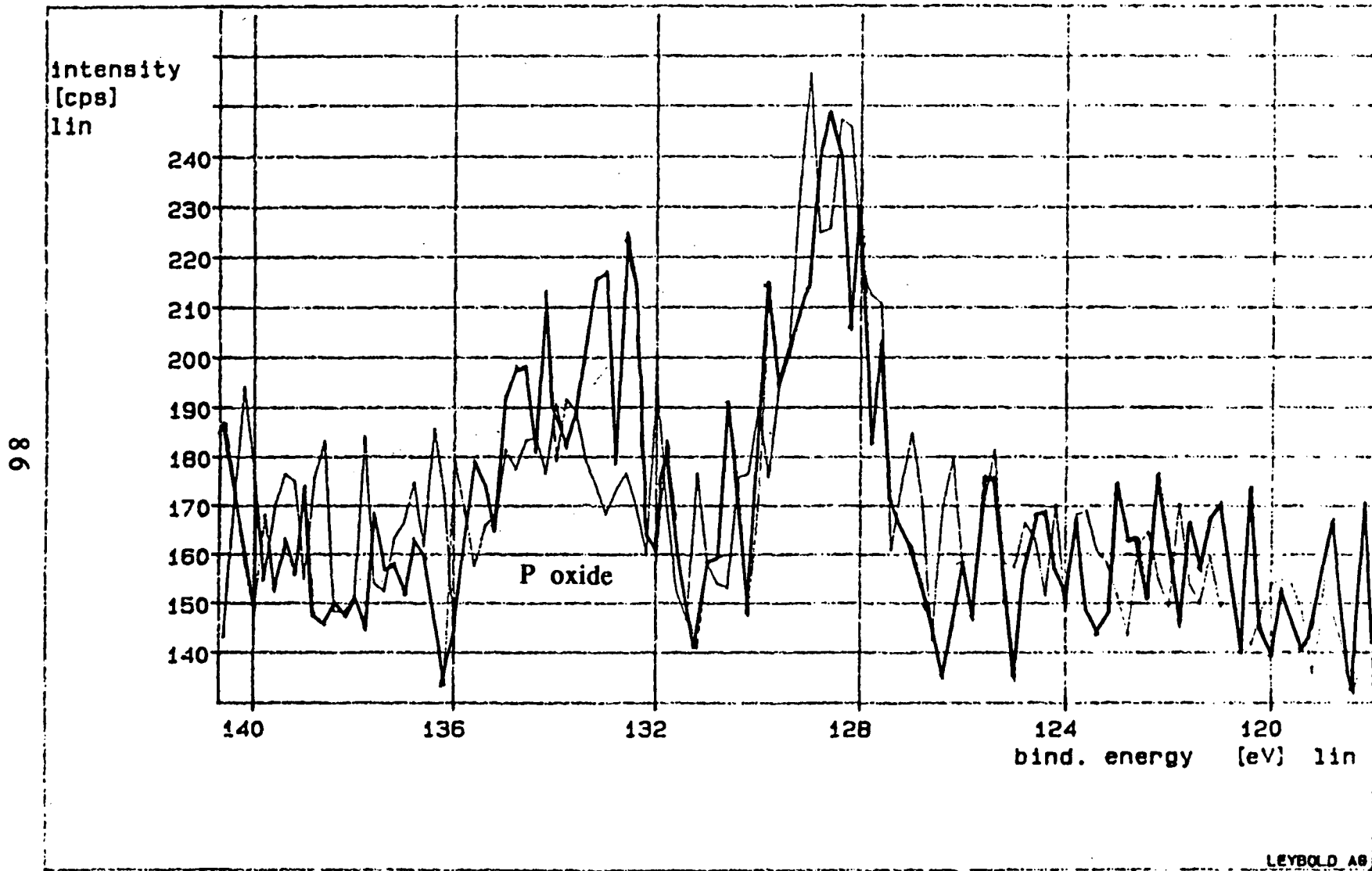
Figure 3.21. XPS spectrum of P 2p, sample # 155. Masked area and
etched area (bold). Note the P oxide chemical shift of 4 - 5 eV.
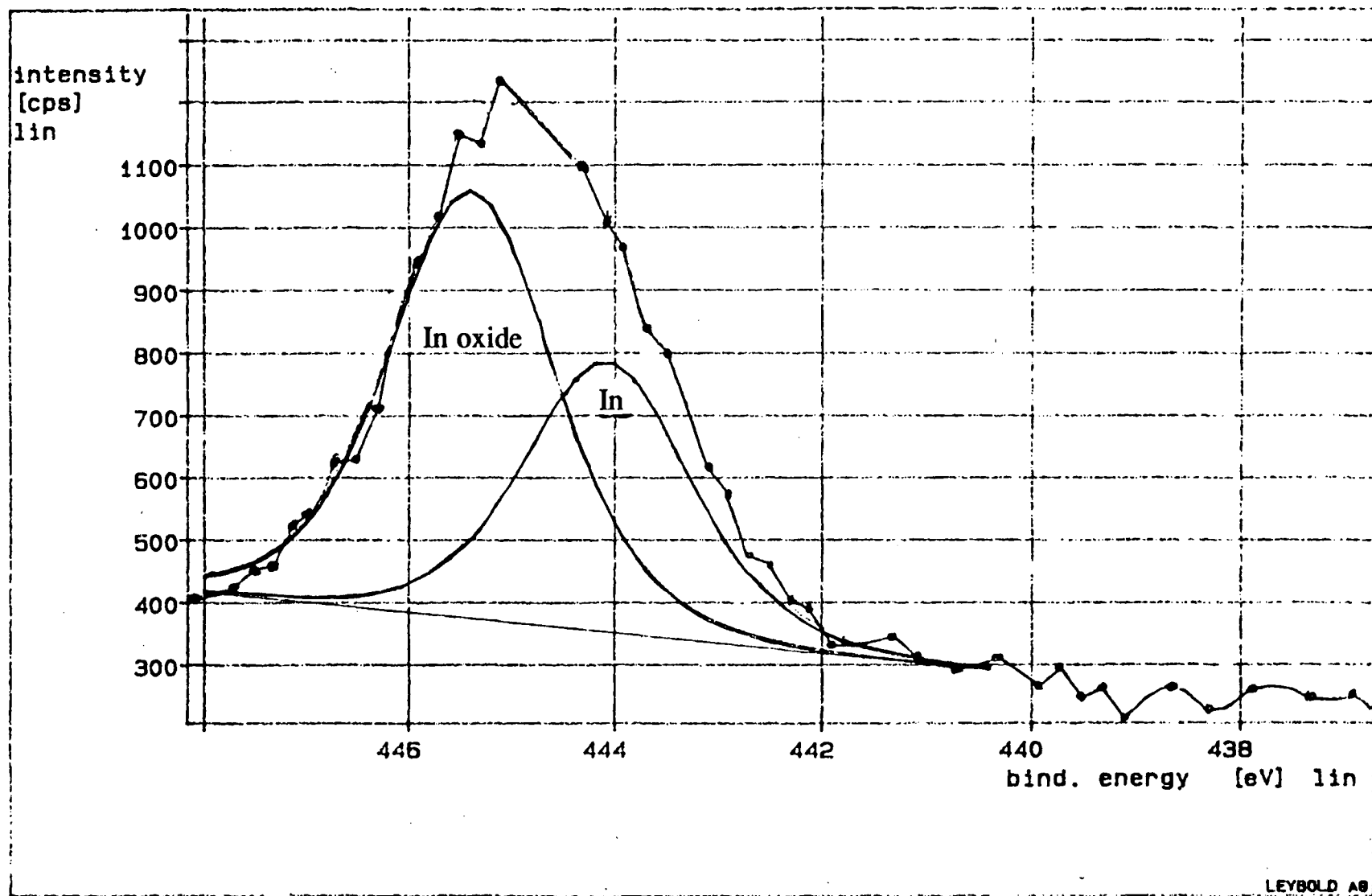
Figure 3.22.  XPS spectrum of In 3d region, sample # 156 etched

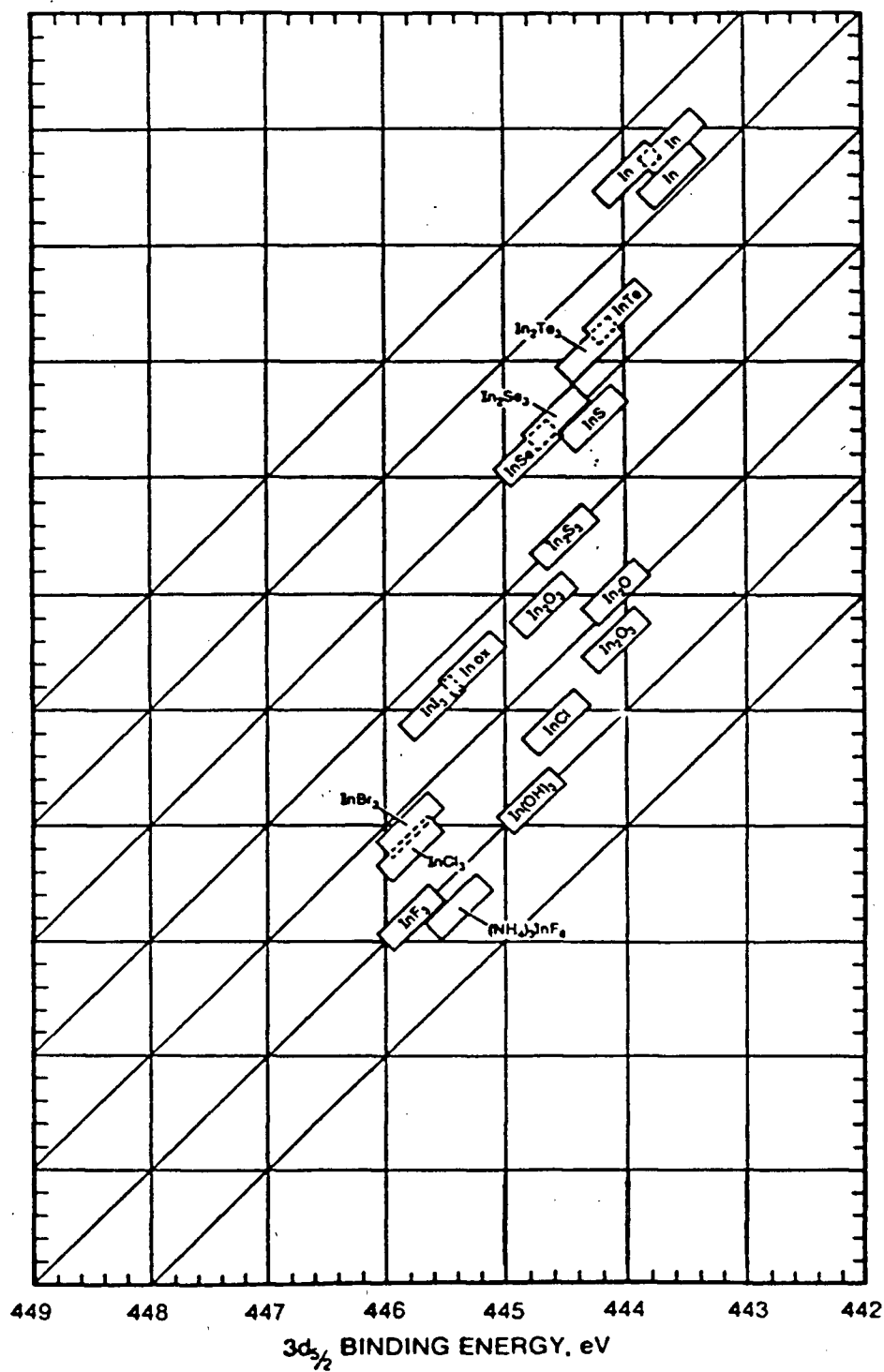area.  The In and In oxide peaks overlap and have been deconvoluted.

Figure 3.23. XPS values for In and some In compounds.

88

Table 3.8. Composition of samples during various stages of H atom and methyl etching.

| Sample # | In/P composition | Oxide composition |
|----------|------------------|-------------------|
| 162 | $In_{0.69}P_{0.31}$ | $In_0 P_0$ |
| 161 | $In_{1.0}P_0$ | $In_{0.2} P_0$ |
| 6 | $In_{1.0}P_0$ | $In_0 P_0$ |
| 160 | $In_{1.0}P_0$ | $In_0 P_0$ |
| 155 | $In_{0.67}P_{0.33}$ | $In_{0.07} P_0$ |
| 157 | $In_{0.57}P_{0.43}$ | $In_0 P_{0.12}$ |
| 163 | $In_{0.56}P_{0.44}$ | $In_0 P_0$ |
| 166 | $In_{0.5}P_{0.5}$ | $In_{0.14} P_{0.04}$ |
| 156 | $In_{0.5}P_{0.5}$ | $In_{0.3} P_{0.25}$ |
| 167 | $In_{0.5}P_{0.5}$ | $In_{0.23} P_{0.43}$ |

from the walls) and the fact that halogens are known to be excellent catalysts for surface oxygenation.

### 3.12.3 SEM analysis of the samples

SEM pictures were taken of some representative samples.

1) After H atom etch:

Plate 3.3 shows sample # 168a which would be at approximately the same time as sample # 6 in figure 3.20. Even though only about 60 - 70% of the surface is covered by indium globules, varying in size from 0.1 $\mu$m to 30 $\mu$m, the XPS of the surface indicates that the remainder is also covered by a layer of indium.

2) $CH_3$ radical etch.

Plate 3.4 shows sample # 156. Here after etching with H atoms for about 1 minute, $CH_3I$ was added and the etching continued. The surface appears quite smooth and no globules of indium are present. However, scattered on the surface are small pieces of material. It is possible that these are an indium or phosphorus oxide.

3) H atoms then $CH_3$ radicals followed by a second short H atom etch.

Plate 3.5 shows the surface of sample # 161, where after an initial H atom etch, $CH_3$ radicals then cleaned up the surface which was then subjected to a second very short H atom etch. The surface appears to be covered intermitantly with seemingly shell like structures, beneath which are a few new indium globules that are seen to be forming. A possible explanation for these shells is that they form an oxide crust on the large globules.
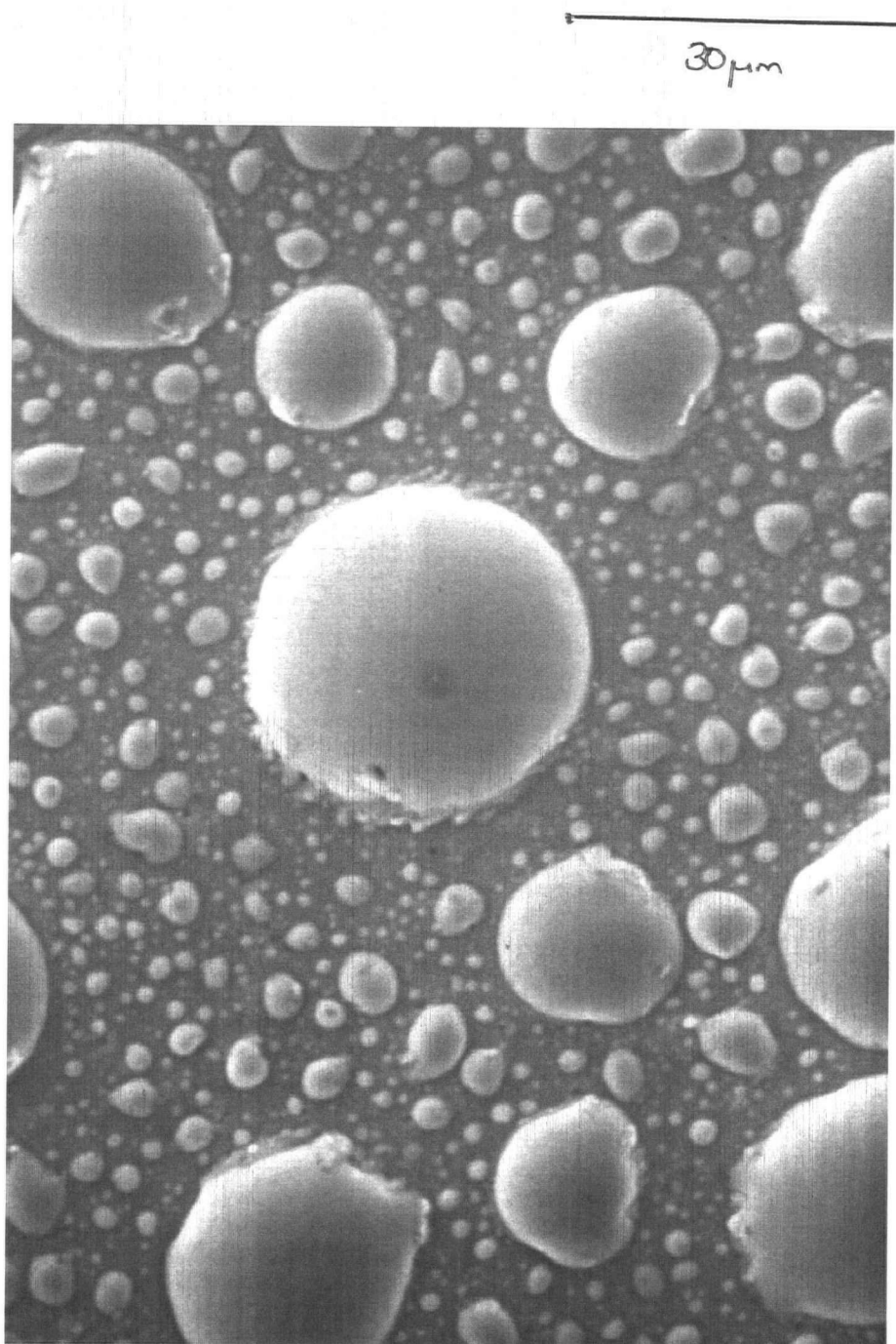
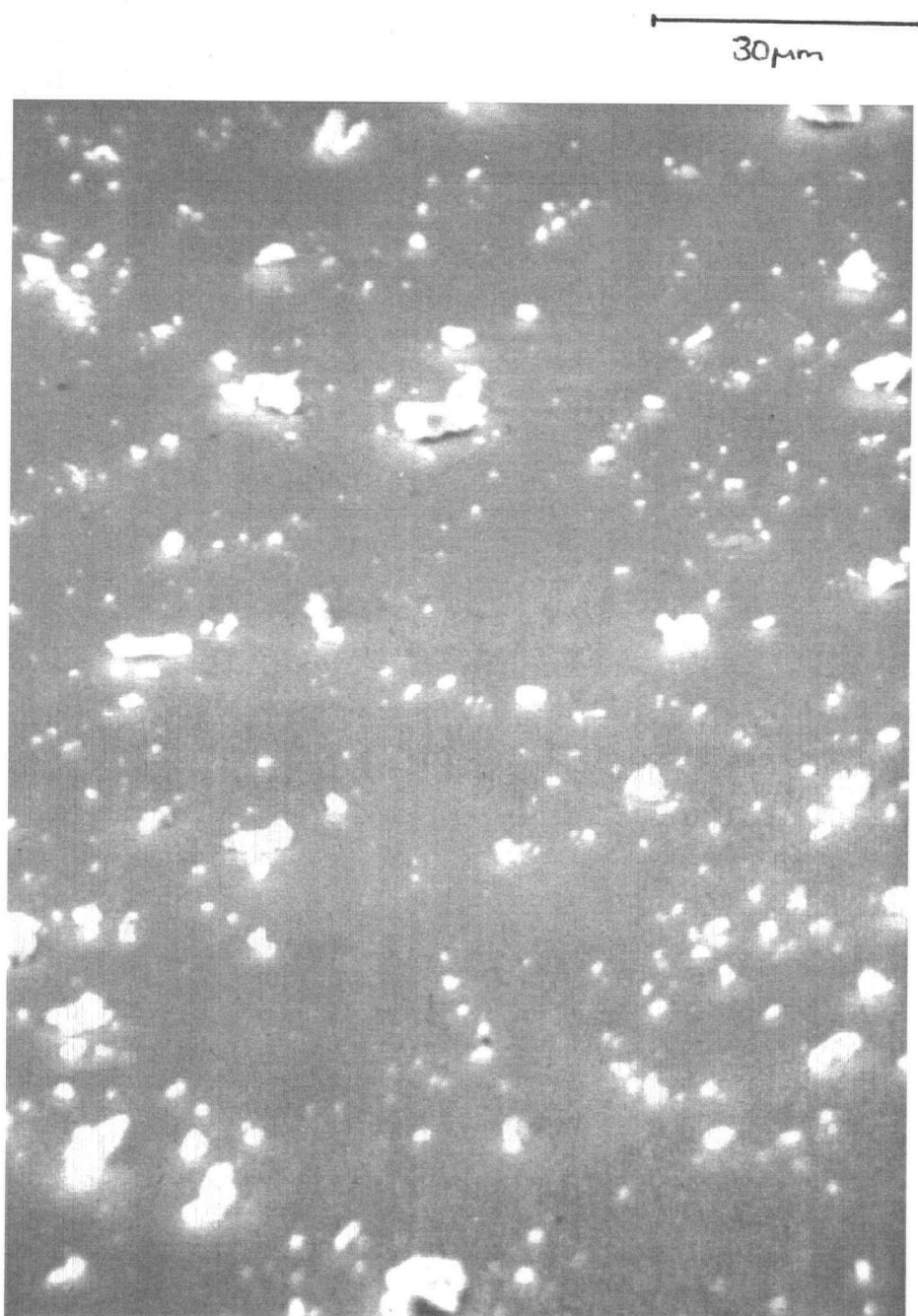Plate 3.3. Sample # 168a H atom etched surface x 6.0k largest globule 30μm.

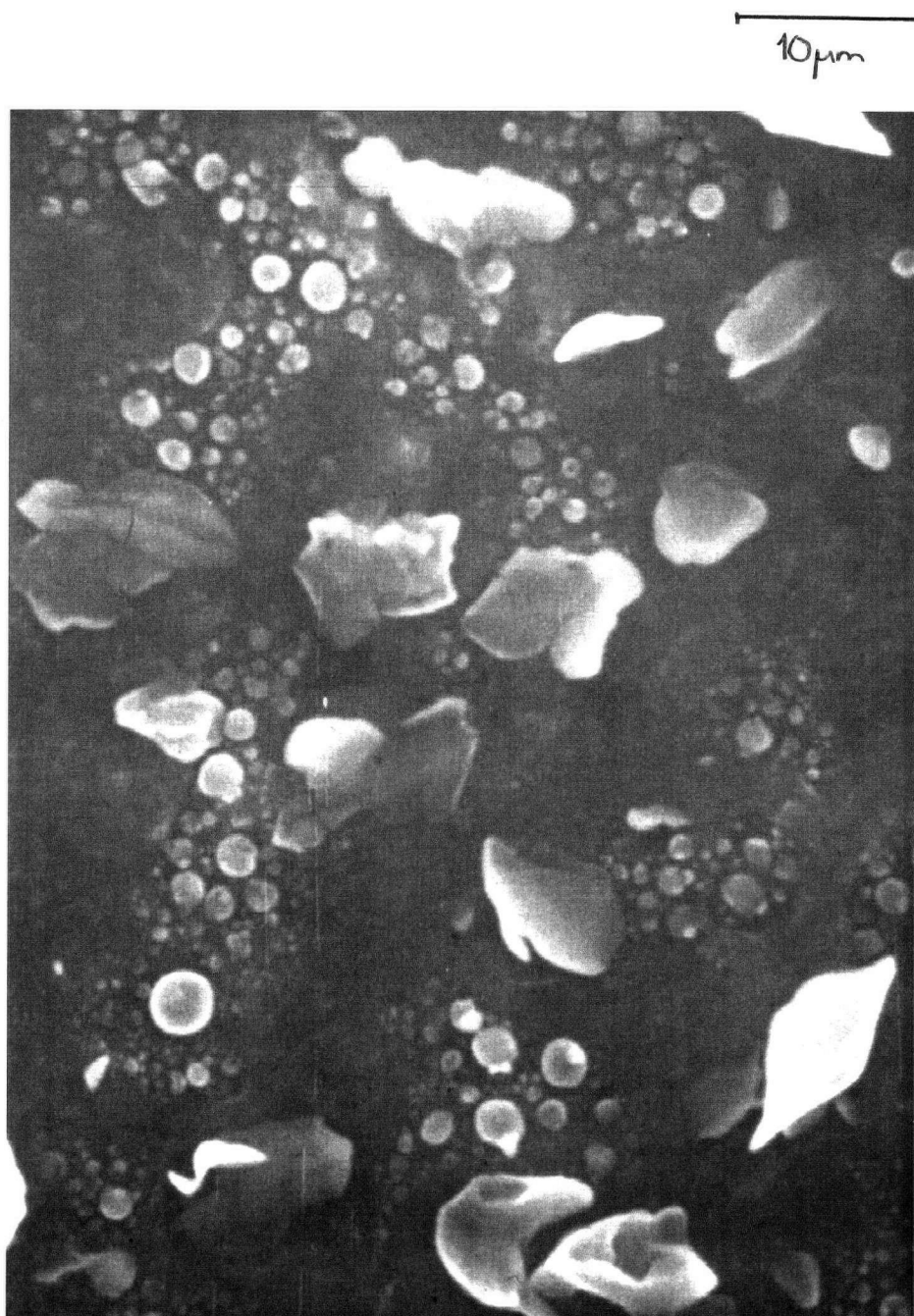Plate 3.4. Sample # 156 after CH$_3$ etch.

Plate 3.5. Sample # 161 H atom and CH$_3$ etching followed by a short H atom etch.

After the indium rich surface has been exposed to the $CH_3$ most of the indium is probably removed except for these shell like oxides, which then are etched away by H atoms, as indicated by the XPS analyses.

### 3.12.4 Profilometry of samples

Profilometry was used to establish the etch depth of the samples, but it can also illustrate differences in the surfaces of the wafers. Figure 3.24 compares a profile of sample # 89 (similar to those shown in figure 3.18) where the wafer has only been etched with H atoms, along with the profile of sample # 161. The latter being H atom etched for a short while, followed by $CH_3$ radical etching of the surface indium with the process being stopped after a further H atom etch had been started. It can be seen that there are no longer large amounts of indium present on the surface and that the etch is much deeper and more uniform than that achieved by H atoms alone.
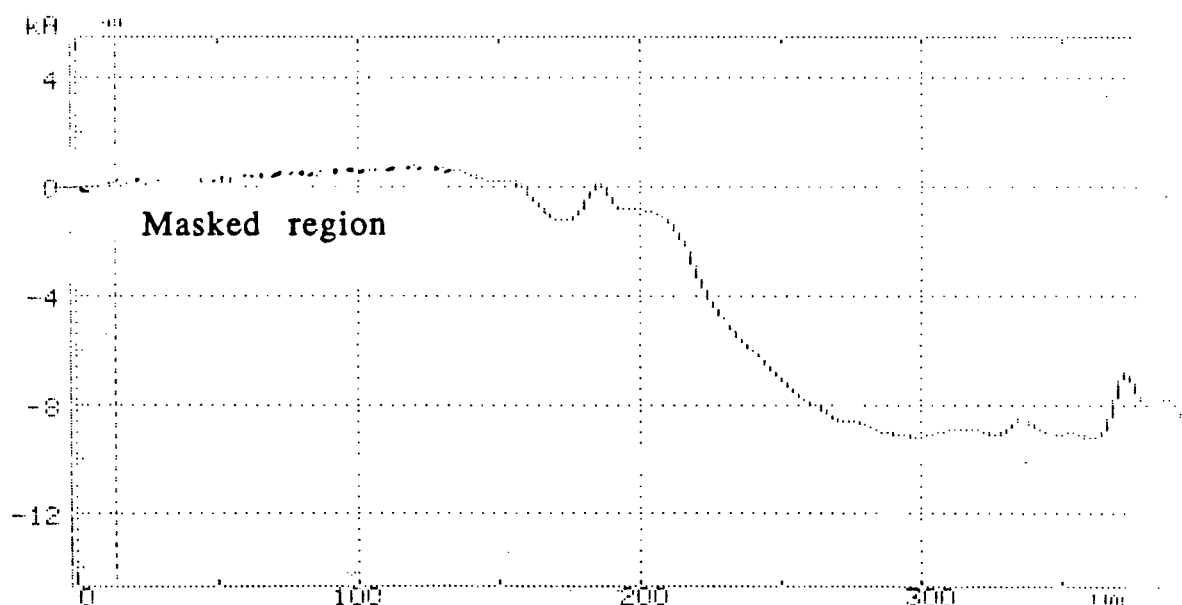
### 3.13 Etching of In metal

The etching of In metal with $CH_3$ was studied by coating microscope cover glasses with In and heating to 250°C - 300°C. The surface oxide was first cleaned off by exposing the sample to the stream of H atoms, $CH_3I$ was then added to the stream to produce $CH_3$ radicals. During the process oxide again forms, discolouring the In, and the sample was intermittantly cleaned. Table 3.9 lists these results and figure 3.25 shows a plot of etch rate against $P_{CH3}$.
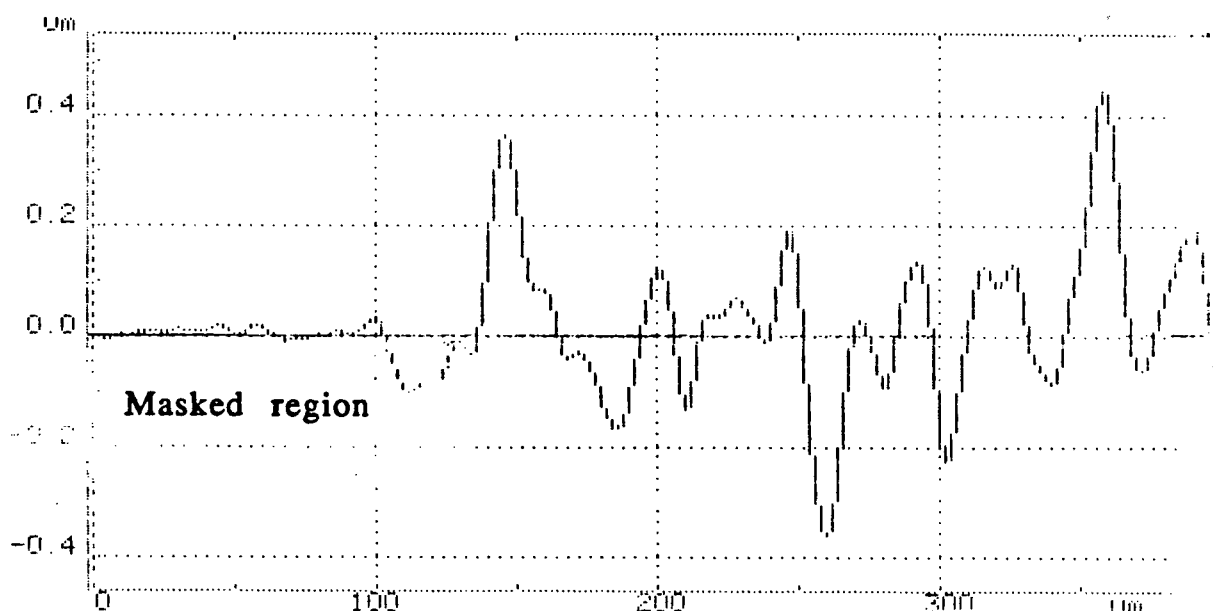
Figure 3.24. Top, profile of sample # 89, only H atom etching. Bottom, sample # 161; H atom etched followed by $CH_3I$ and then H atoms again.

Table 3.9.  Etch rate of In with $CH_3I$ and H atoms.

| Sample # | Mass loss (mg) | Etch rate (μm/min) | Partial pressure of $CH_3$ (Pa) |
|----------|----------------|--------------------|--------------------------------|
| 194 | 1.67 | 0.27 | 15.54 |
| 172 | 0.22 | 0.26 | 17.13 |
| 189 | 2.33 | 0.10 | 4.82 |

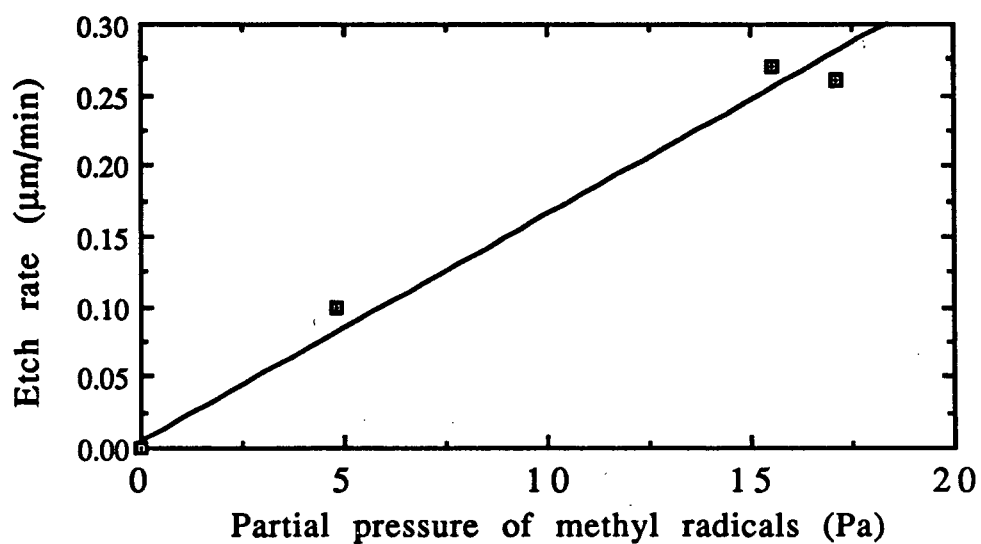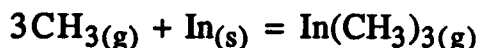Slope $(k_2) = 0.0145 \pm 0.0016$ $\mu$m/min.Pa$^{-1}$

Figure 3.25. Graph of the partial pressure of $CH_3$ against etch rate of In.

The data in figure 3.25 is consistent with a first order dependence upon the partial pressure of $CH_3$ ($P_{CH3}$) for the reaction;

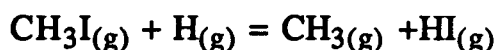$$3CH_{3(g)} + In_{(s)} = In(CH_3)_{3(g)}$$

where $k_2$ = rate constant and is given by the slope of figure 3.25.

Using a least squares fit of the points yields a value of,

$$k_2 = 0.0145 \pm 0.0016 \ \mu m.min^{-1}.Pa^{-1}.$$

### 3.14. Continuous etching of InP

The source of methyl radicals that we have used namely:

$$CH_3I_{(g)} + H_{(g)} = CH_{3(g)} + HI_{(g)}$$

allows us to only partially titrate the H atoms with the $CH_3I$ and thus obtain an etching mixture containing any ratio of H:$CH_3$ desired. A fresh sample of InP was introduced into the reaction chamber at 300°C and an initial partial pressure of 0.19 Pa. The $CH_3I$ flow was then adjusted to produce a continuous etch shown in figure 3.26. The flow of $CH_3I$ required to produce this continuous etch was found to require a partial pressure of 0.13 Pa of $CH_3I$. This yields a partial pressure of $CH_3$ = 0.13 Pa and an untitrated partial pressure of 0.06 Pa of H atoms, that is a ratio of $P_{CH3}/P_H = 2$.

In view of the conclusions drawn earlier, the etching of InP by H atoms and $CH_3$ radicals can proceed through the following two steps;

$$3H_{(g)} + InP_{(s)} = In_{(s)} + PH_{3(g)}$$
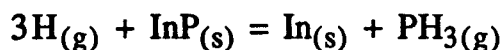
with $k_1 = 0.0305 \ \mu m.min^{-1}.Pa^{-1}$

$$3CH_{3(g)} + In_{(s)} = In(CH_3)_{3(g)}$$
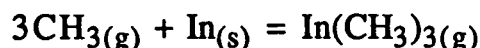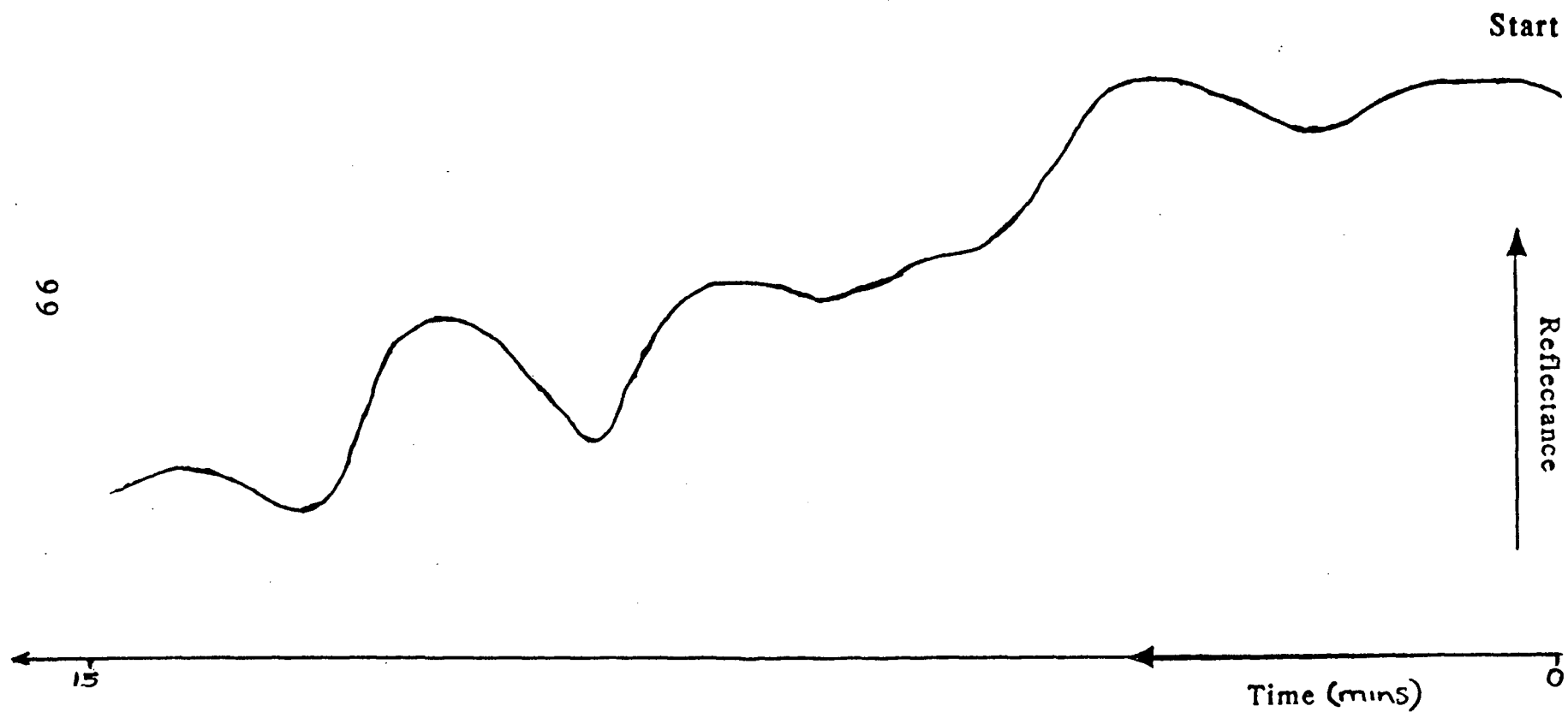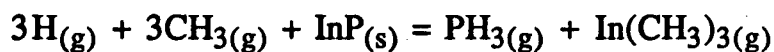
with $k_2 = 0.0145 \ \mu m.min^{-1}.Pa^{-1}$.

Figure 3.26.   Interferogram showing 5 interference maxima,
produced by etching InP with H atoms in a small MeI flow.

The net reaction is

$$3H_{(g)} + 3CH_{3(g)} + InP_{(s)} = PH_{3(g)} + In(CH_3)_{3(g)}$$

The rate of first step is,

$$ER_H = k_1P_H$$

and the rate of the second step is,

$$ER_{CH3} = k_2P_{CH3}$$

Such a steady state etch rate occurs when

$$ER_H = ER_{CH3}$$

that is,

$$k_1P_H = k_2P_{CH3}$$

and should therefore occur at,

$$P_{CH3}/P_H = k_1/k_2 = 2$$

which is in excellent agreement with the direct measurement of the partial pressure of $CH_3$ and H required for continuous etching.

## 4 Conclusion

The etching of InP by H atoms was found to occur at 160°C and not below, leaving the surface rich in indium metal globules. Although at temperatures lower than the melting point of indium (156.6°C) etching of the very uppermost surface layers ( up to 0.8 nm[16]) probably occurs, the bulk material does not etch until globulation occurs to reveal more phosphorus. The rate constant ($k_1$) for the reaction;

$$3H_{(g)} + InP_{(s)} = PH_{3(g)} + In_{(l)}$$
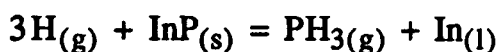
was found to be $0.0307 \pm 0.0018$ μm.min$^{-1}$.Pa$^{-1}$ at 300°C.

$CH_3$ radicals were found not to react with InP however the rate constant ($k_2$) for the reaction;

$$In_{(l)} + 3CH_{3(g)} = 3In(CH_3)_{3(g)}$$
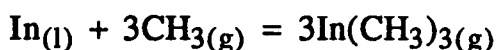
was found to be $0.0145 \pm 0.0016$ μm.min$^{-1}$.Pa$^{-1}$ at 300°C.

The surface composition of the InP wafer was determined at various stages along the process, whereby H atoms were followed by $CH_3$ radical etching of the residual indium. XPS showed that the indium rich surface was cleaned up by the $CH_3$ radicals, although upon extended exposure to the $CH_3I$ flow oxidation was found to occur. Studies of the resulting surfaces by SEM and profilometry established that the uniformity of the etch was greatly improved.

A method was developed where etching of both the constituent components was performed simultaneously and was found to depend upon the condition that;

$$P_{CH3}/P_H = 2$$
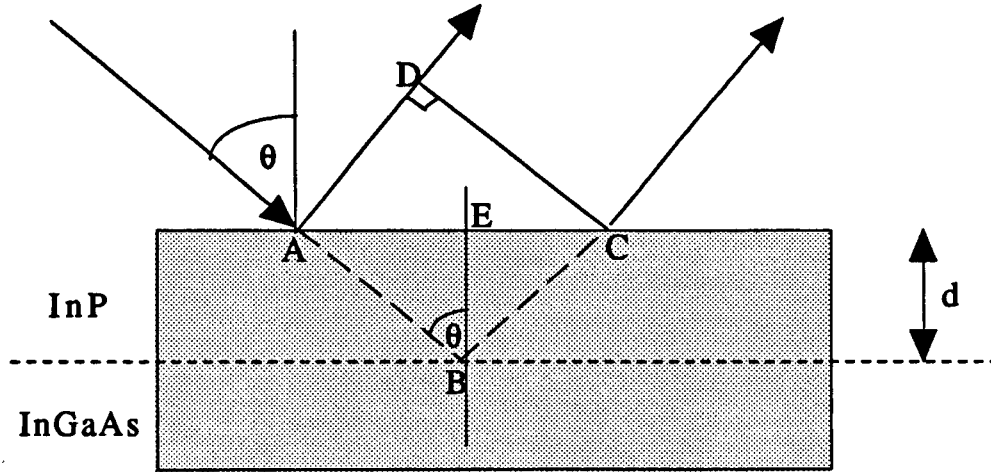
$d$ = depth etched,

$\theta$ = angle of incident laser beam.

The difference in the optical path, L, is given by;

$$L = (AB + BC) - AD$$

$$= (AB + BC) - 2AB\sin^2\theta$$

$$= 2AB(1-\sin^2\theta)$$

$$= 2d\cos\theta.$$

For constructive interference,

$$n\lambda_{InP} = 2d\cos\theta \qquad \text{where } \lambda_{InP} =$$

wavelength of laser in InP

When $\theta = 0$ $\qquad n\lambda_{InP} = 2d \qquad\qquad$ (i)

Now,

$$\lambda_{InP} = v/f \qquad \text{where } f = \text{frequency of light}$$

and v = velocity of light in InP.

$$\lambda_{InP} = v/f$$

As,
$$\lambda_{air} = c/f,$$

$$\lambda_{InP} = \lambda_{air}v/c$$

$$= \lambda_{air}\eta_{air}/\eta_{InP} \qquad \text{since, } v/c = \eta_{InP}/\eta_{air}$$

Substituting into equation (i) gives,

$$d = n\lambda_{air}\eta_{air}/2\eta_{InP}$$

Etch rate = $d/t$, where $t$ = time between interference peak maxima.

Hence, Etch rate = $n\lambda_{air}\eta_{air}/2\eta_{InP}t$.

# Appendix B

A least squares linear regression program with errors in both coordinates was used to fit the data.[36] The algorithm used is based upon the view that the errors in the slope and intercept are dependent upon $\sigma^2$ and not upon the precision of the measurements. The errors in the individual data points were calculated as follows.

1) Error in etch rate by interferometry.

$$\text{Etch rate} = \lambda/2 \cdot \eta_{air}/\eta_{InP} \cdot 1/T.$$

Error only from measuring the time between the peak maxima = 0.025 mins.

2) Error in $F_H$.

The error in measuring the atom flow was calculated to be around 22% as shown in the sample calculation shown below.

From page 36 we have,

$$F_H = (i_1^2 - i_2^2) \cdot R/(4.18 \times D/2)$$

assuming the errors to be random we obtain,

$$(\Delta F_H)^2 = (4.18D/2)^{-2}[(2i_1R)^2(\delta i_1)^2 + (2i_2R)^2(\delta i_2)^2 + (i_1^2 - i_2^2)^2(\delta R)^2]$$

Using values of; $R= 0.35\Omega$, $\Delta R= 0.01\Omega$, $i_1=1.010$ amps, $i_2= 0.950$ amps and $\Delta i= 0.01$ amps we get,

$$\Delta F_H = 4.4 \times 10^{-8} \text{ moles/s and } \Delta F_H/F_H = 0.22$$

3) Error in $P_H$.

$$P_H = P_{total}\{1-1/(1+F_H/F_{H2})\}$$

Since the error in $F_{H2}$ is very small compared to that in $F_H$, $\Delta F_{H2}$ will be assumed to be negligable.

$$(\delta P_H)^2 = (P_{total})^2[(1 + F_H/F_{H2})^2 F_{H2}^{-1}]^2 \Delta F_H^2$$

using values of $\Delta F_H = 7 \times 10^{-8}$, $P_{tot} = 40$ Pa, $F_H = 2 \times 10^{-7}$ mole/s and $F_{H2} = 7 \times 10^{-4}$ moles/s

$$=> \Delta P_H = 2.5 \times 10^{-3} \text{ and } \Delta P_H / P_H = 0.23$$

4) Error in $P_{CH3}$.

This is assumed to be the same as the error in $P_H$ as calculated above.

5) Error in the etch rate ($\Delta$ER) of In with $CH_3$.

$$\Delta ER = (\Delta weight/weight) + (\Delta time/time)$$

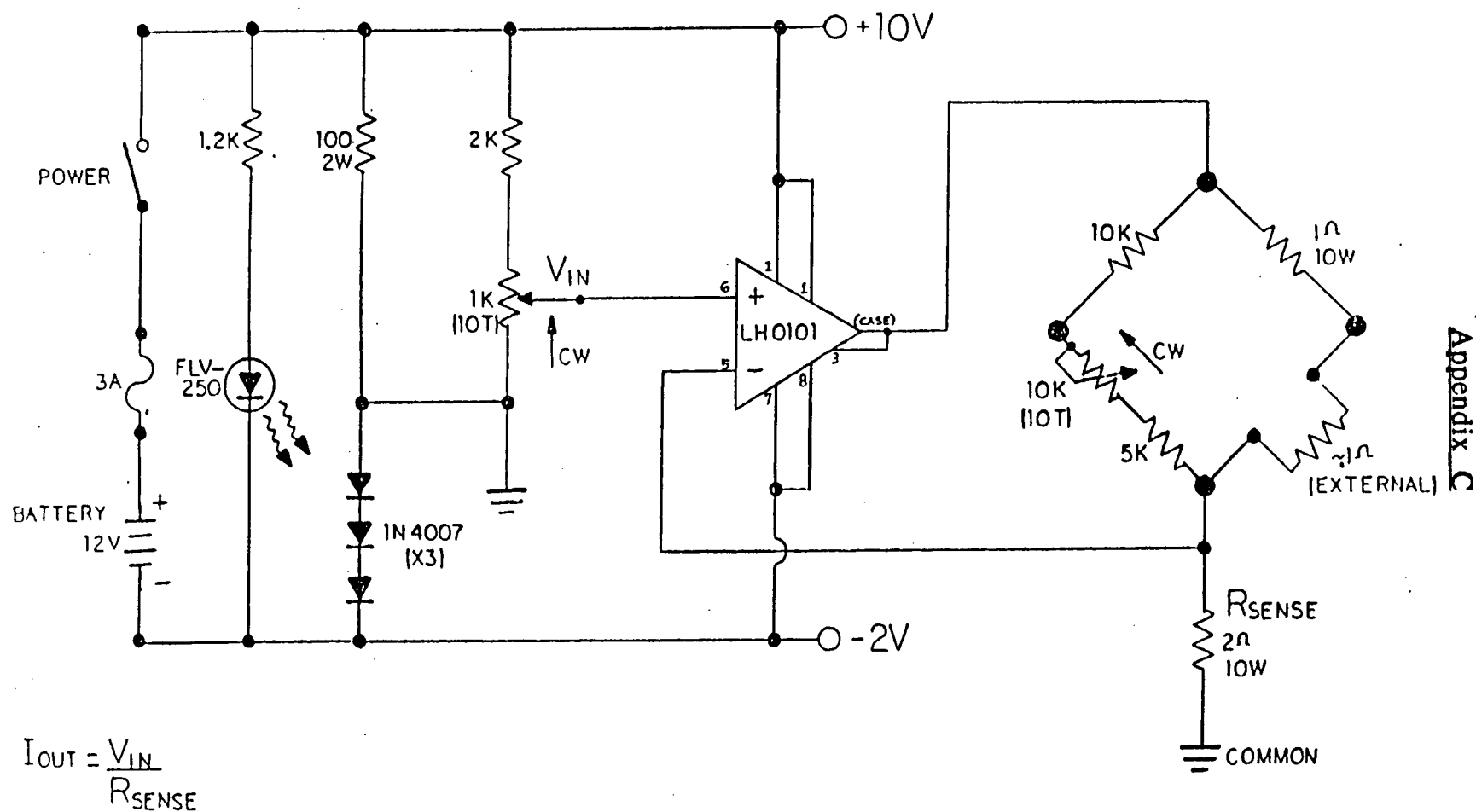$\Delta$time is estimated to be +/- 5% and $\Delta$weight is +/- 0.00006g.

6) Data input for fits.

a: For low $P_H$ against etch rate of InP.

| $P_H$ (Pa) | $\Delta P_H$(Pa) | Etch rate μm/min | ΔEtch rate μm/min |
|------------|------------------|------------------|-------------------|
| 1.11 | 0.24 | 0.040 | 0.001 |
| 0.66 | 0.15 | 0.029 | 0.001 |
| 0.36 | 0.08 | 0.018 | 0.001 |
| 1.67 | 0.37 | 0.056 | 0.001 |
| 1.19 | 0.26 | 0.045 | 0.001 |

b: Data for $P_{CH3}$ against etch rate of In.

| $P_{CH3}$(Pa) | $\Delta P_{CH3}$(Pa) | Etch rate μm/min | ΔEtch rate μm/min |
|---------------|----------------------|------------------|-------------------|
| 4.82 | 1.06 | 0.10 | 0.01 |
| 15.5 | 3.41 | 0.27 | 0.01 |
| 17.1 | 3.76 | 0.26 | 0.01 |

POWER

1.2K

100 2W

2K

$V_{IN}$

1K (10T)

CW

LH0101

(CASE)

10K

1Ω 10W

CW

10K (10T)

5K

~1Ω (EXTERNAL)

3A

FLV-250

1N4007 (X3)

BATTERY 12V

-2V

+10V

$R_{SENSE}$ 2Ω 10W

COMMON

Appendix C

106

$$I_{OUT} = \frac{V_{IN}}{R_{SENSE}}$$

OUTPUT: 0 - 1.5A

TITLE — CONSTANT CURRENT BRIDGE

DWG NO

DATE 03/90

BUILT BY D.T.

Dr. FOR OGRYZLO

CHECKED

PAGE NO 1

623

CONSTANT CURRENT SET-UP
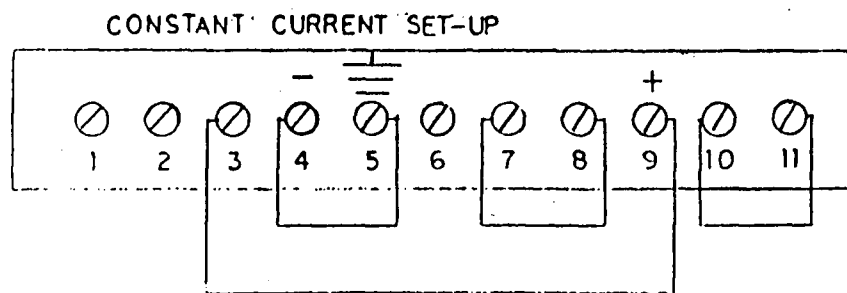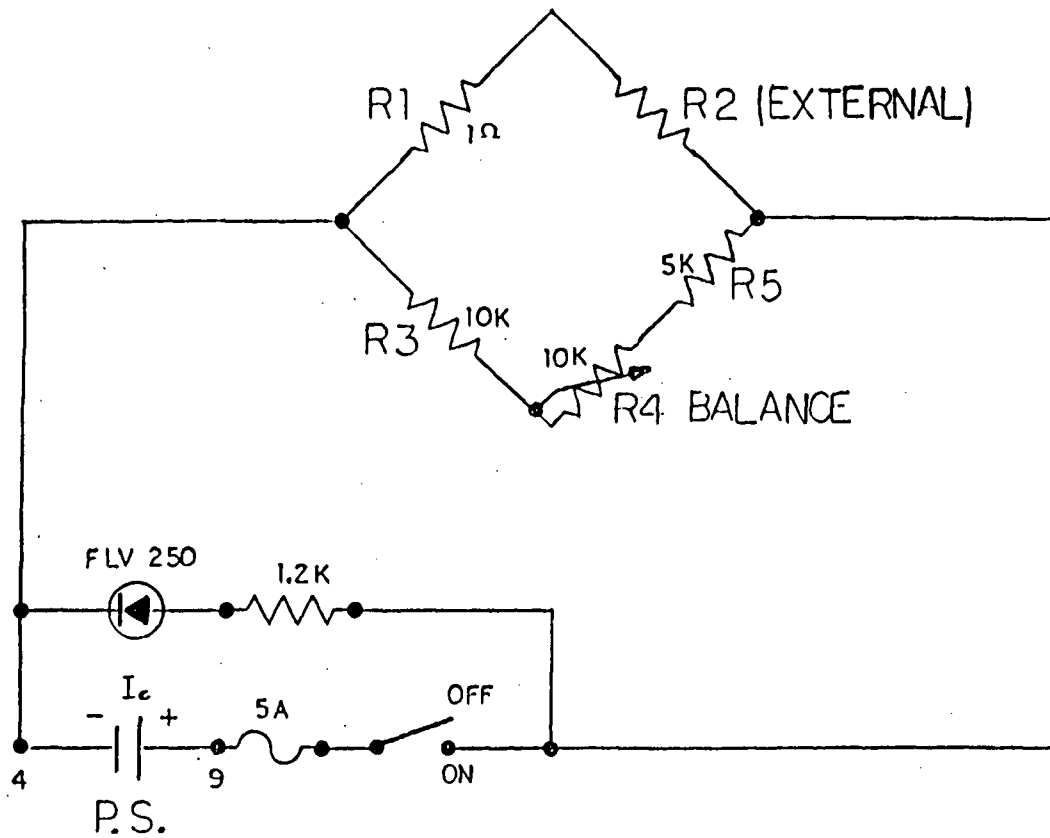
(REAR VIEW LAMBDA P.S.)

# REFERENCES

1. W. S. Ruska, in "Microelectronic Processing"; (McGraw Hill,1987), p 59 - 62.

2. S. K. Ghandhi, in "VLSI Fabrication Principles, Silicon and Gallium Arsenide", (Wiley Interscience,1982) p88.

3. M. L. Cohen and T. K. Bergstresser, Phys. Rev., 144, 789 (1966)

4. H. L. Chang and L. G. Meiners, J. Vac. Sci. Tech., B3, 1625 (1985)

5. "Semiconductor International", P. H. Singer Ed., 22 April 1989

6. H. W. Brandhorst, in SPIE vol 1144 (Oklahoma 1989); "InP & Related Materials For Advanced Electronic And Optoelectronic Devices", p12

7. C. J. Kleavey and M. B. Spitzer, Appl. Phys. Lett., 52, 1439 (1988)

8. Moss, Burrel and Ellis, in "Semiconductor Optoelectronics" (Wiley), 192-198

9. I. Weinberg, C. K. Swartz and R. E. Hart, in Proc. 20th. IEEE PV Conf. (1988) p893-897

10. K. Ando and M. Yammaguchi. Appl.Phys.Lett., 47, 846 (1985)

11. Ross, in "Optoelectronic Devices & Optical Imaging Techniques", (Wiley) p68-85

12. H. Kressel, in "Semiconductor Devices for Optical Communication", (Wiley), p82.

13. W. A. Gault, J. Crystal Growth, 74, 491, (1986)

14. D. J. Elliott, in "Integrated circuit fabrication technology", (McGraw Hill 1989) p.1-70

15. S. C. McNevin, J. Vac. Sci. Tech., **B4**, 1216 (1986)

16. R. J. Contolini, J. Electrochem. Soc., **135**, 929 (1988)

17. V. M. Donnely, D. L. Flamm, C. W. Tu and D. E. Ibbotson, J. Electrochem. Soc: Solid - State Science and Technology, **129**, 2533 (1982)

18. T. Tadokoro, F. Koyama and K. Iga, Jpn. J. Appl. Phys., (i), **27**, 389 (1988)

19. L. Henry, C. Vaudry and P. Granjoux, Electronics Lett., **23**, 1255 (1987)

20. R. P. H. Chang, C. C. Chang and S. Darack, J. Vac. Sci. Tech., **20**, 45 (1982)

21. R. P. H. Chang, C. C. Chang and S. Darack, J. Vac. Sci. Tech., **20**, 490 (1982)

22. C. W. Tu, R. P. H. Chang and A. R. Schiler, Appl. Phys. Lett., **41**, 80 (1982)

23. H. L. Chang, J. Vac. Sci. Tech., **B3**, 1625 (1985)

24. U. Niggebrugge, M. Klug and G. Garus, Inst. Phys. Conf. Ser., **79**, 367 (1985)

25. S. Doughty, S. Thomas, V. Law and C. D. W. Wilkinson, Vacuum, **36**, 803 (1986)

26. L. Henry, Electronics Lett., **23**, 1255 (1987)

27. T. Matsui, H. Sugimoto, T. Ohishi and H. Ogato, Electronics Lett., **24**, 798 (1988)

28. D. A. Roberts, M. A. Pate and P. A. Claxton, J. Vac. Sci. Tech., **B8**, 57 (1990)

29. H. Bonhoeffer, Z. Physik. Chem., **113**, 492 (1924)

30. E. E. Tollefson and D. J. Le Roy, J. Chem. Phys., **16**, 1057 (1948).

31. "Progress in reaction kinetics" G. Porter, Ed. (Pergamon 1961); vol 1 p105-129, vol 3 p63-97.

32. E. W. R. Steacie, in "Atomic and free radical reactions", (Reinhold 1946), p73-147 and p462-485.

33. F. K. McTaggert, in "Plasma Chemistry in Electrical Discharges" (Elsevier 1967), p105-120

34. W. M. Lau and R. N. S. Sodhi, J. Vac. Sci. Tech., **A6**, 1371 (1988).

35. R. Cheung, S. Thomas, S. P. Beaumont, G. Doughty, V. Law and C. D.W. Wilkinson, Electronics Lett., **23**, 857 (1987).

36. D. P. Chong, Submitted to Am. J. Phys., Feb 1990. "Comment on Linear least square fits with errors in both coordinates."